UNIVERSITAT POLITÈCNICA DE CATALUNYA BARCELONATECH

Morpho-functionality of the toothed whale external ear canal

by
Steffen De Vreese

ADVERTIMENT La consulta d'aquesta tesi queda condicionada a l'acceptació de les següents condicions d'ús: La difusió d'aquesta tesi per mitjà del repositori institucional UPCommons (http://upcommons.upc.edu/tesis) i el repositori cooperatiu TDX (http://www.tdx.cat/) ha estat autoritzada pels titulars dels drets de propietat intel·lectual **únicament per a usos privats** emmarcats en activitats d'investigació i docència. No s'autoritza la seva reproducció amb finalitats de lucre ni la seva difusió i posada a disposició des d'un lloc aliè al servei UPCommons o TDX. No s'autoritza la presentació del seu contingut en una finestra o marc aliè a UPCommons (*framing*). Aquesta reserva de drets afecta tant al resum de presentació de la tesi com als seus continguts. En la utilització o cita de parts de la tesi és obligat indicar el nom de la persona autora.

ADVERTENCIA La consulta de esta tesis queda condicionada a la aceptación de las siguientes condiciones de uso: La difusión de esta tesis por medio del repositorio institucional UPCommons (http://upcommons.upc.edu/tesis) y el repositorio cooperativo TDR (http://www.tdx.cat/?locale-attribute=es) ha sido autorizada por los titulares de los derechos de propiedad intelectual **únicamente para usos privados enmarcados** en actividades de investigación y docencia. No se autoriza su reproducción con finalidades de lucro ni su difusión y puesta a disposición desde un sitio ajeno al servicio UPCommons No se autoriza la presentación de su contenido en una ventana o marco ajeno a UPCommons (*framing)*. Esta reserva de derechos afecta tanto al resumen de presentación de la tesis como a sus contenidos. En la utilización o cita de partes de la tesis es obligado indicar el nombre de la persona autora.

WARNING On having consulted this thesis you're accepting the following use conditions: Spreading this thesis by the institutional repository UPCommons (http://upcommons.upc.edu/tesis) and the cooperative repository TDX (http://www.tdx.cat/?locale- attribute=en) has been authorized by the titular of the intellectual property rights **only for private uses** placed in investigation and teaching activities. Reproduction with lucrative aims is not authorized neither its spreading nor availability from a site foreign to the UPCommons service. Introducing its content in a window or frame foreign to the UPCommons service is not authorized (framing). These rights affect to the presentation summary of the thesis as well as to its contents. In the using or citation of parts of the thesis it's obliged to indicate the name of the author.

Joint PhD programme in Veterinary and Marine Sciences

MORPHO-FUNCTIONALITY of the TOOTHED WHALE EXTERNAL EAR CANAL

Thesis submitted to obtain the title of Doctor in Veterinary Sciences by the Università degli Studi di Padova and Doctor in Marine Sciences by the Universitat Politècnica de Catalunya

Doctoral dissertation by
Steffen De Vreese

Supervisors
Prof. Dr. Sandro Mazzariol
Prof. Dr. Michel André

Coordinators
Prof. Dr. Valentina Zappulli
Prof. Dr. Agustín Sanchez-Arcilla

Department of Comparative Biomedicine and Food Science (BCA), Università degli Studi di Padova (UniPd), Italy
Laboratory of Applied Bioacoustics (LAB), Universitat Politècnica de Catalunya (UPC), Spain

University with Administrative Responsibility: Università degli Studi di Padova
Hosting University: Universitat Politècnica de Catalunya
Performed with the financial contribution of the Cariparo Foundation

GENERAL TABLE OF CONTENTS

Detailed tables of contents are provided at the beginning of each chapter

ANNEXES

ANNEXES

1 Anatomopathological findings and case reports

1.1 Otitis externa

1.1.1 Striped dolphin (ID293/18)

There was a chronic active purulent inflammation with macrophages and neutrophils around and in the left ear canal in the superficial half of the canal from the skin down to the medial end of the ventral curvature where the canal turns horizontal again. There was a mild to moderate adenitis (possibly bacterial) and panniculitis, with likely inclusion bodies situated inside the glandular units (Figure 315, Figure 316, Figure 317, Figure 320, Figure 321, Figure 322, Figure 323). There was hyperplasia of the epithelium, and in one section, there was ulceration of the epithelium (Figure 324, Figure 325, Figure 326). There was no degeneration of the nervous tissues. The aetiology could have been associated with either a reaction to an external influence with skin reaction (e.g. parasites: *Penella* around the ear opening), or an infectious agent with epitheliotrope character (e.g. Herpes, or a secondary infection associated with Morbillivirus) and secondary infection with bacteria in the ear canal and glands. The right ear canal was used for studies using Sihler´s method, and therefore not histologically analysed.

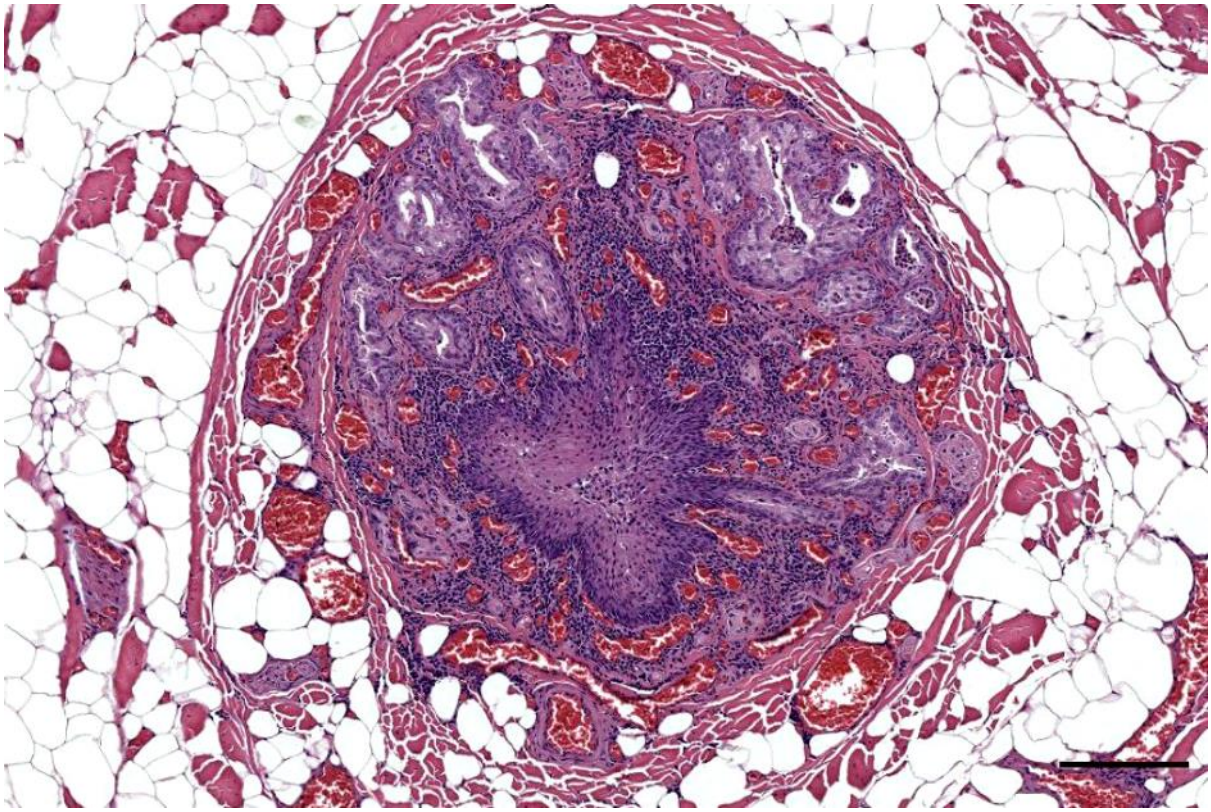

Figure 315. Histological cross-section (HE staining) of the left ear canal in a striped dolphin (293/18_L2). Overview of the ear canal, glands and immediate surroundings. Note the inflammation, the absent lumen, and the intense vascularization. Scale bar 200 µm

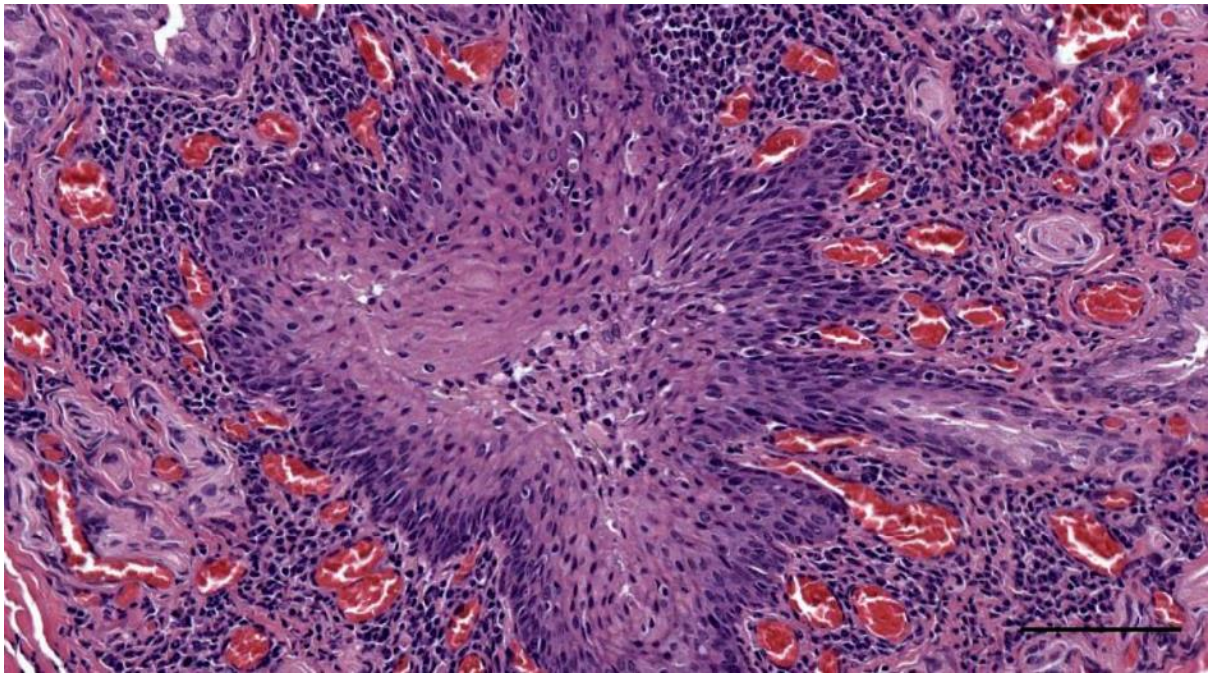

Figure 316. Detail of Figure 315. Artificial lumen filled with epithelial cells and mononuclear cells. There is an abundant presence of inflammatory cells (lymphocytes and macrophages) surrounding the ear canal. Scale bar 100 µm

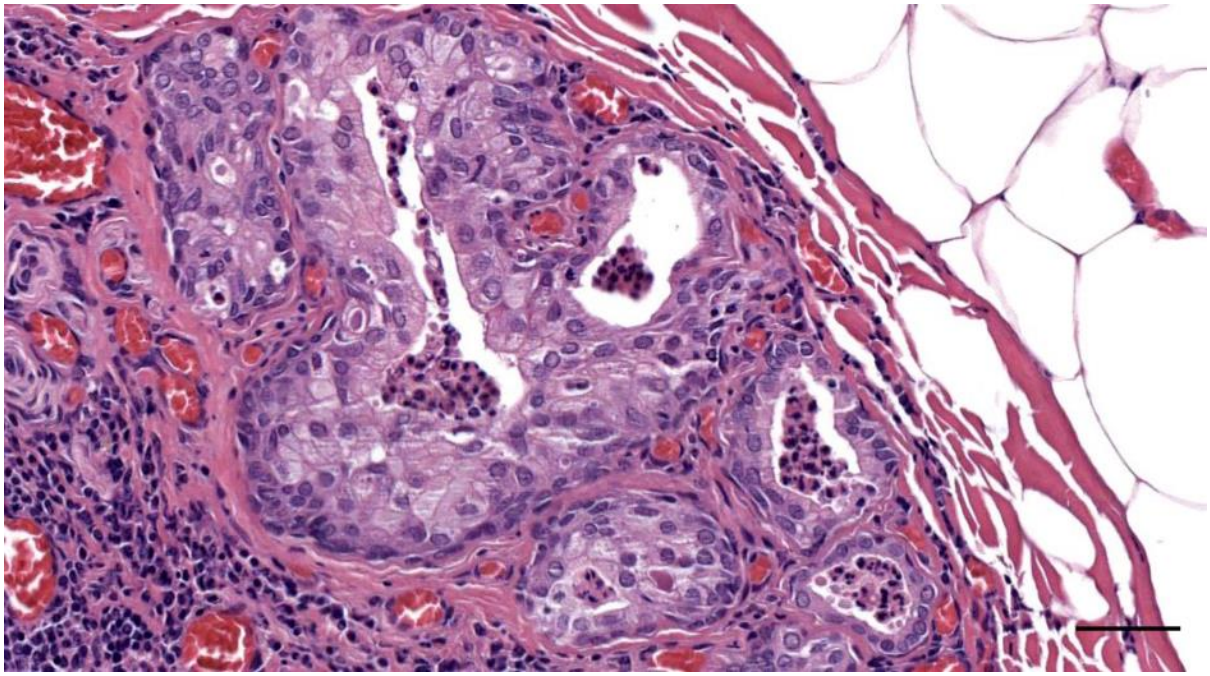

Figure 317. Detail of Figure 315. Inflammatory cells in the glandular secretory/excretory ducts; also not the abundant presence of mononuclear cells in the stroma between glands and ear canal (bottom left). Scale bar 50 µm

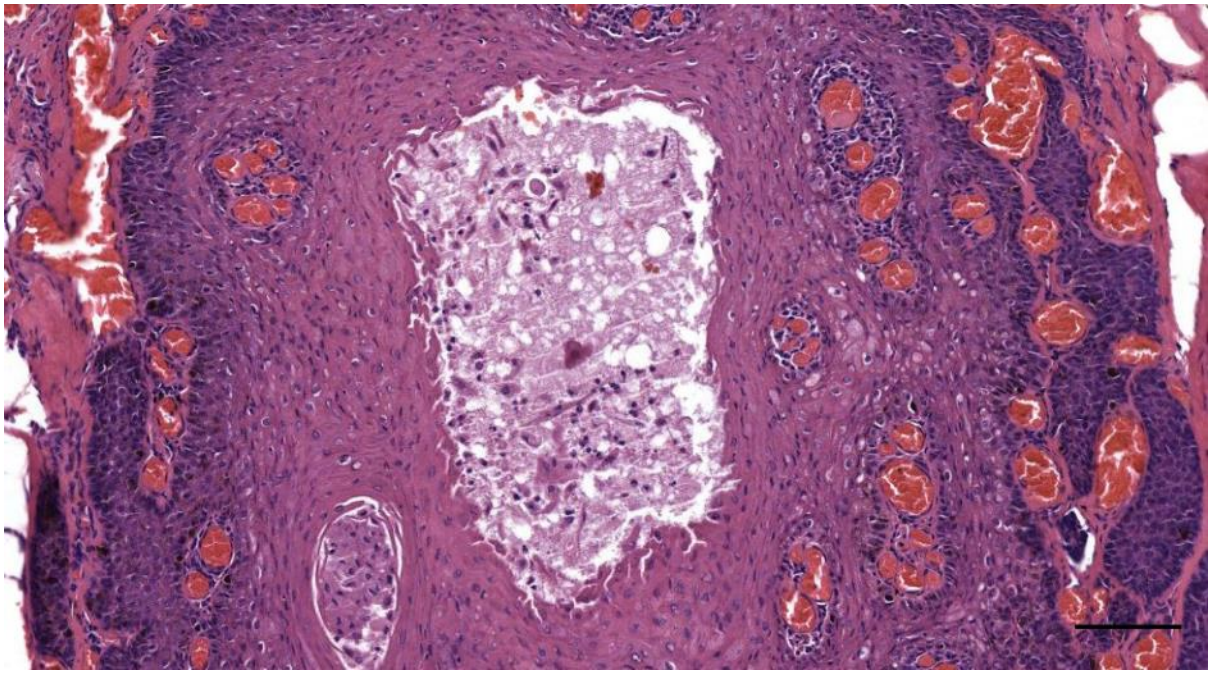

Figure 318. Histological transverse section through the ear canal of a striped dolphin (ID293/18) at the medial end of the external ear opening. The lumen is filled with a mixed content of degenerated epithelial cells, mononuclear inflammatory cells, possible glandular cells with pyknotic nuclei, and a homogenous eosinophilic matter. Scale bar 100 µm

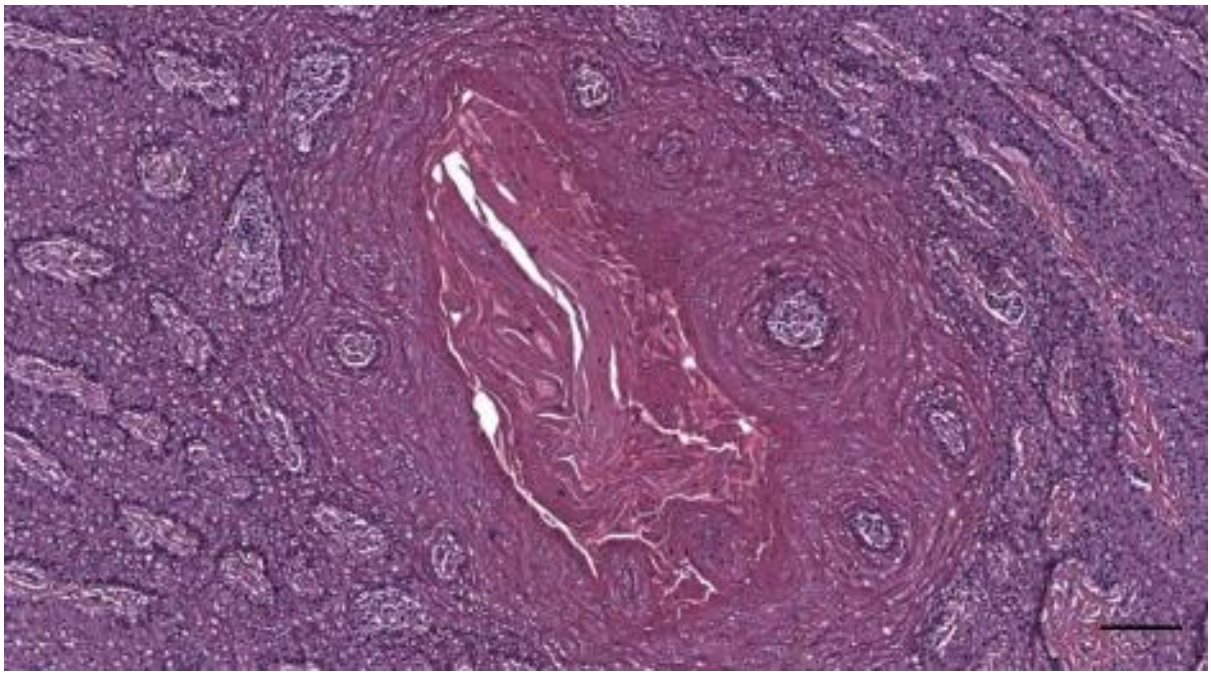

Figure 319. Histological cross-section (HE staining) of the left external ear opening in a striped dolphin (293/18_L1) Ear canal lumen with proteinaceous content, cells with pyknotic nuclei, and mononuclear inflammatory cells. Scale bar 100 µm

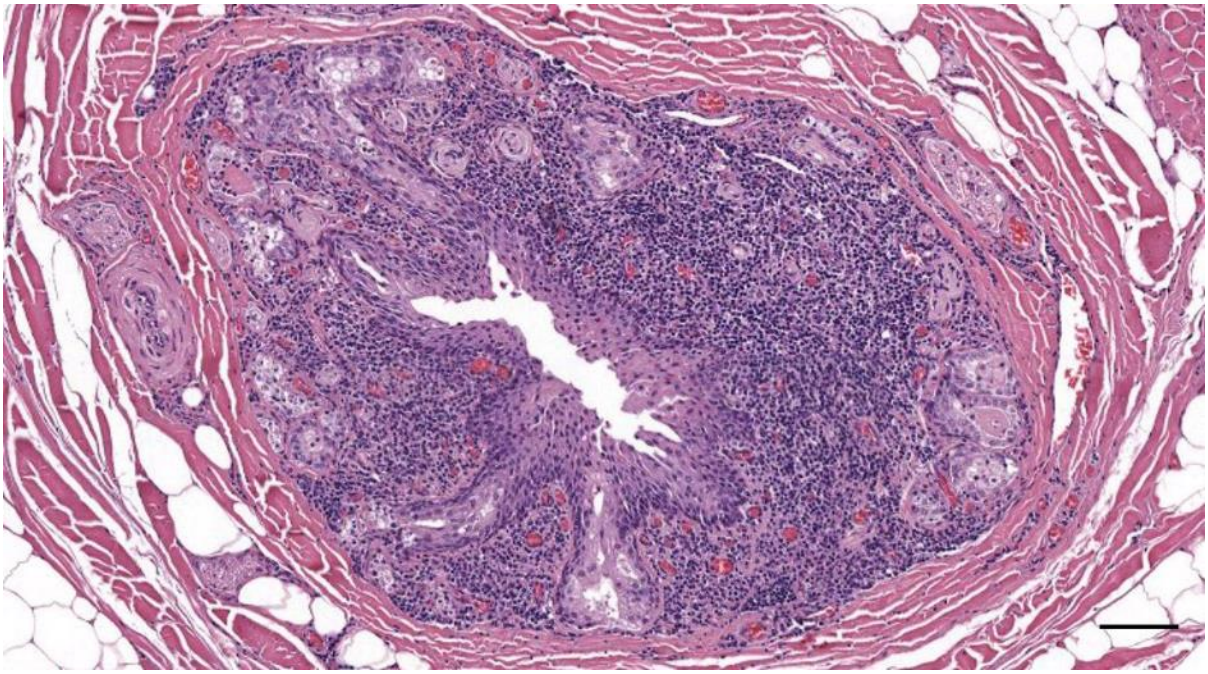

Figure 320. Histological cross-section (HE staining) of the left ear canal in a striped dolphin (293/18_L3). There is an inflammation of the ear canal and glands, with the abundant presence of mononuclear cells in the subepithelial tissue. Scale bar 100 µm

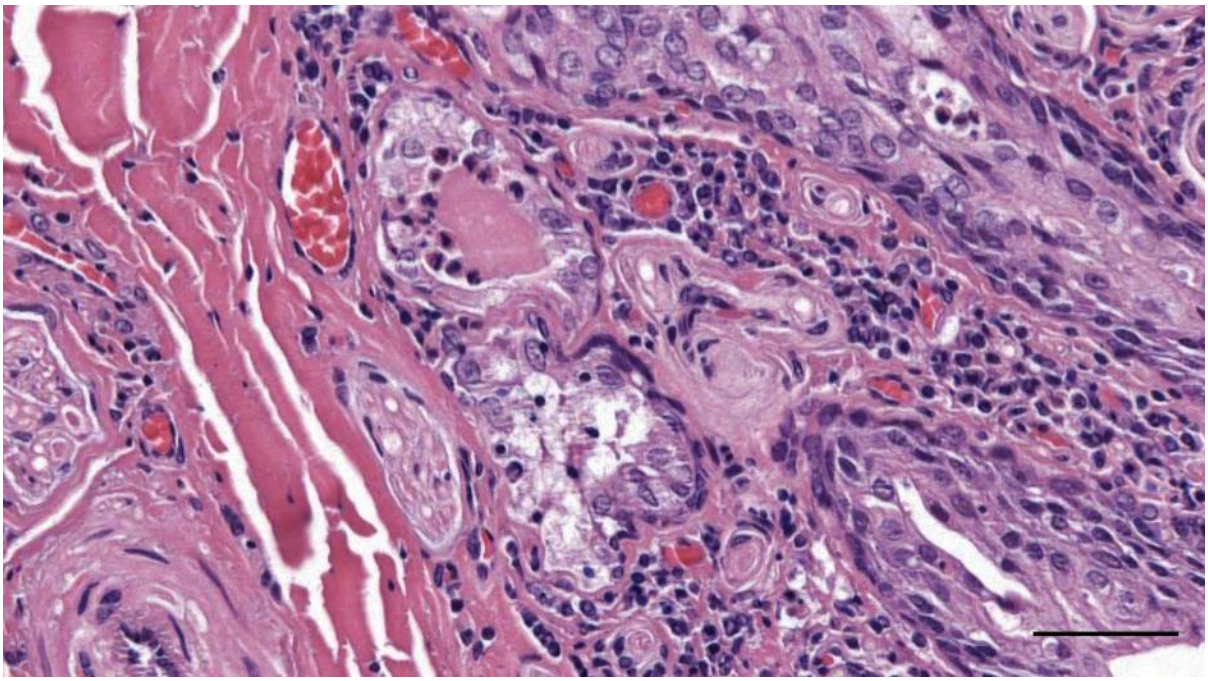

Figure 321. Detail of Figure 320 with a focus on the glandular units with normal cells, cells with pyknotic nuclei, and inflammatory cells, and a homogenous proteinaceous content. Scale bar 50 µm

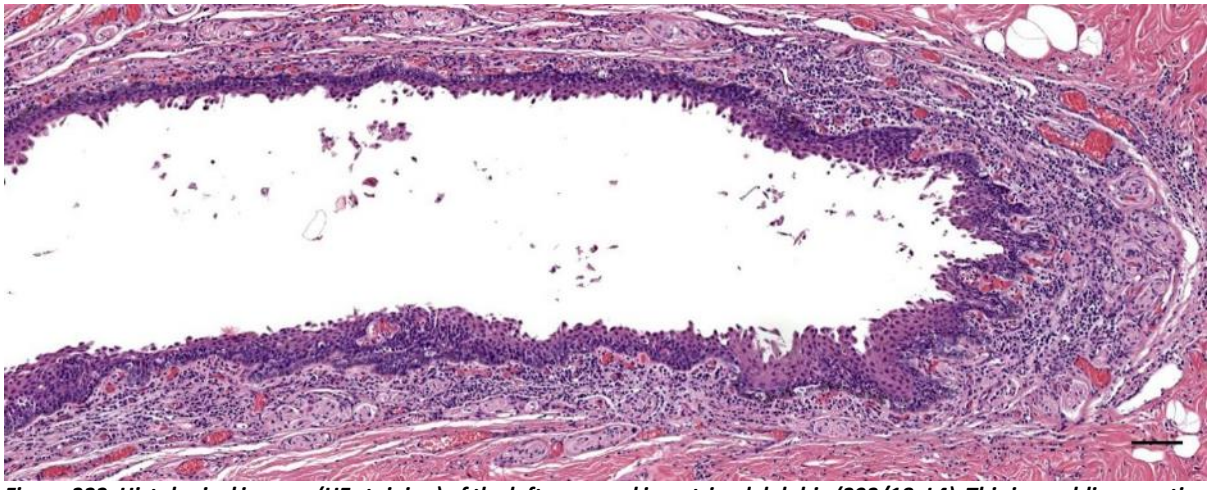

Figure 322. Histological images (HE staining) of the left ear canal in a striped dolphin (293/18_L4). This is an oblique section through the ear canal at the level of the ventral curvature, with mononuclear cells in the subepithelial tissue and abundant lamellar corpuscles and small nerves. Scale bar 100 µm

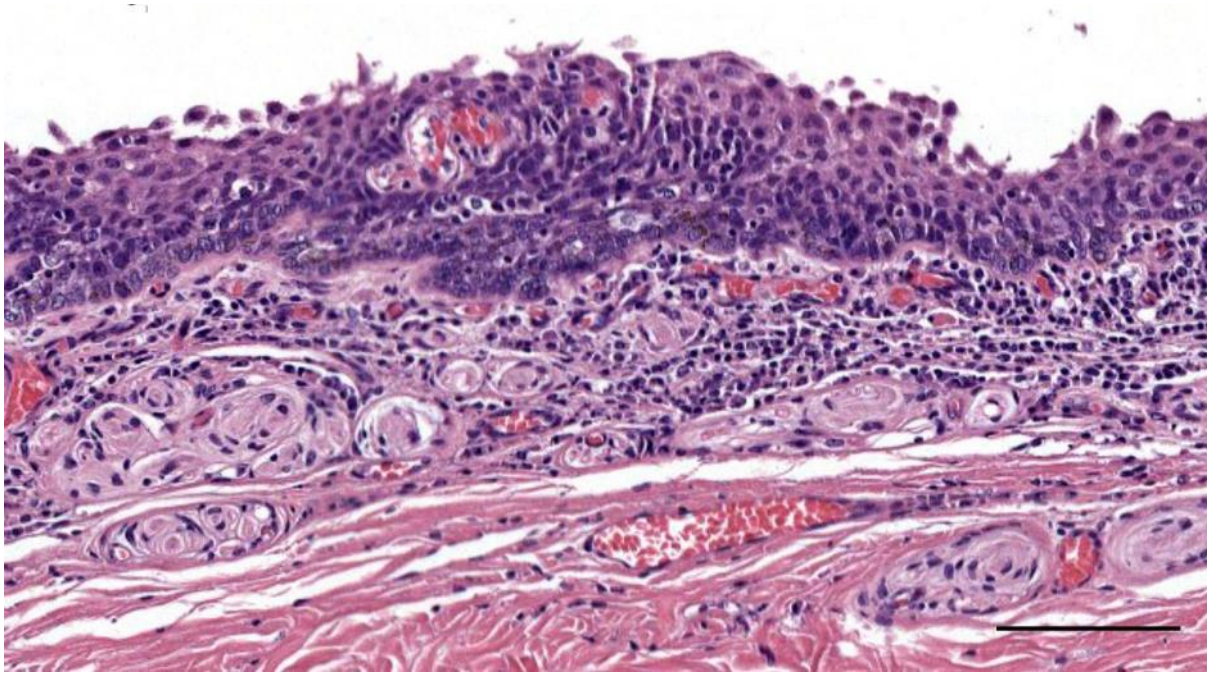

Figure 323. Detail of Figure 322, highlighting the abundant presence of corpuscles and nerves. Scale bar 100 µm

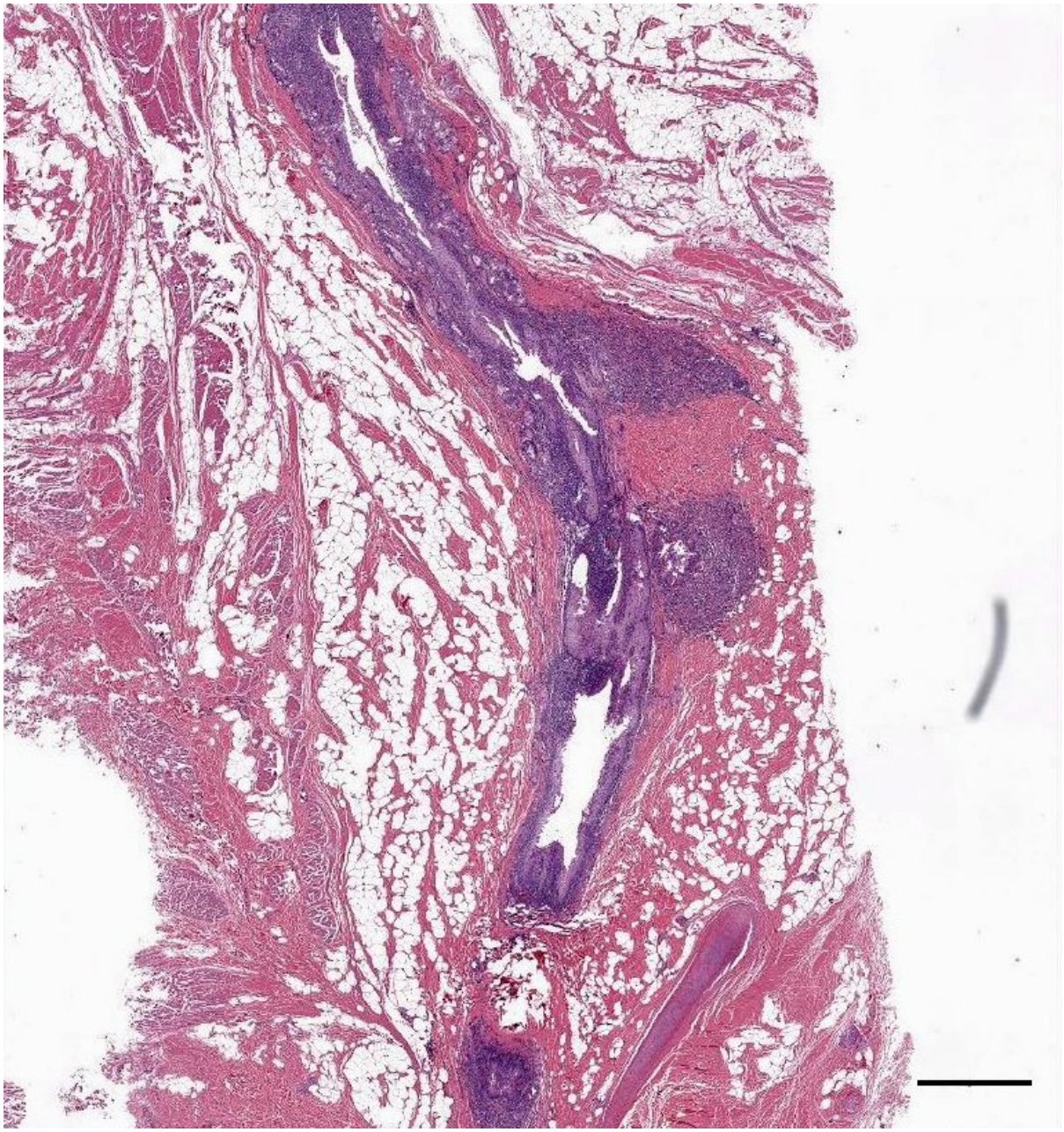

Figure 324. Longitudinal HE-stained section through the ear canal at the level of the ventral curvature (293/18_L5). Note the intense inflammation with ulceration of the epithelium. There are glandular structures with excretory ducts on both sides of the canal. Scale bar 1 mm

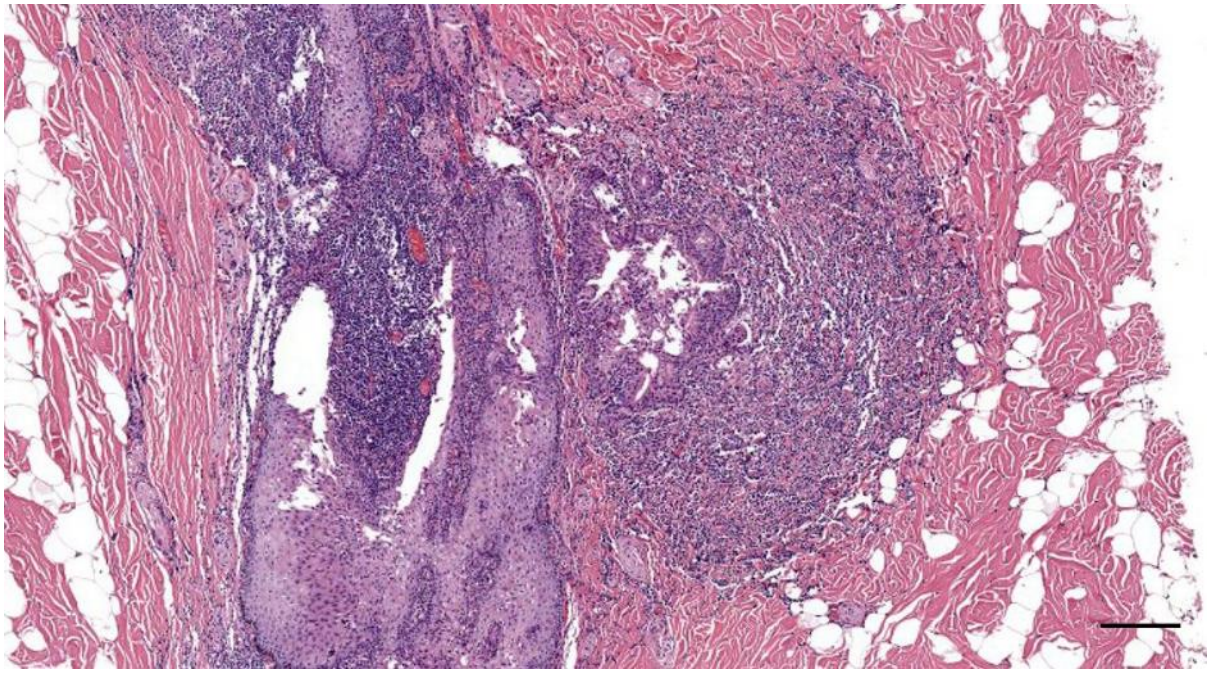

Figure 325. Detail of Figure 324. Scale bar 200 µm

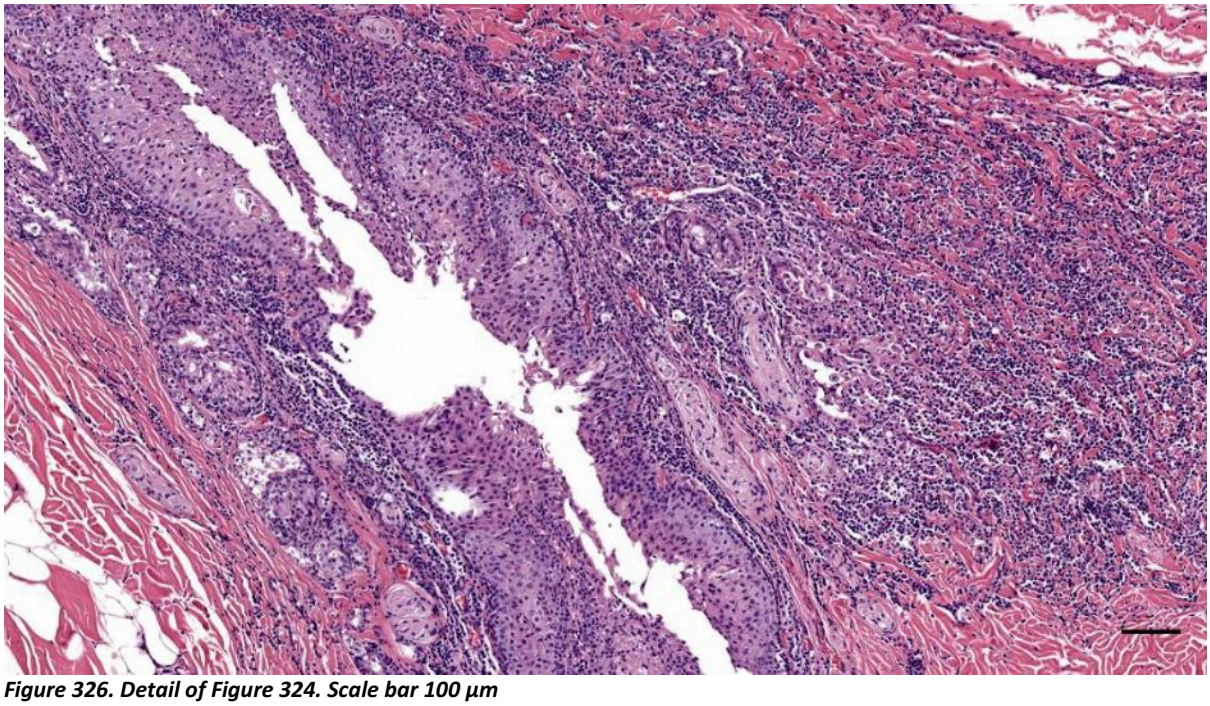

Figure 326. Detail of Figure 324. Scale bar 100 µm

1.1.2 Striped dolphin (ID2926)

There was a **purulent otitis externa** in several transverse sections of the ear canal of this individual there was the presence of desquamated epithelial cells, macrophages and neutrophils in the lumen of the canal, indicative of a purulent otitis externa. There was the presence of much cellular debris, and we noted many necrotic changes. The surrounding tissue did not show obvious signs of inflammation except for a slight leucocytosis associated with the larger blood vessels.

Two different gram stains were carried out (See Annex for protocols), both of which stained Gram + and Gram – bacteria. No bacteria were detected with certainty. Many coccoid elements were present

that could be consistent with bacteria, often clustered in packs or rows. There were also similar elements that varied in size and shape and were often refringent, consistent with degeneration of the nucleus of the present cells, or which were part of the nucleus of mature/degenerated neutrophils. There were also unidentified structures that could likely be attributed to sloughed epithelial keratinocytes without a nucleus, or parasitic infection. No eosinophilic cells could be identified in neither the HE nor Gram stain, therefore favouring the former possibility of epithelial content. To get an absolute identification of these structures, two more HE sections at 25 and 50 µm medial to the first section to check if the same structures were present over such a distance, and also a PAS[1] (Figure 331) and a pan-cytokeratin IHC stain (Figure 332), situated between the two, were carried out to distinguish parasites from epithelial structures. None of these techniques showed any other structures apart from epithelial and inflammatory cells.

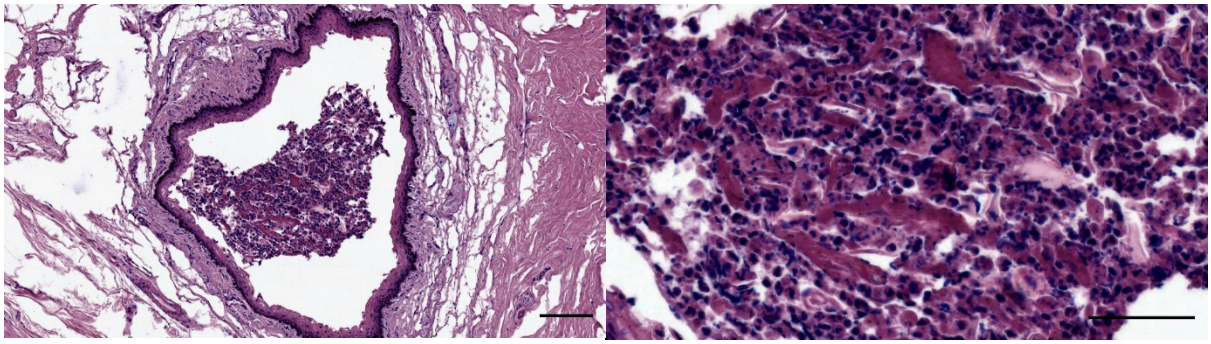

Figure 327. Histological images (Gram staining) of a transverse section through the ear canal of a striped dolphin (ID2926) with the presence of inflammatory cells such as macrophages, neutrophils and also desquamated epithelial cells within the lumen of the canal. Scale bars: left 100 µm, right 50 µm

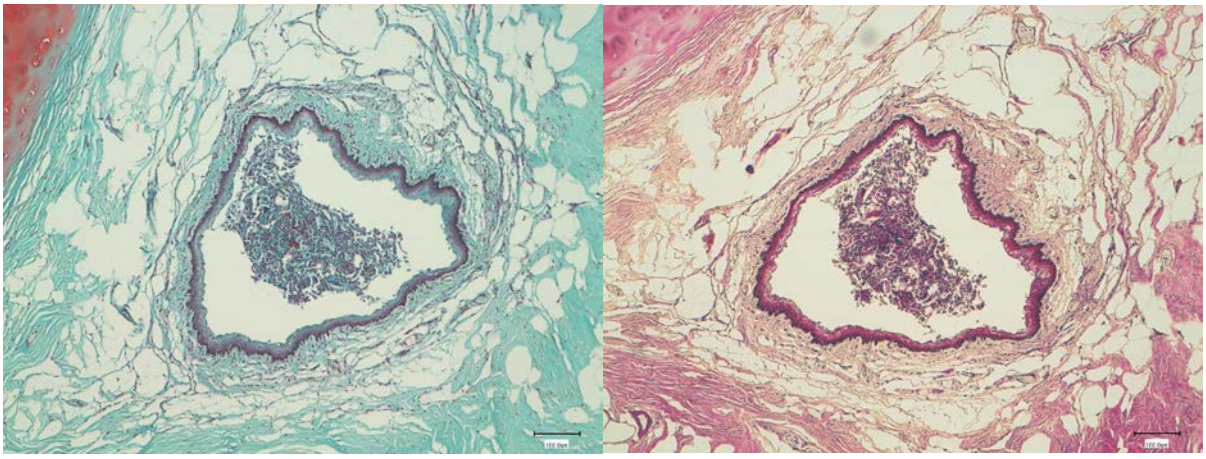

Figure 328. Histological images of a transverse section through the ear canal of a striped dolphin (ID2926) stained with Gram 1 and 2, left and right respectively. Scale bars 100 µm

[1] The PAS (Periodic Acid Schiff) stain stains carbohydrate macromolecules in the basement membrane, glycogen, mucopolysaccharides and some mucins, and can be used for the detection of parasites. PAS (Periodic Acid-Schiff). PathologyOutlines.com website. http://www.pathologyoutlines.com/topic/stainspas.html. Accessed April 19th, 2018.

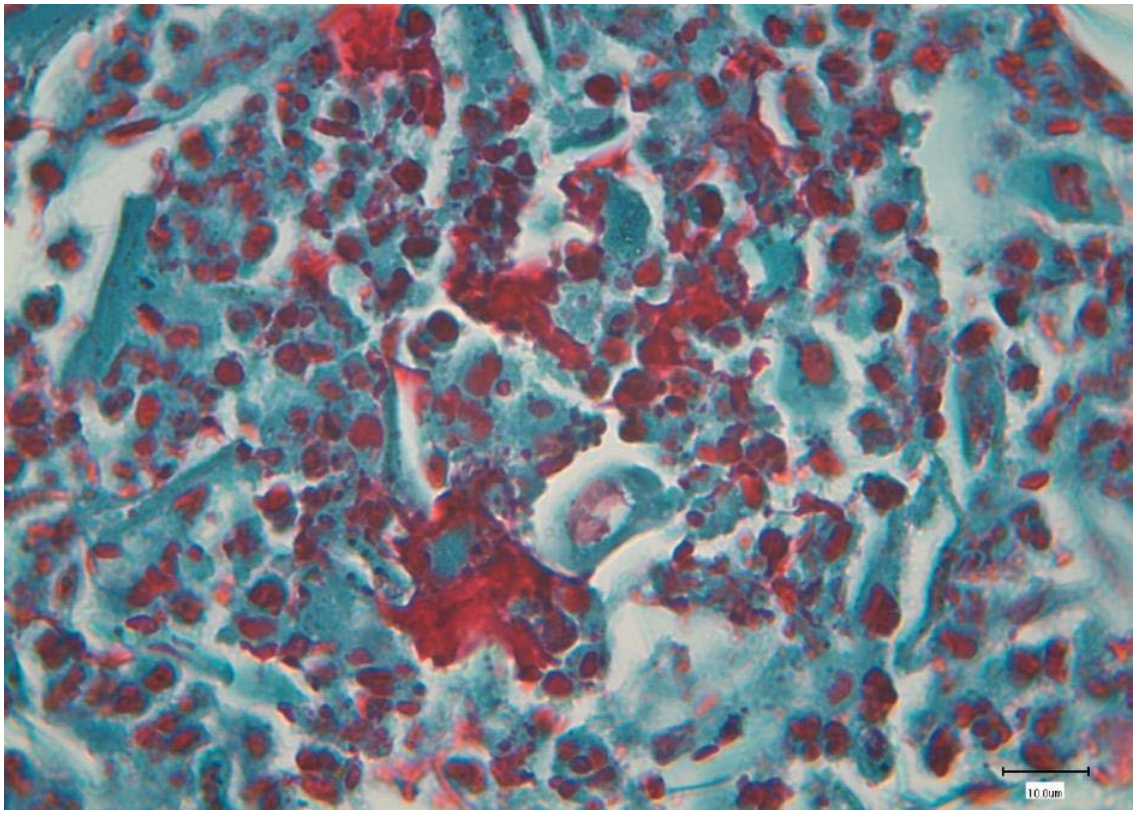

Figure 329. Histological detail of ear canal content stained with 'Gram 1'. Note the coccoid structures, epithelial cells with or without nucleus, neutrophils, and macrophages. Scale bar 10 µm

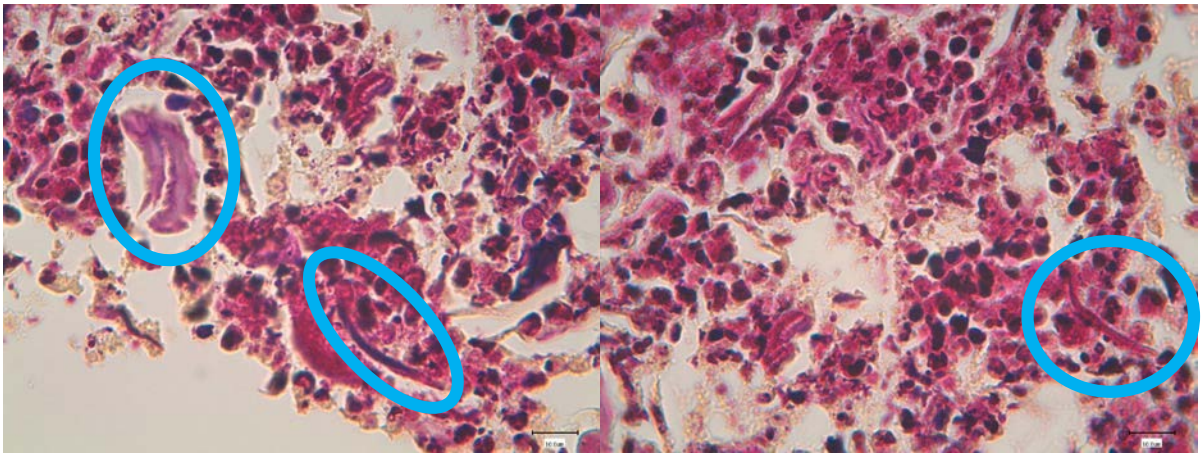

Figure 330. Detail of Gram 2 stain. The blue circles indicate parasite or more likely a sloughed epithelial cell. Scale bars 10 µm

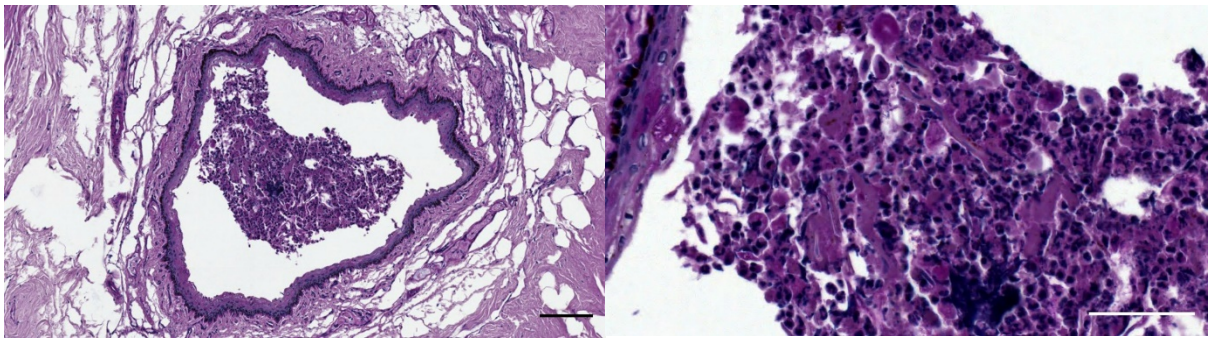

Figure 331. Histological images of a transverse section through the ear canal of a striped dolphin (ID2926), PAS stain. Scale bar 100 and 50 µm

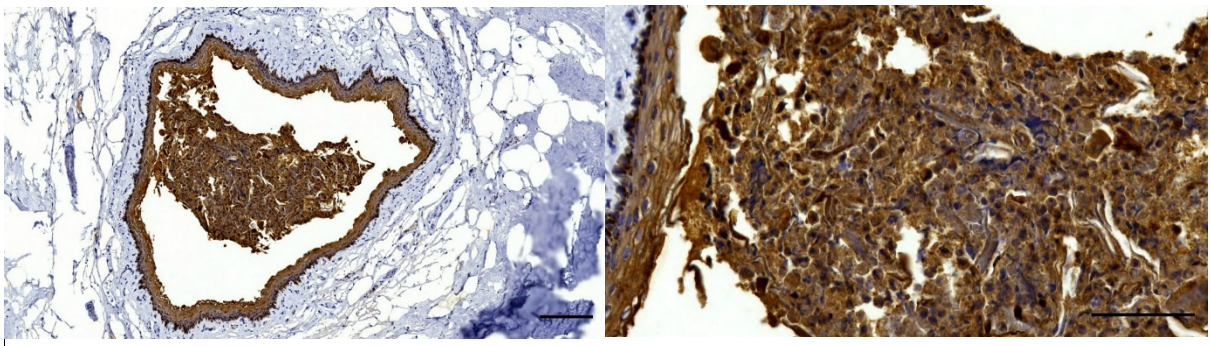

Figure 332. Histological images of a transverse section through the ear canal of a striped dolphin (ID2926), anti-pan-cytokeratin IHC stain. Scale bar 100 µm

1.1.3 Striped dolphin (ID488/17)

Purulent otitis externa: A striped dolphin with inflammatory cells (lymphocytes, neutrophils) inside the ear canal lumen. We did not note any inflammation in the surrounding tissue, but this was possibly missed as it could have been present in more proximal tissue, which was not at our disposal.

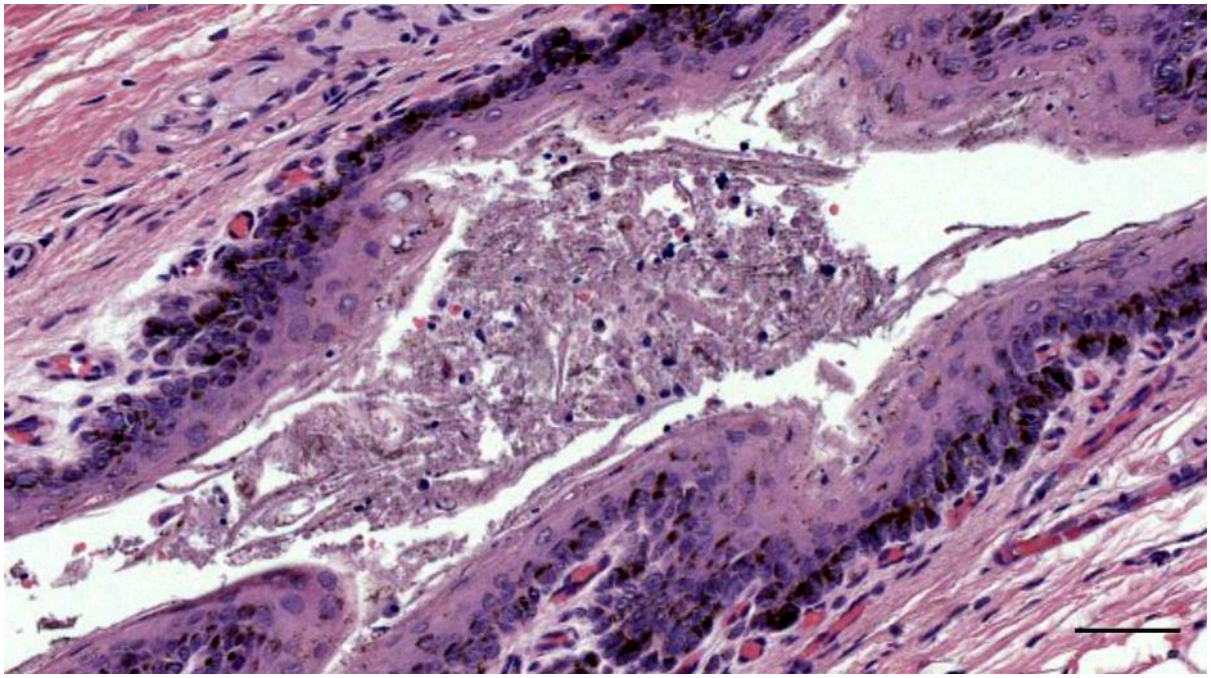

Figure 333. Histological detail (HE staining) of the ear canal content in a striped dolphin (488/17_L8) Purulent otitis: Inflammatory cells (lymphocytes, neutrophils), and cells with pyknotic nuclei (possible glandular cells), together with epithelial sloughs in the ear canal lumen. Scale bar 50 µm

1.1.4 Bottlenose dolphin (ID444)

There was a **bilateral inflammation of the external ear canal**, both at the level of the glands (L5-8, R5-7)(Figure 421, Figure 344, Figure 353) and in deep sections where there was cartilage. The inflammation consisted of activation of the resident ECALT with the presence of a mixed cell inflammatory reaction in the subepithelial tissue at two locations. In one location, there was an interruption of the basal membrane with the presence of melanocytes in the propria, together with

apoptotic changes in the epithelium (Figure 343). This animal also presented a multifocal mixed inflammatory reaction in the middle ear corpus cavernosum

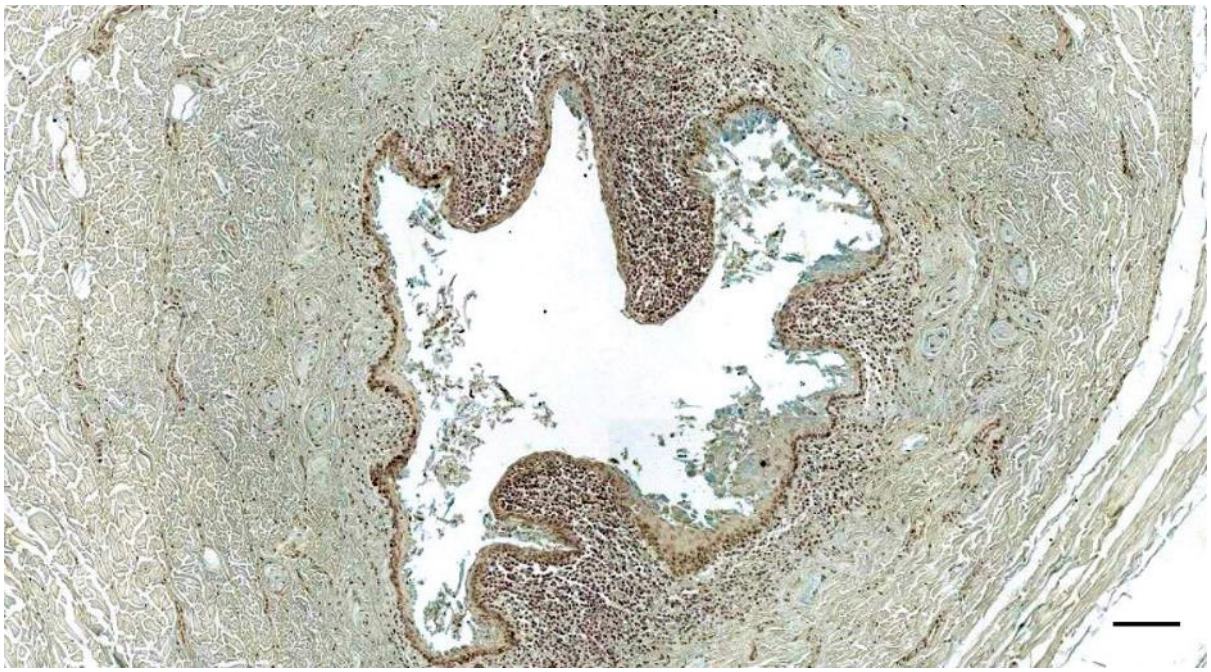

Figure 334. Histological cross-section (Alcian blue staining) of the right ear canal of a bottlenose dolphin, at about 2 cm beneath the skin (ID444_R5). Note the inflammation. Scale bar 100 µm

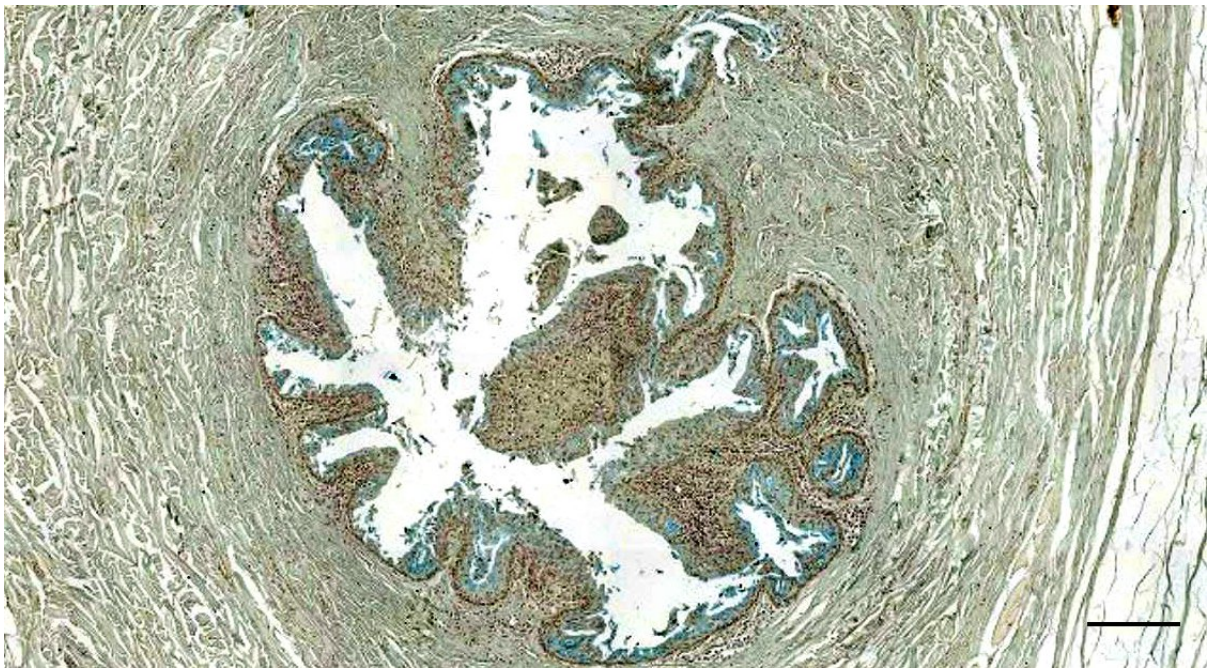

Figure 335. (444_R6) Alcian blue. Glands and inflammation (Scale bar 200 µm)

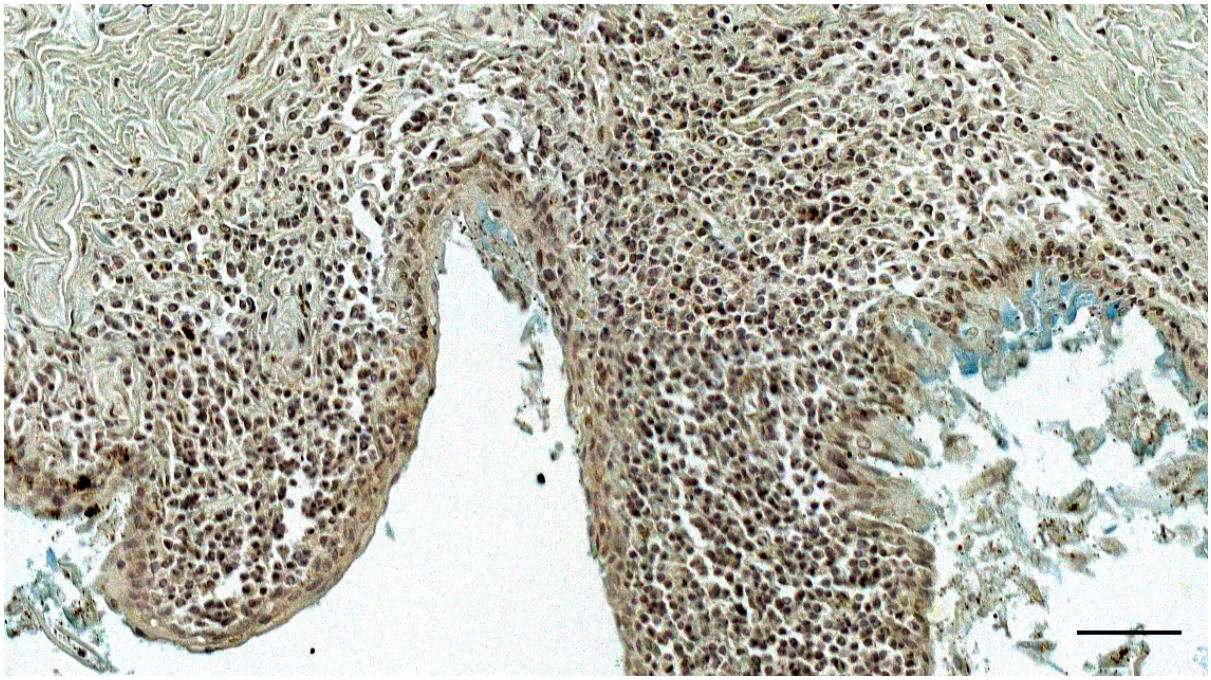

Figure 336. Detail of Figure 334 (Alcian blue stain). Note the subepithelial abundant presence of mononuclear cells, and the abrasive epithelium of the ear canal, showing a blue staining. Scale bar 50 µm

In some cases, such as in this bottlenose dolphin, it was not clear whether their was an activation of the resident ECALT. For instance, there was an infiltration of **mononuclear cells** (lymphocytes, plasma cells, and few macrophages and neutrophils) in the subepithelial tissue, at the level of the glands but also medial to the glands, and focally concentrated in association with the excretory ducts (e.g. Figure 337, Figure 338), which included subjectively too many cells to be a normal finding.

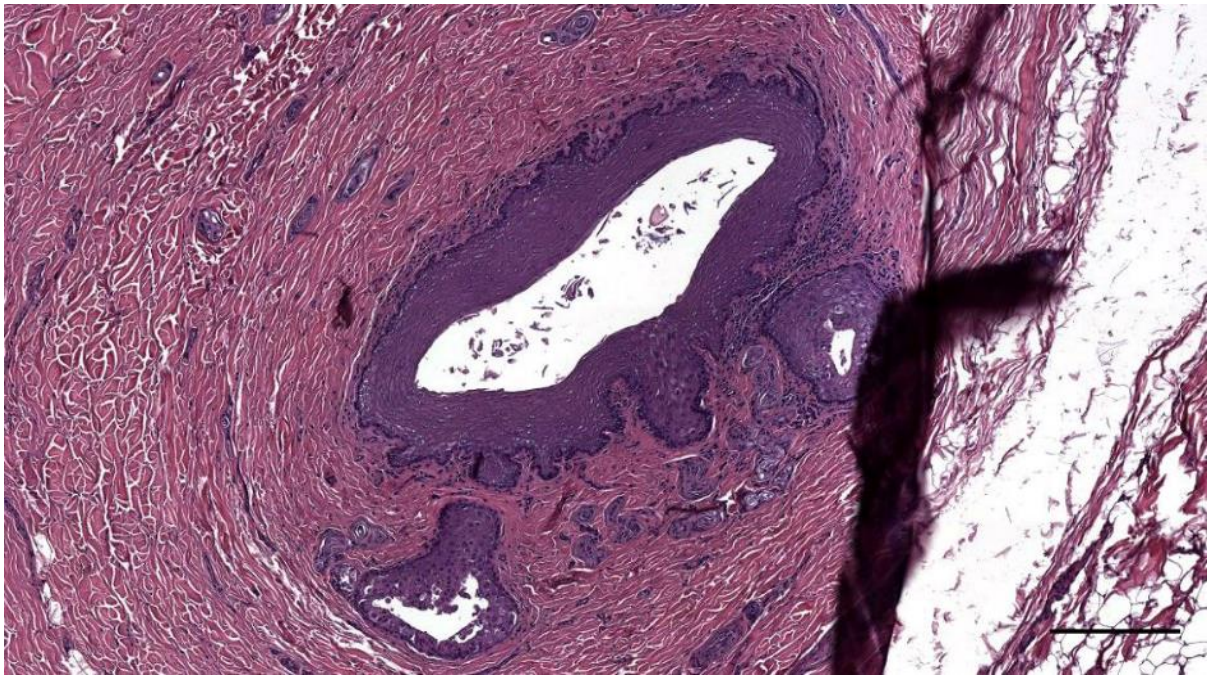

Figure 337. (457_R6) Ear canal with glandular excretory ducts, and mononuclear infiltration. Scale bar 250 µm

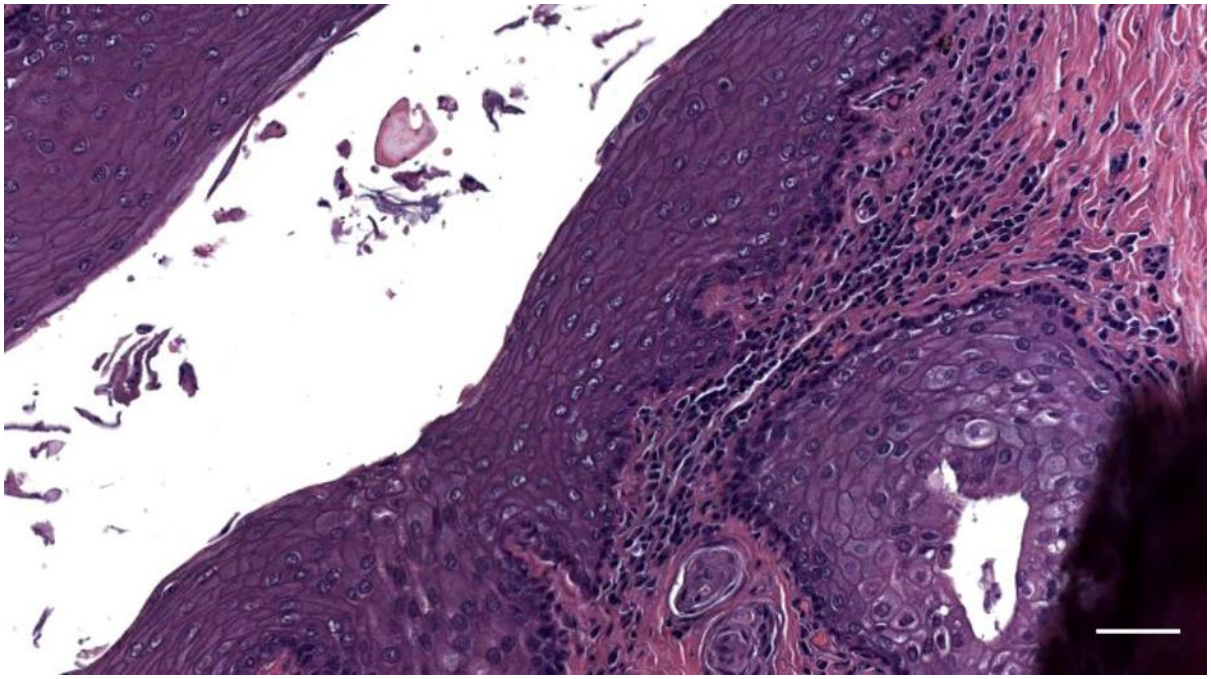

Figure 338. (457_R6) Ear canal with glandular excretory ducts, and mononuclear infiltration in a bottlenose dolphin. Scale bar 50 µm

1.1.4.1 other findings

Left side

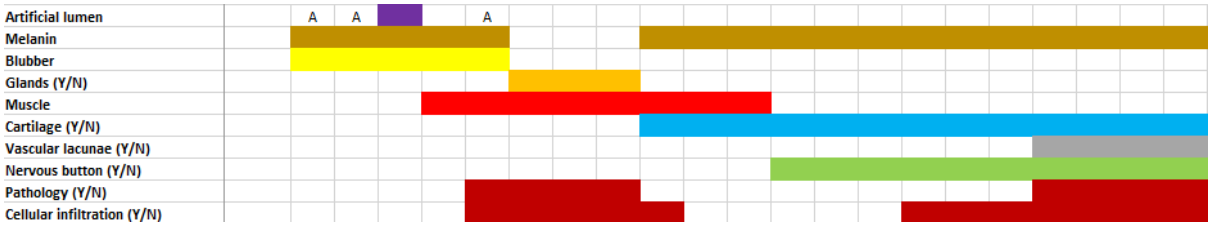

Right side

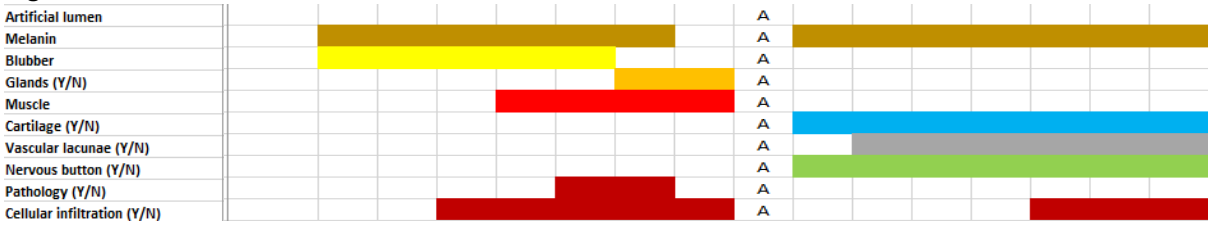

The ear canal epithelium presented an apparent transition from squamous (L4) to single columnar or pseudostratified (likely glandular)(L5-8)(Figure 339, Figure 340, Figure 341, Figure 342, Figure 356, Figure 357, Figure 358, Figure 359, Figure 360) to squamous (Figure 347, Figure 348, Figure 349). There were also glandular structures separate from the ear canal (Figure 345, Figure 346, Figure 354, Figure 355, Figure 335), with pyknotic nuclei and eosinophilic cytoplasm (Figure 355).

The Alcian blue showed a positive reaction in the glandular structures, while the squamous epithelium of ear canal in bottlenose dolphin stained negative, also in sections where we noted a change in epithelium from squamous to single columnar or pseudostratified (possibly glandular). The situation in common dolphin and bottlenose dolphin was very similar in that the distinction between ear canal

and glands, or squamous epithelium and glandular epithelium was not fully clear. (Figure 352, Figure 334, Figure 335)

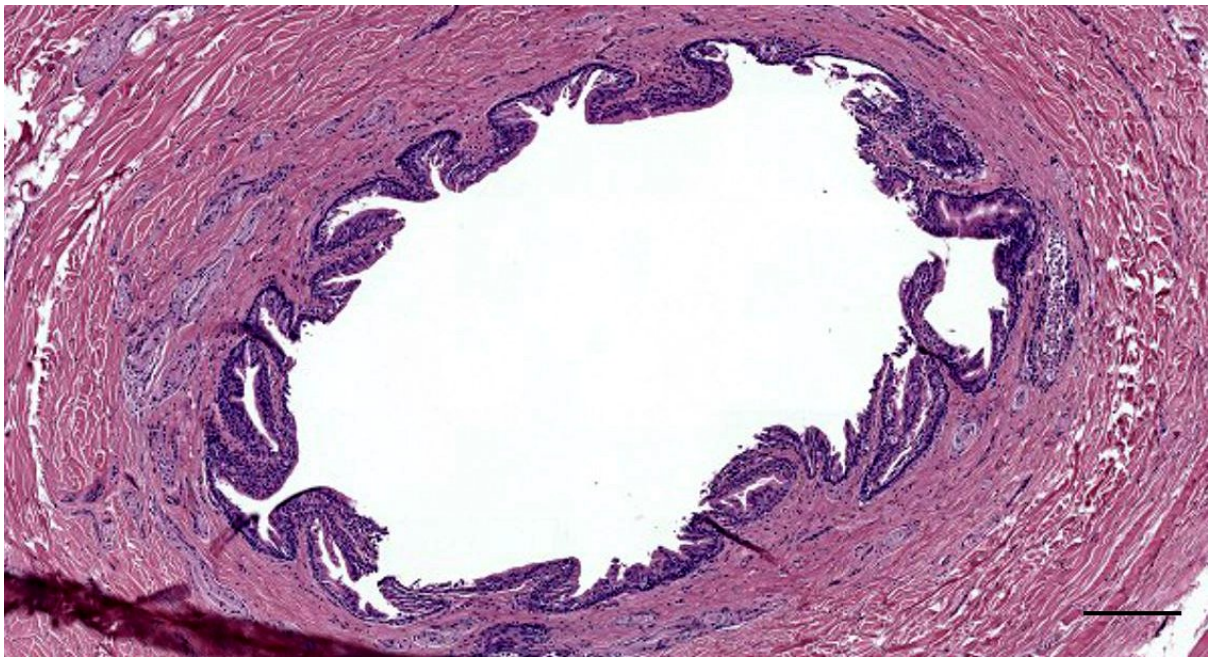

Figure 339. Histological image (HE staining)(444_L6) Ear canal and glands/glandular epithelium in a bottlenose dolphin (Scale bar 200 µm)

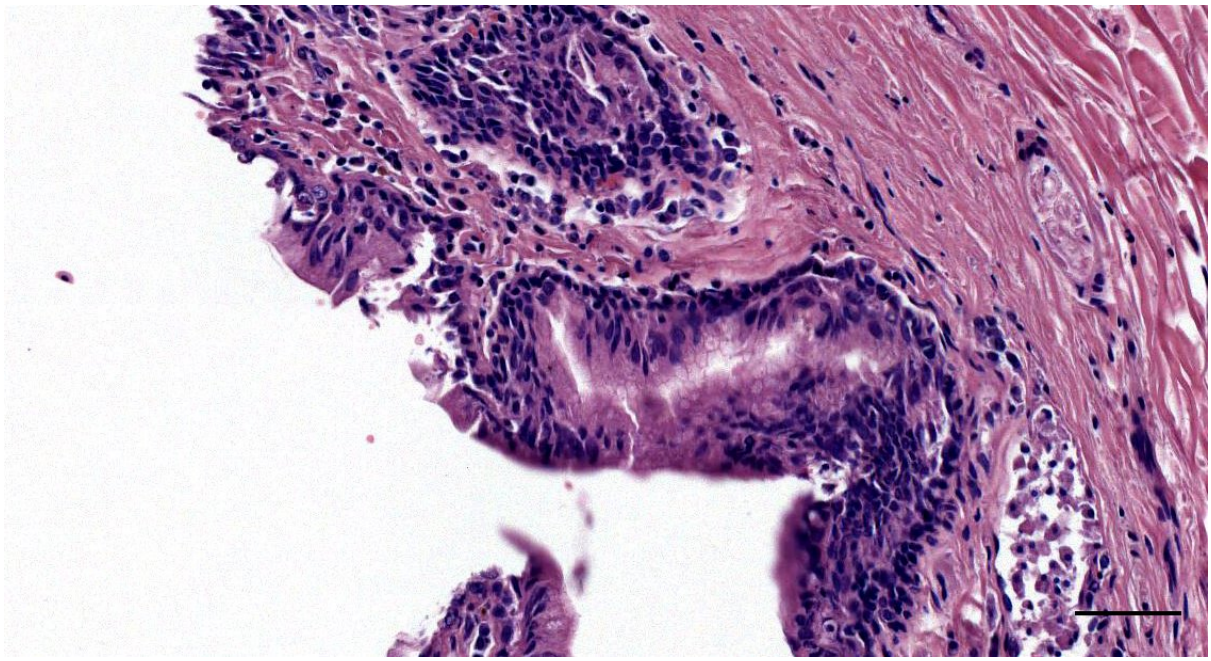

Figure 340. Histological image (HE staining) (444_L6) Ear canal and glands/glandular epithelium in a bottlenose dolphin (Scale bar 50 µm)

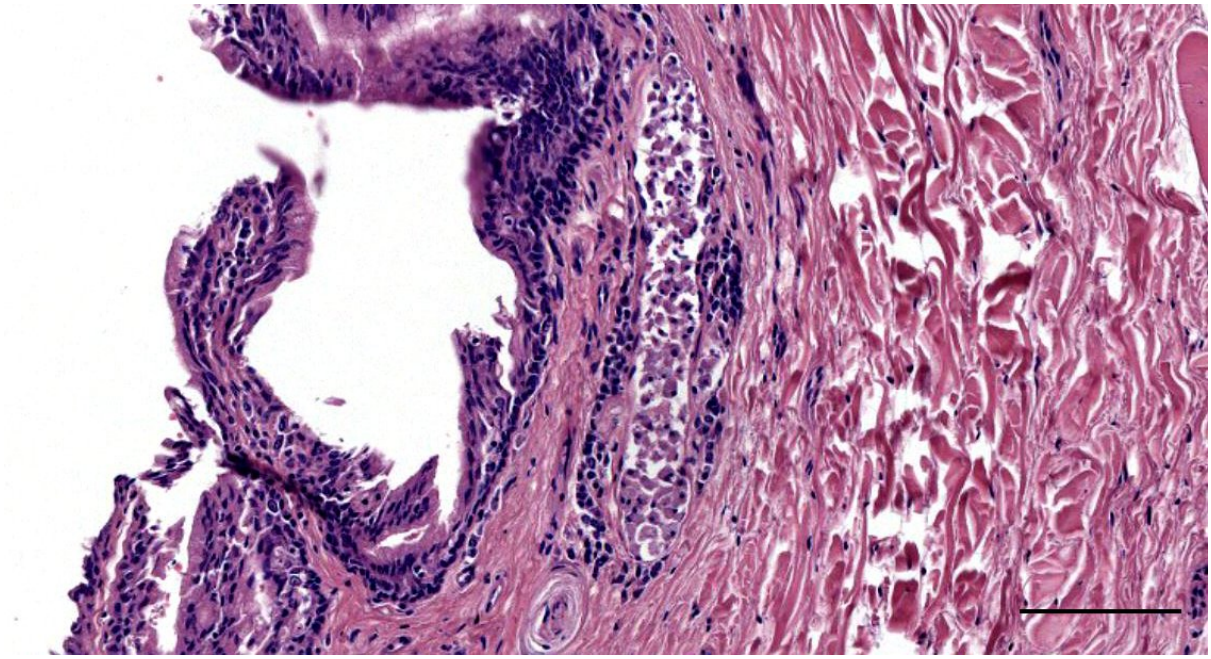

Figure 341. Histological image (HE staining) (444_L6) Ear canal and glands/glandular epithelium in a bottlenose dolphin (Scale bar 100 µm)

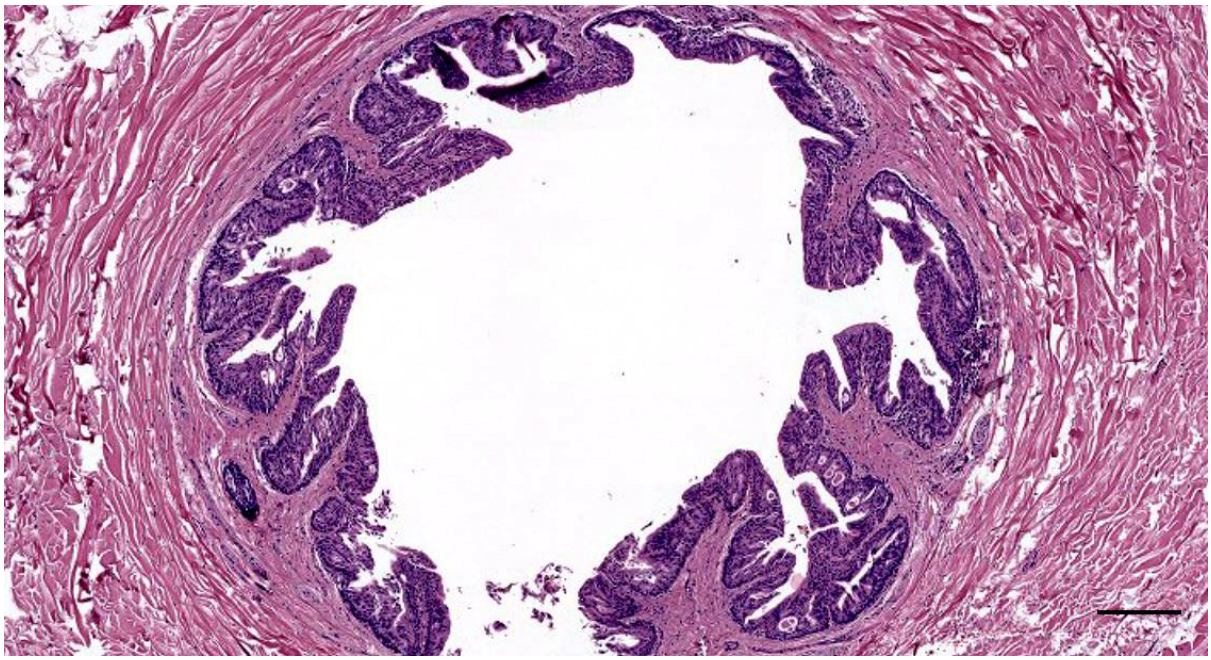

Figure 342. Histological image (HE staining) (444_L7) Ear canal and glands/glandular epithelium in a bottlenose dolphin (Scale bar 200 µm)

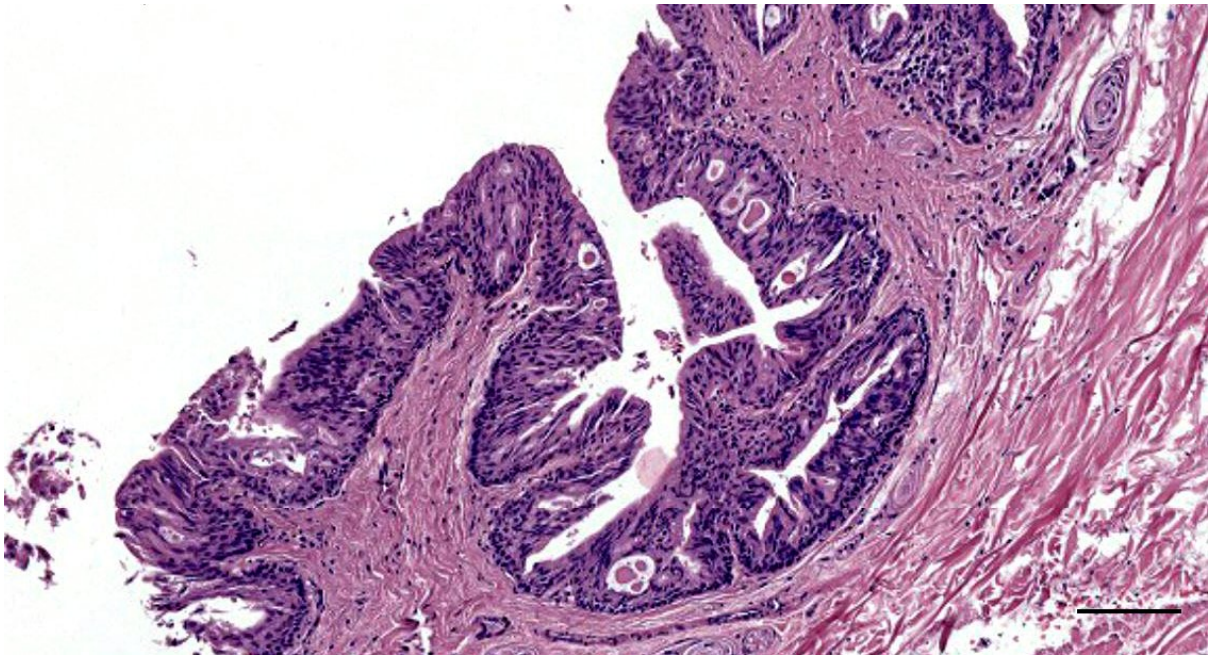

Figure 343. Histological image (HE staining) (444_L7) Ear canal and glands in a bottlenose dolphin. Note the apoptotic changes in the glandular epithelium (Scale bar 100 µm)

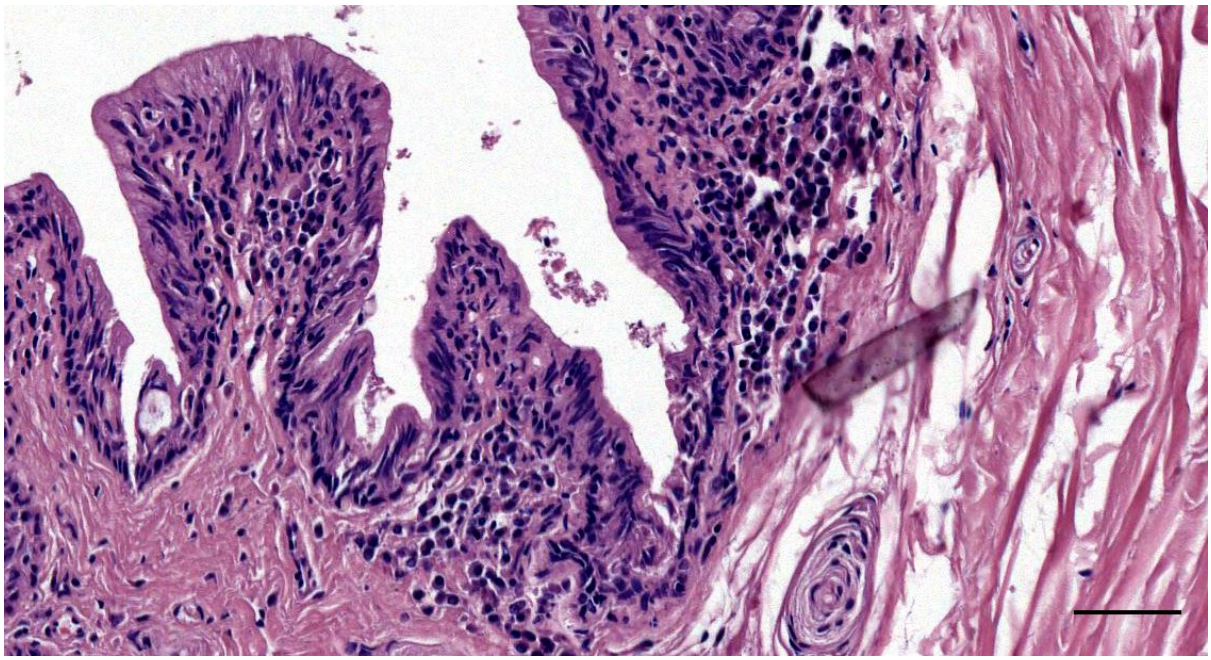

Figure 344. Histological image (HE staining) (444_L7) Ear canal and glands in a bottlenose dolphin. Note the mononuclear infiltrate in the superficial propria (Scale bar 100 µm)

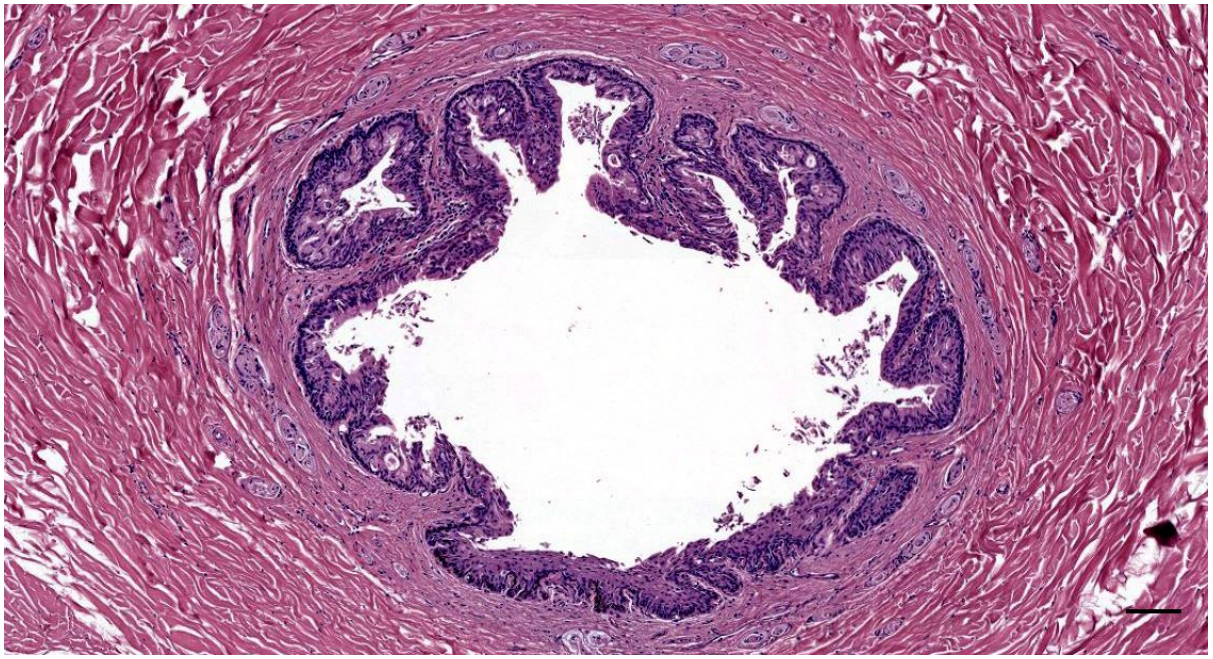

Figure 345. Histological image (HE staining) (444_L8) Ear canal and gland in a bottlenose dolphin (Scale bar 100 µm)

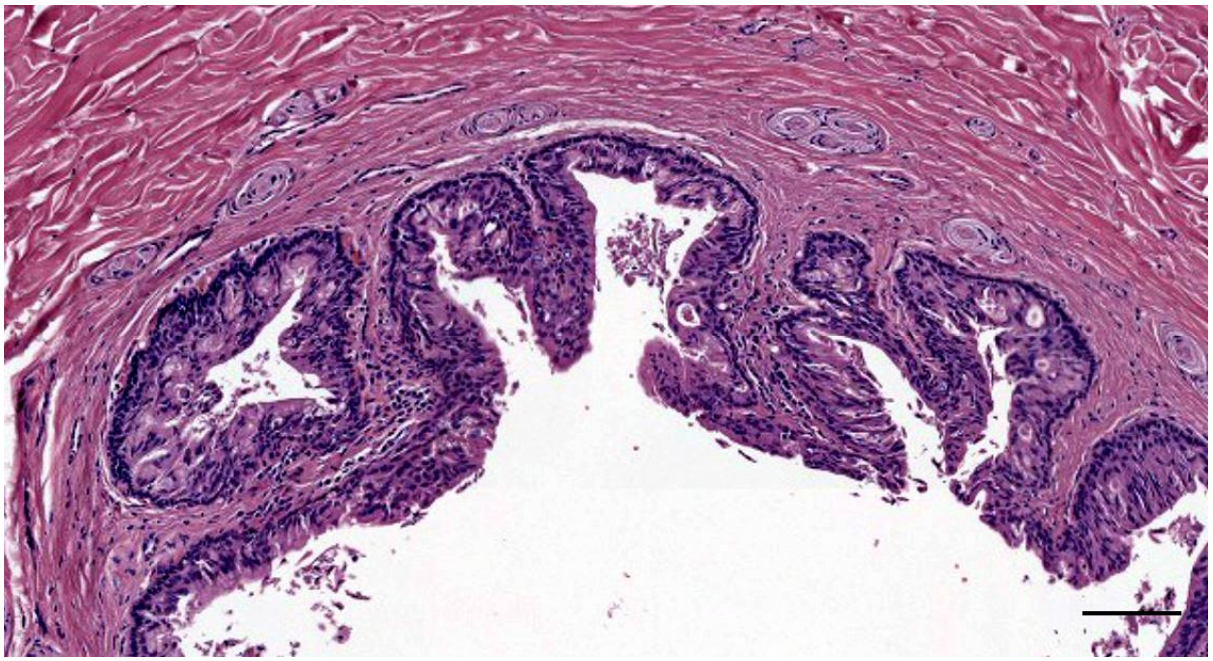

Figure 346. Histological image (HE staining) (444_L8) Ear canal and glands, note the lamellar corpuscles and the lymphocytic infiltrate in the superficial lamina propria, in a bottlenose dolphin (Scale bar 100 µm)

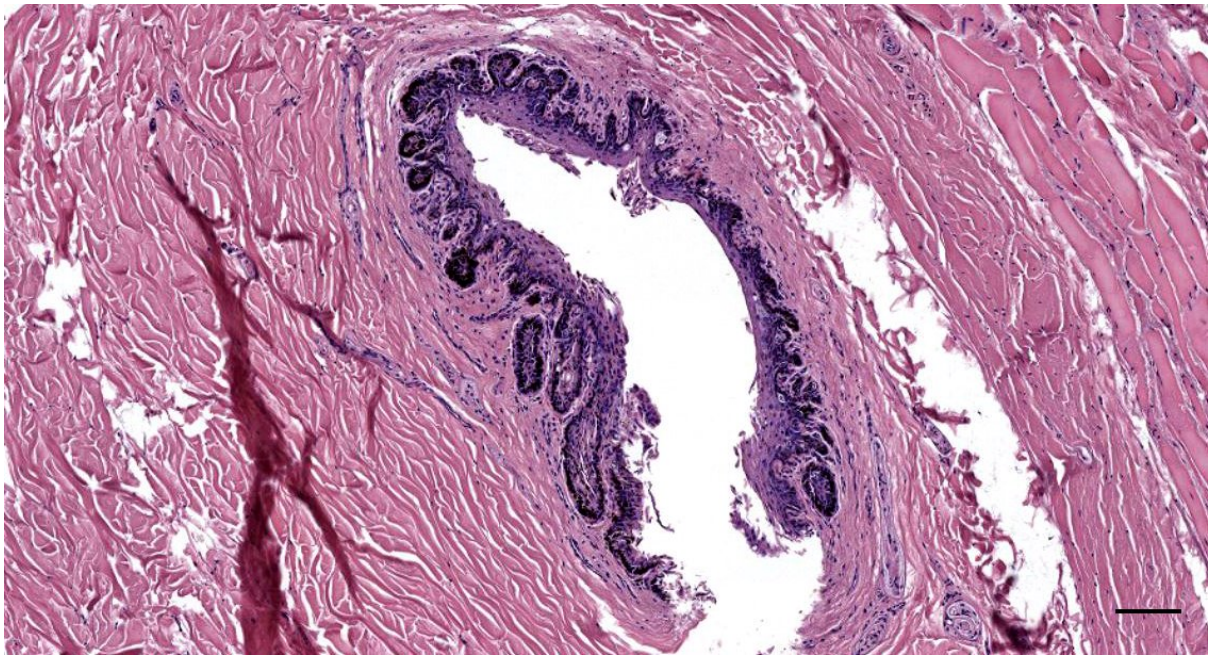

Figure 347. Histological image (HE staining) (444_L9) Ear canal with squamous epithelium in a bottlenose dolphin (Scale bar 100 µm)

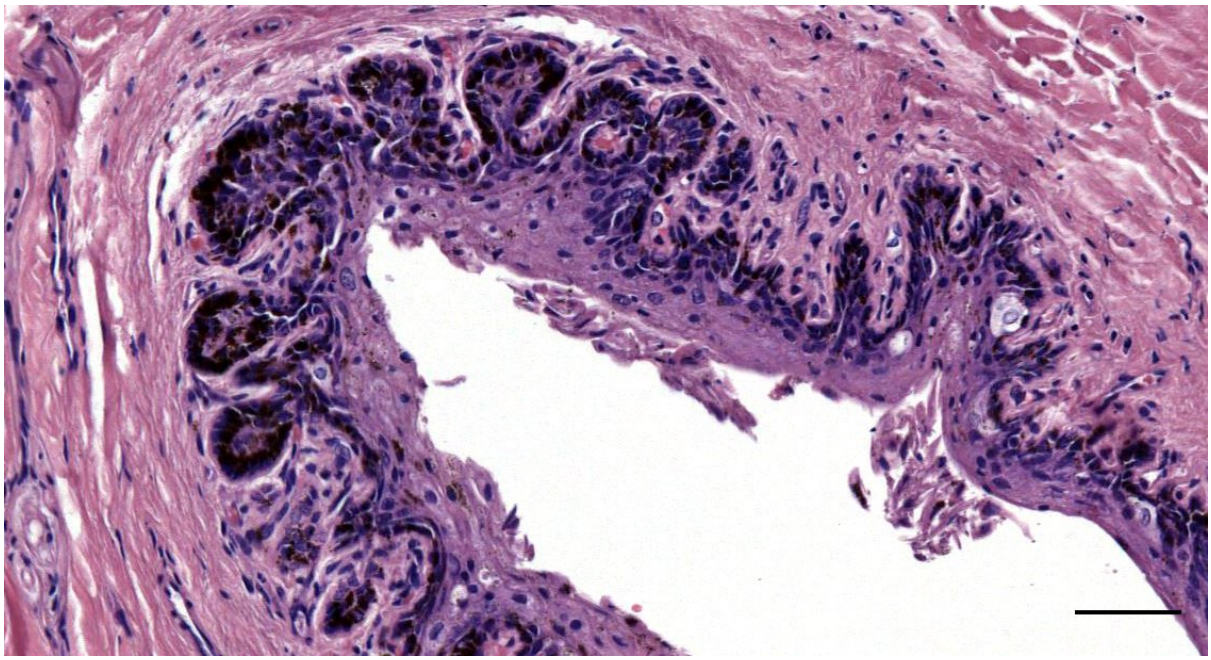

Figure 348. Histological image (HE staining) (444_L9) Ear canal with squamous epithelium in a bottlenose dolphin (Scale bar 50 µm)

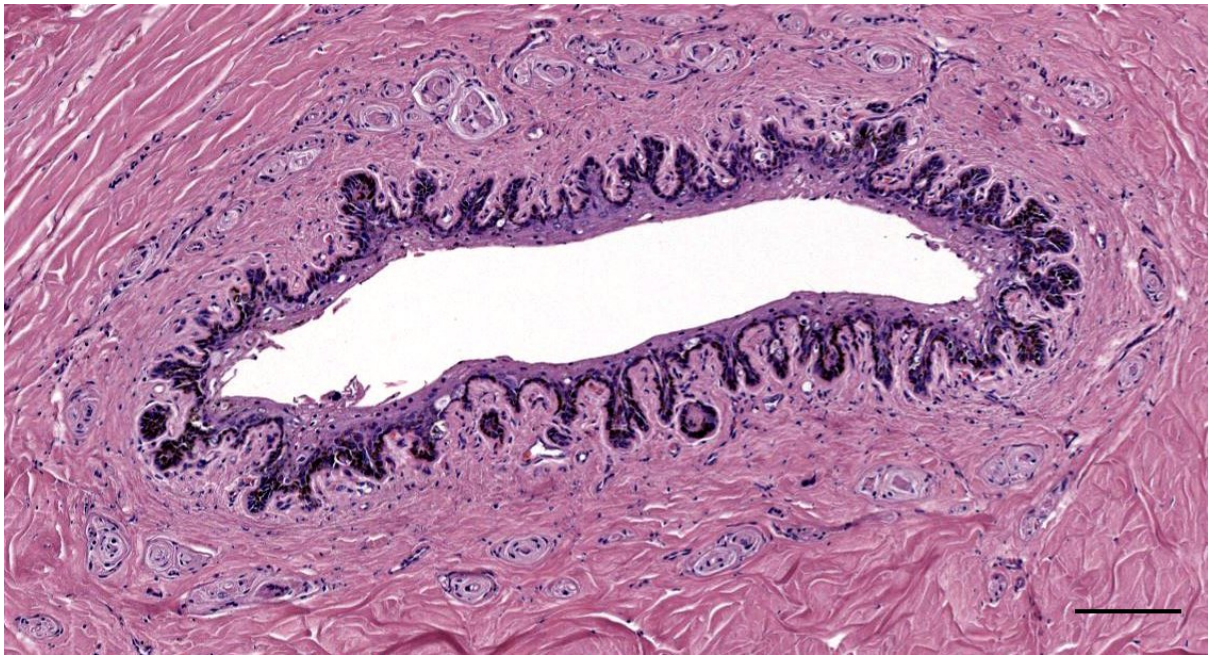

Figure 349. Histological image (HE staining) (444_L10) Ear canal in a bottlenose dolphin (Scale bar 100 µm)

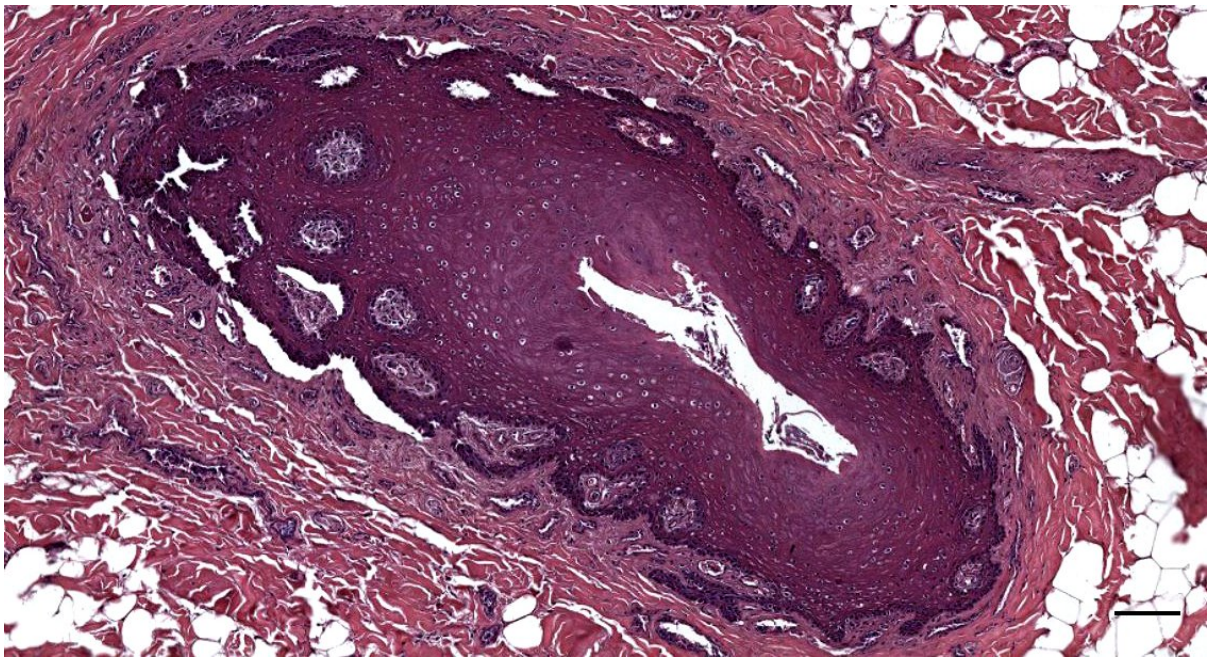

Figure 350. Histological image (HE staining) (444_R1) Ear canal at the level of the porus acusticus externus in a bottlenose dolphin (Scale bar 100 µm)

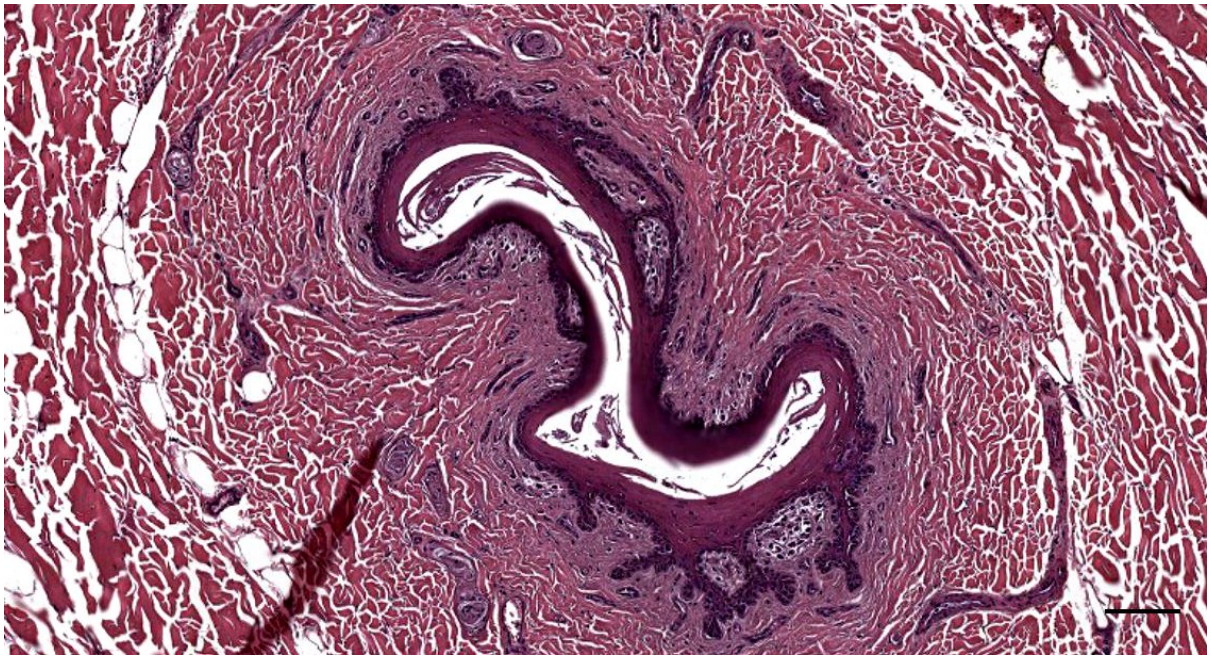

Figure 351. Histological image (HE staining) (444_R3) Ear canal in a bottlenose dolphin (Scale bar 100 µm)

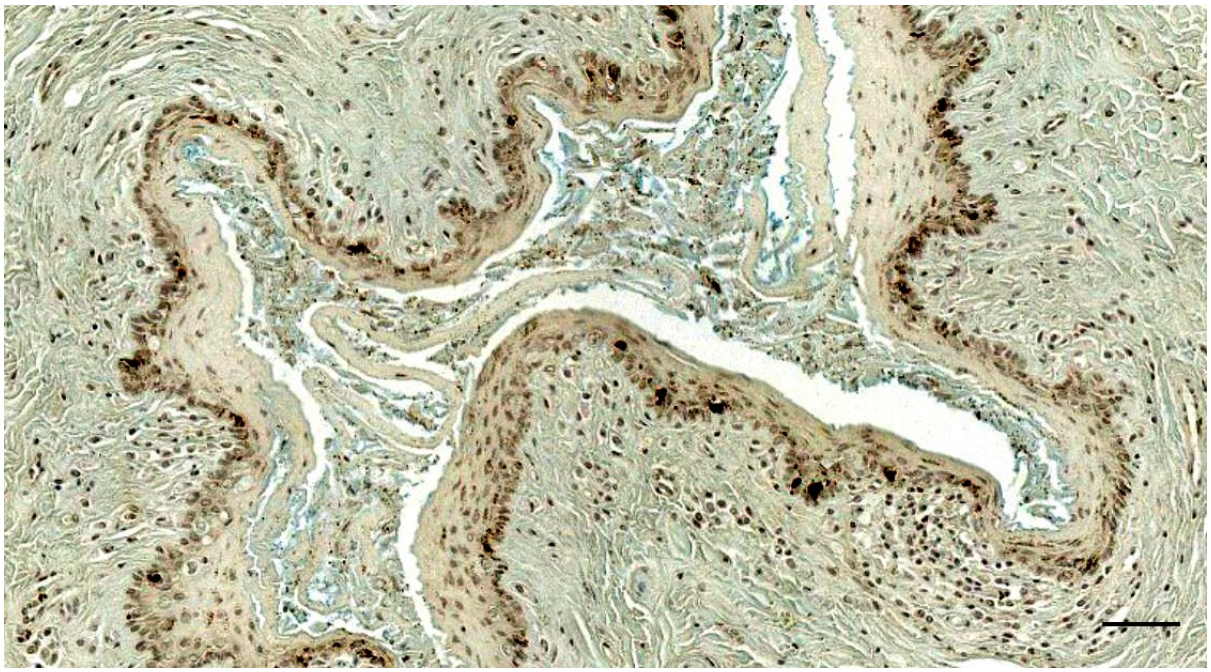

Figure 352. Histological image (444_R4)(Alcian blue) of the ear canal and content in a bottlenose dolphin. (Scale bar 50 µm)

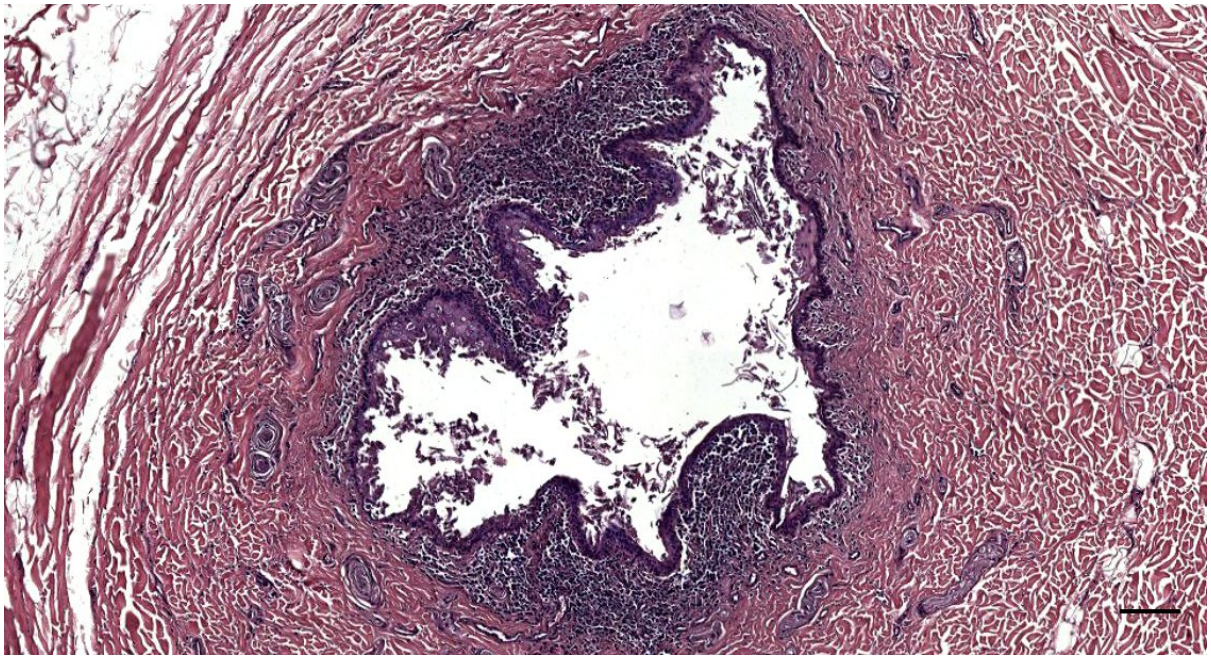

Figure 353.Histologicalcross-section (HE staining) (444_R5) of aar canal inflammation in a bottlenose dolphin (Scale bar 100 µm)

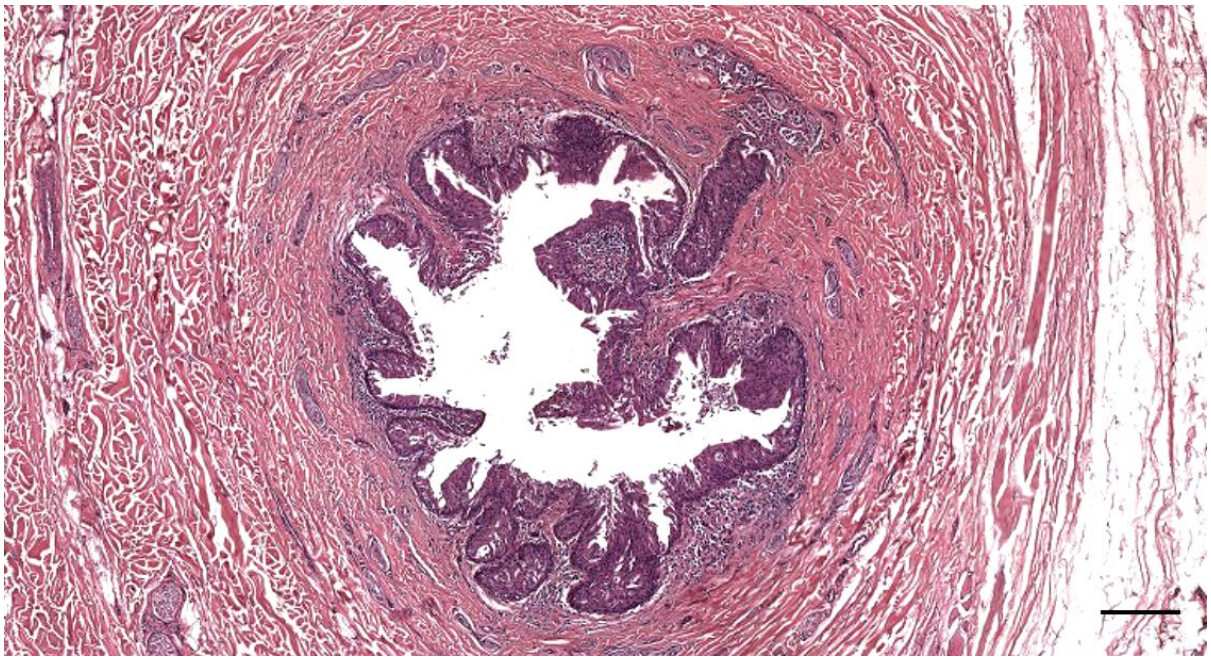

Figure 354. Histologicalcross-section (HE staining) (444_R6)of the ear canal and glands in a bottlenose dolphin (Scale bar 200 µm)

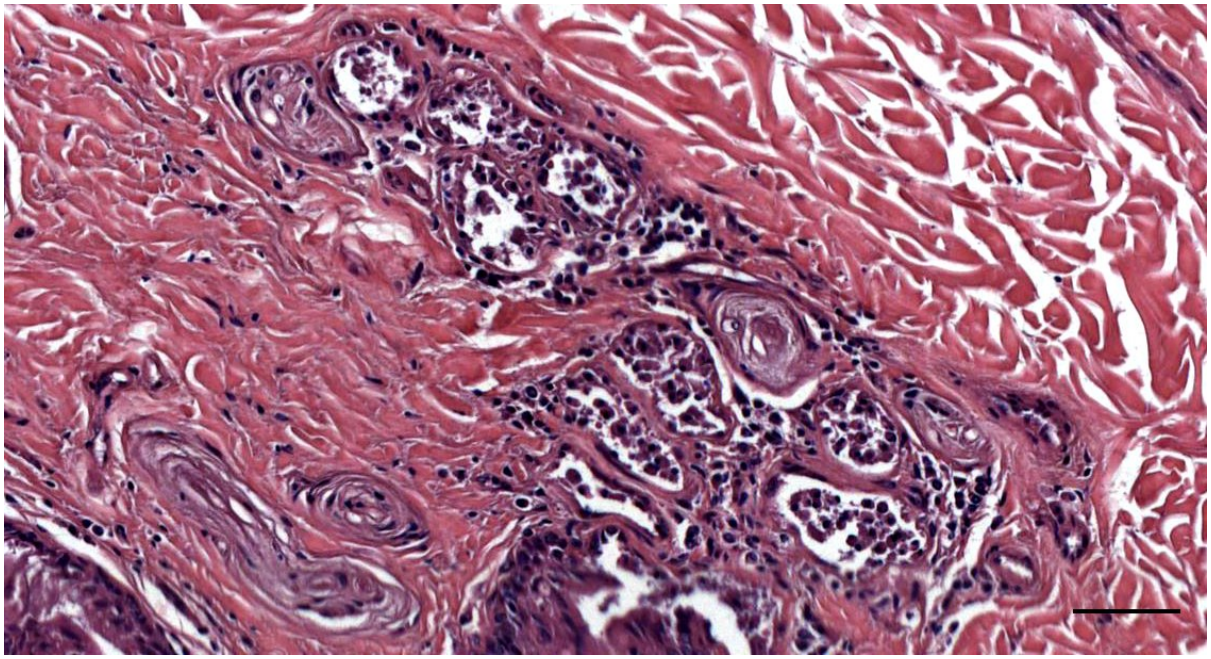

Figure 355.Histological detail image of (HE staining) (444_R6) of the ear canal glands in a bottlenose dolphin (Scale bar 50 µm)

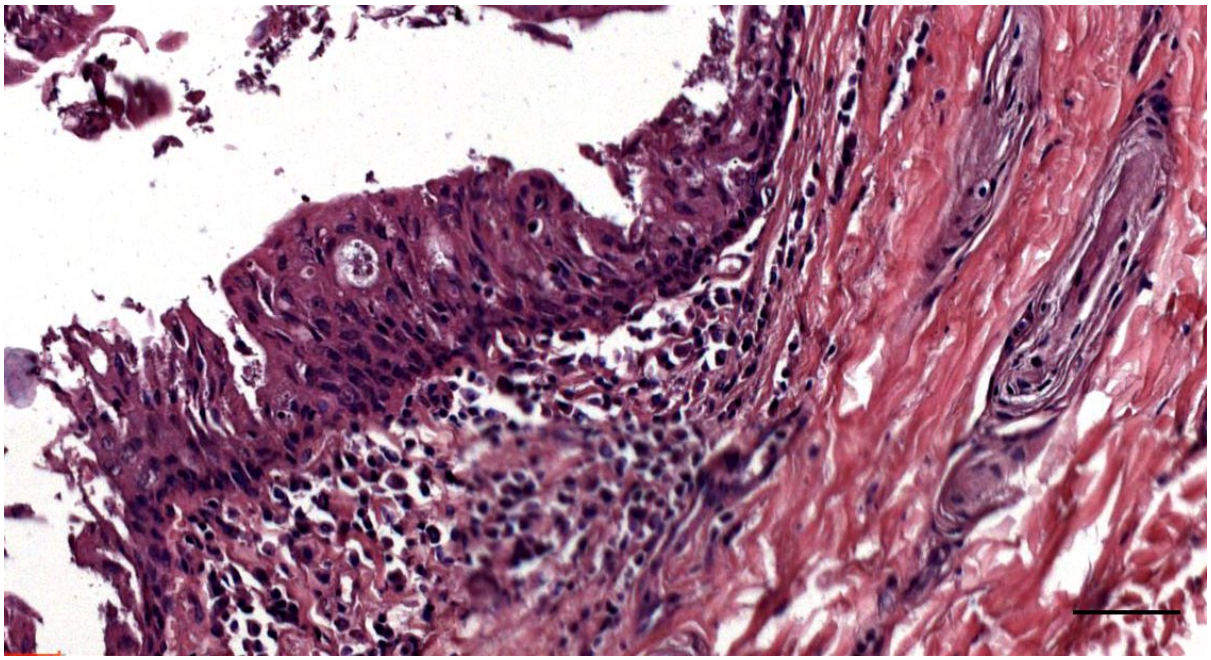

Figure 356. Histological detail image of (HE staining)(444_R6) of the ear canal pseudostratified epithelium in a bottlenose dolphin (Scale bar 50 µm)

Figure 357. Histological cross=-section (HE staining) (444_R7) of the ear canal at the level of the glands in a bottlenose dolphin (Scale bar 100 µm)

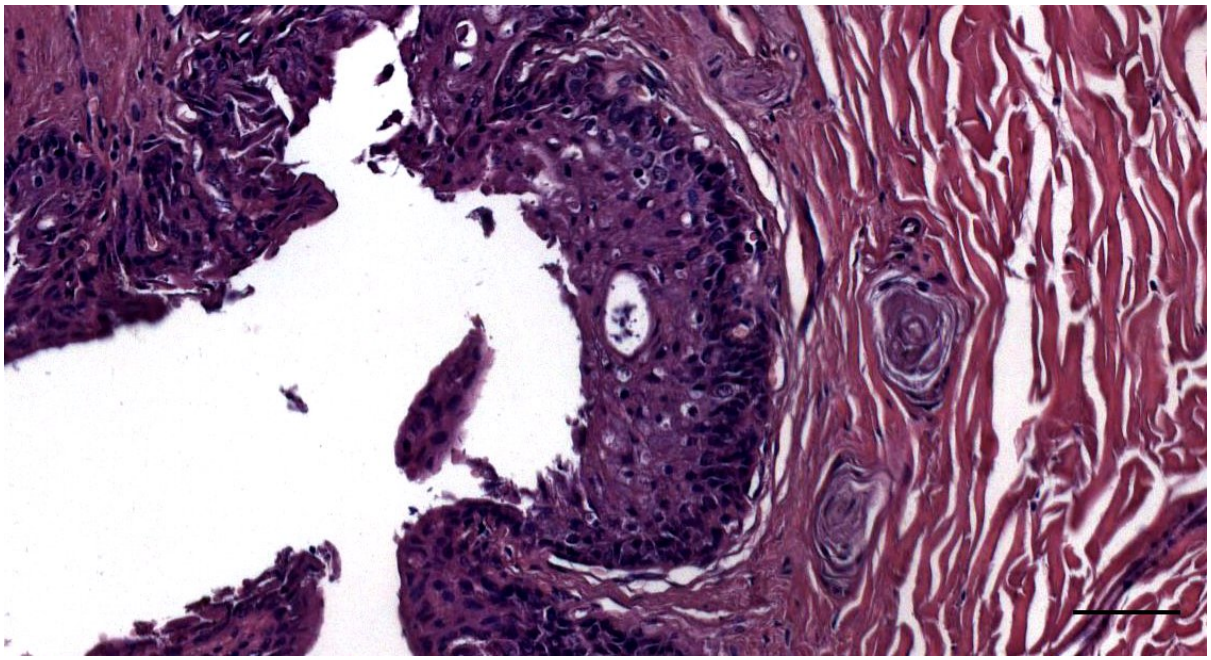

Figure 358. Histological detai l(HE staining) of the ear canal epitheliumin a bottlenose dolphin (444_R7) (Scale bar 50 µm)

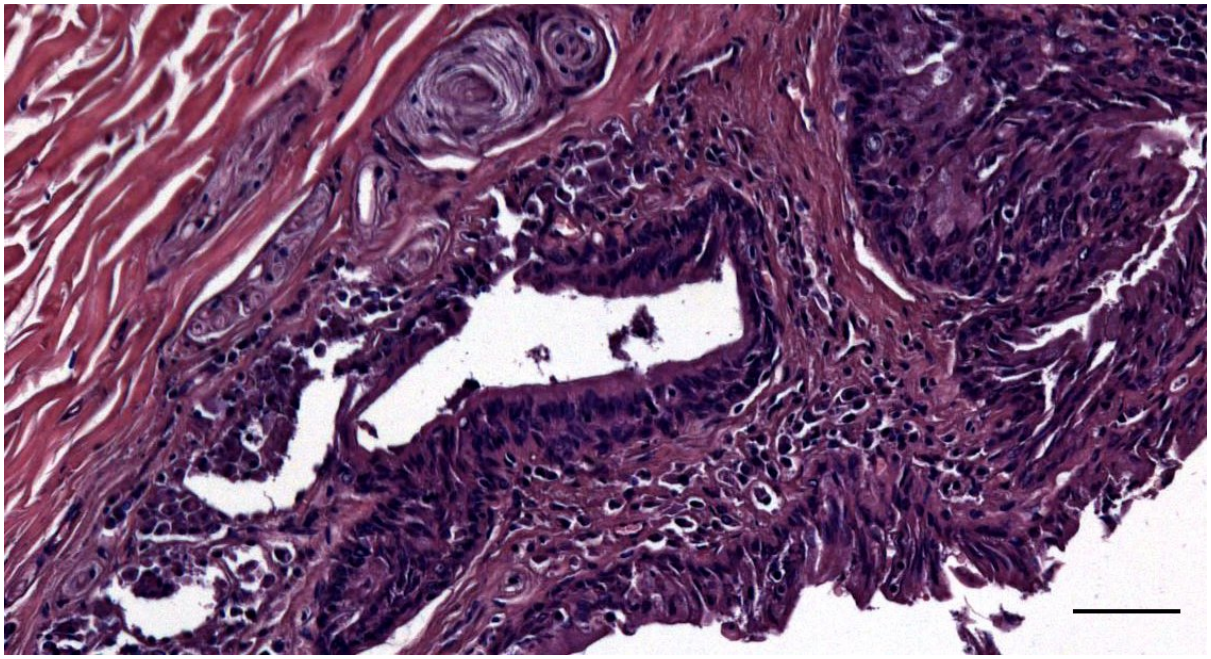

Figure 359. Histological detail l(HE staining)of the double layered epithelium in a possible glandular structure in a bottlenose dolphin (444_R7) (Scale bar 50 µm)

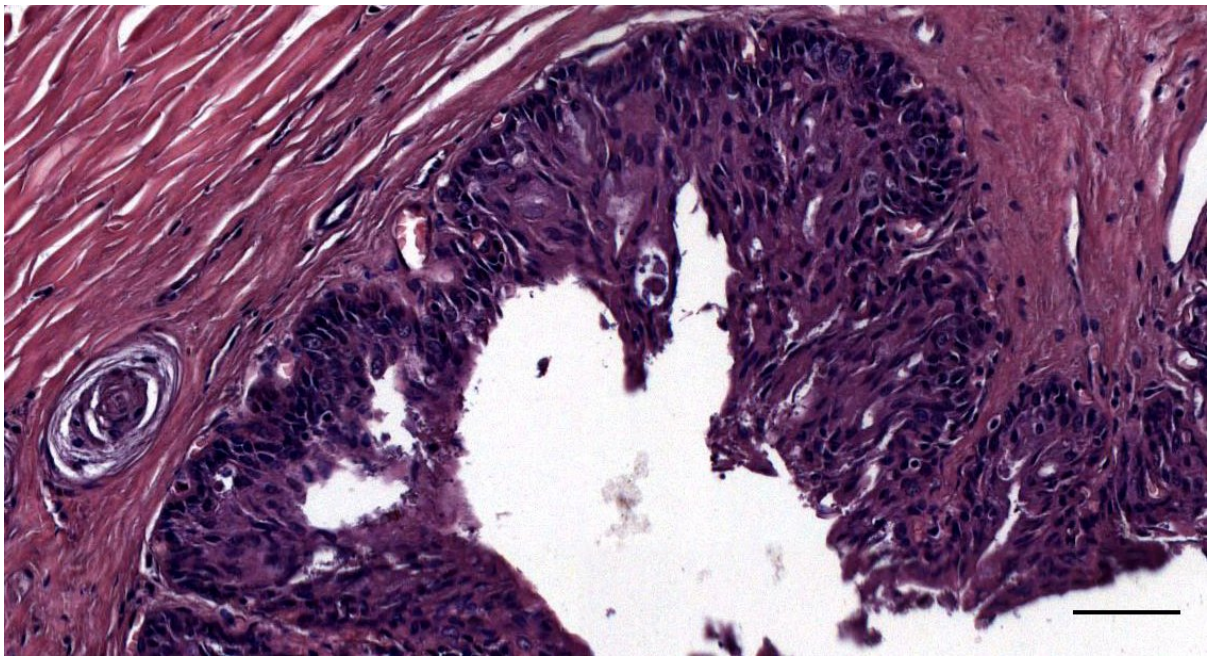

Figure 360. Histological detail l(HE staining) of the ear canal epithelium in a bottlenose dolphin (444_R7)(Scale bar 50 µm)

1.1.5 Long-finned pilot whale (ID441)

Purulent otitis with bilateral chronic granulomatous dermatitis, although more pronounced on the left side (Figure 361, Figure 362, Figure 363). There was a granulomatous dermatitis with hyperplastic pigment-laden macrophages, likely as a reaction to a bacterial infection. There were bacteria present in the subepithelial tissue where they stained positive for Gram1 and 2, and Giemsa stain (Figure 364, Figure 365), and also few bacteria were found in the ear canal lumen (Figure 366). The origin of the bacteria was not ascertained, although likely coming from the ear canal surroundings as there was a local epithelial erosion, with damage of the epithelial-subepithelial junction which caused melanin to appear in the subepithelial tissue, where it got phagocytised by macrophages (melanophages). The diagnosis was, therefore, a purulent otitis externa with granulomatous dermatitis, with interface pattern. We could not identify other types of cells in the infiltrate, although it was likely mononuclear (macrophages, lymphocytes).

Both Gram1 and 2 stains showed the presence of scant bacteria in the ear canal, many bacteria in the subepithelial tissue (pre-mortem) (Figure 365), and also many rod bacteria in the blood vessels (post-mortem) (Figure 366). All the bacteria positive in the Gram stain also stained positive (pink) in the Giemsa stain(Figure 364). The PAS stain did not provide additional information, as it stained the basement membrane of the epithelium, but no extraneous organisms were detected. (Figure 367).

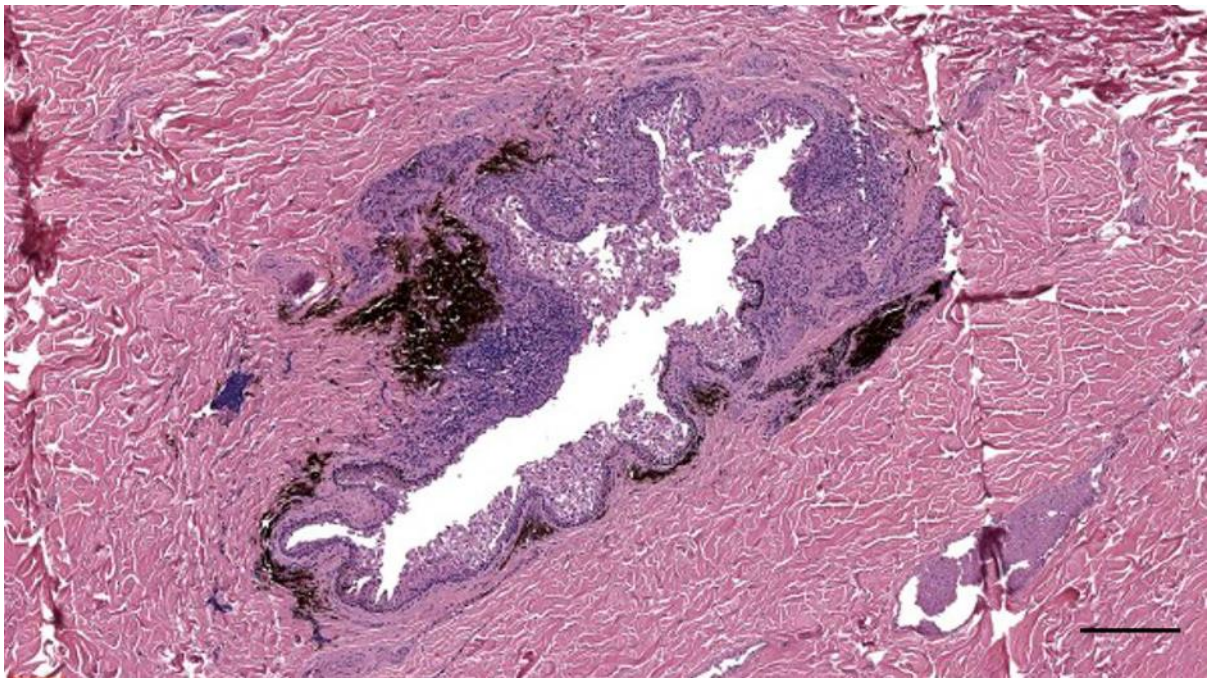

Figure 361. Histological image (HE staining) of a cross-section through the ear canal of a long-finned pilot whale (441_L8) at about 4 cm beneath the skin, showing the ear canal with subepithelial inflammation and large amounts of melanin pigment. Scale bar 200 µm

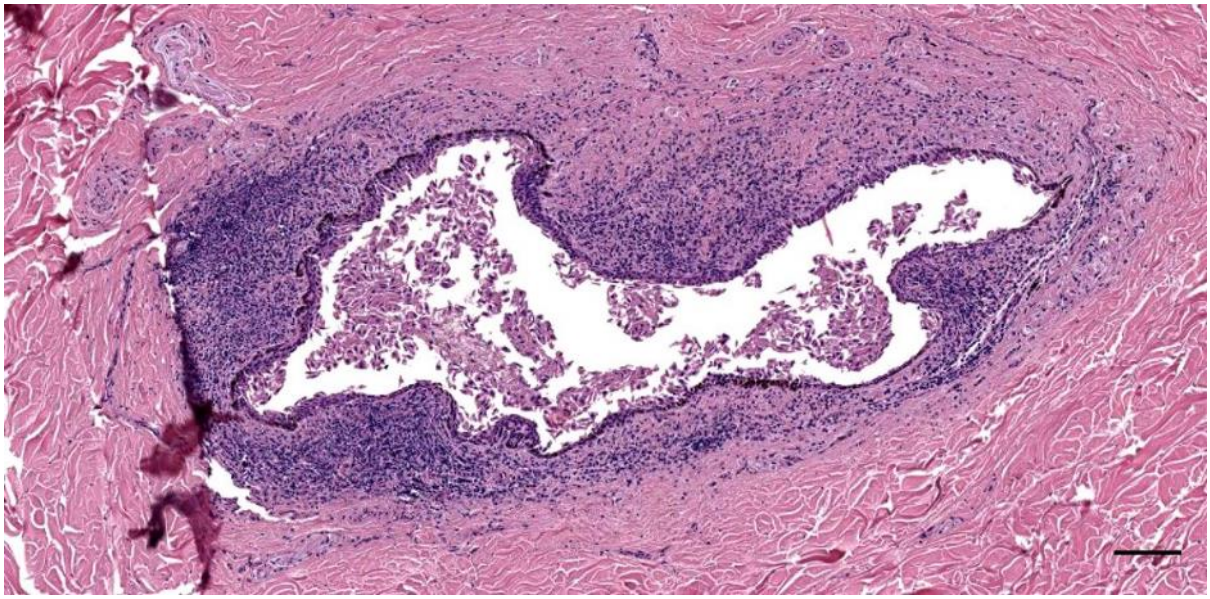

Figure 362. Histological image (HE staining) of a cross-section through the ear canal of a long-finned pilot whale (441_L11) at about 5.5 cm beneath the skin, showing the ear canal with an intense infiltration of inflammatory cells. Scale bar 100 µm

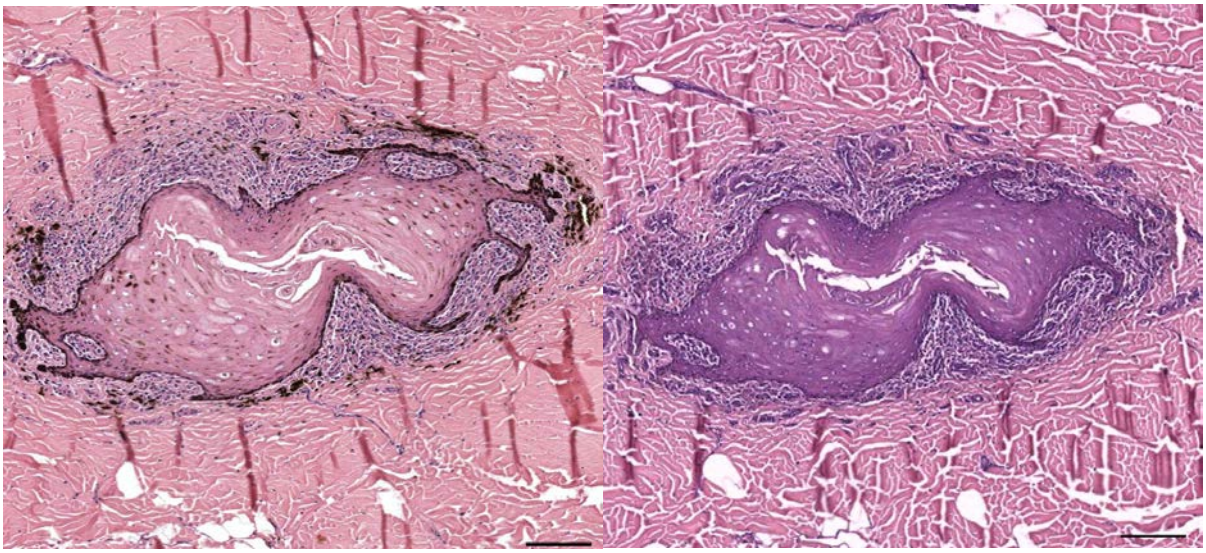

Figure 363. Histological images of a cross-section through the ear canal of a long-finned pilot whale (441_L5) at about 3 cm beneath the skin. Left is standard HE and right is HE with bleaching of melanin (right). Scale bars 100 µm

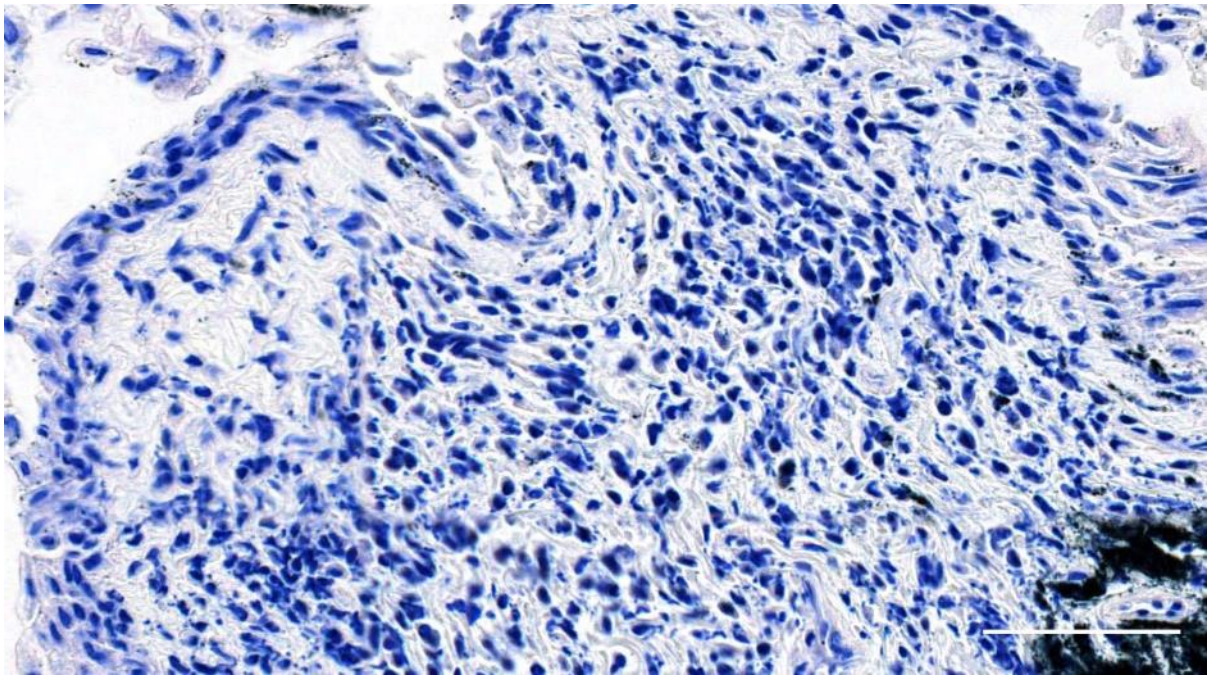

Figure 364. Histological images (Giemsa staining) of a cross-section through the ear canal of a long-finned pilot whale (441_L9) at about 4.5 cm beneath the skin, showing the ear canal´s subepithelial tissue with the presence of bacteria. Scale bar 50 µm

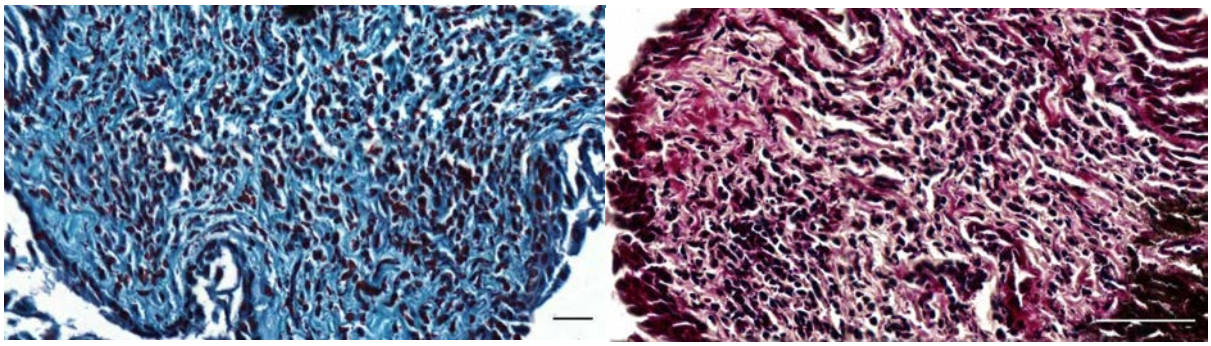

Figure 365. Histological images (Gram stains: 1, left, and 2, right) of a cross-section through the ear canal of a long-finned pilot whale (441_L9) at about 4.5 cm beneath the skin, showing the ear canal´s subepithelial tissue with the presence of bacteria. Scale bar 20 µm

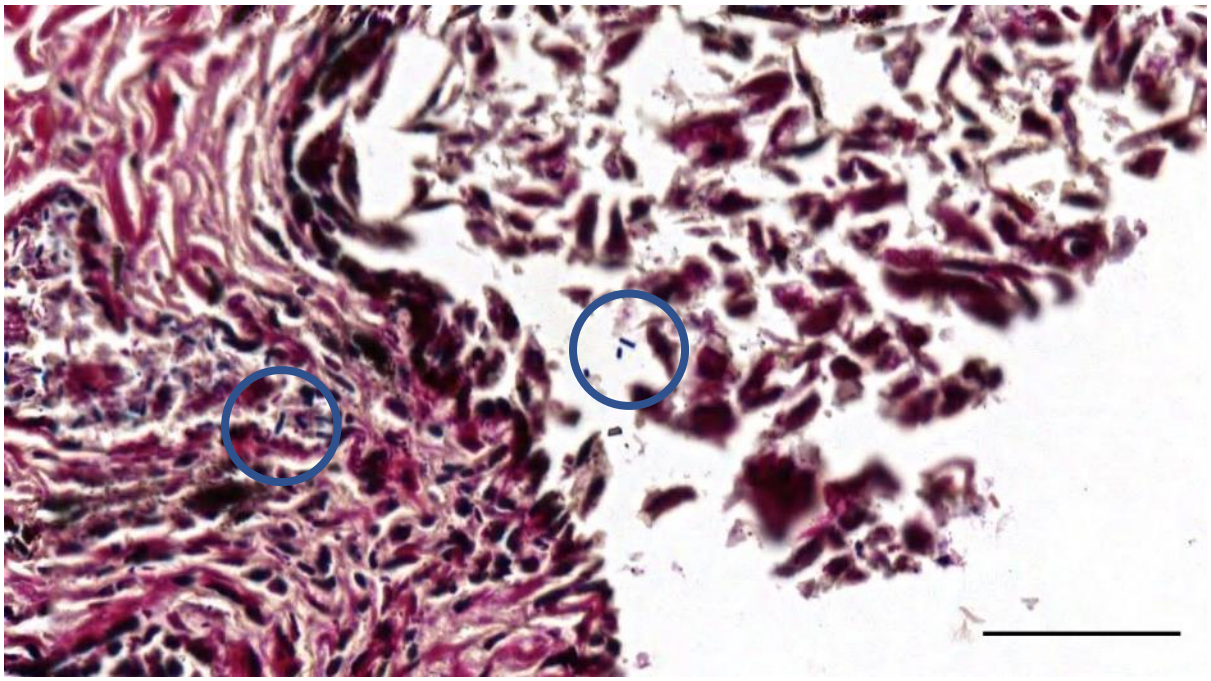

Figure 366. Histological images (Gram2 staining) of a cross-section through the ear canal of a long-finned pilot whale (441_L9) at about 4.5 cm beneath the skin, showing the ear canal´s subepithelial tissue, eroded epithelium and luminal content with the presence of rod bacteria (circles). Scale bar 50 µm

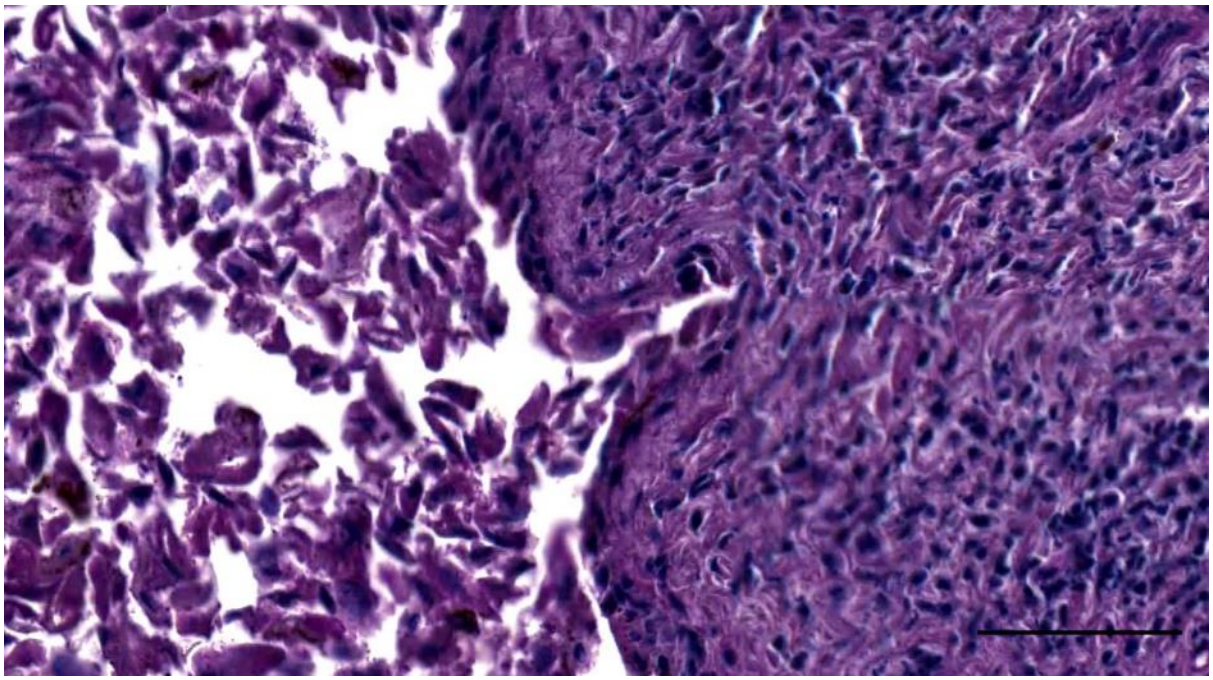

Figure 367. Histological images (PAS staining) of a cross-section through the ear canal of a long-finned pilot whale (441_L9) at about 4.5 cm beneath the skin, showing the ear canal lumen with detached epithelial cells, basal layer, and subepithelial tissue. Scale bar 50 µm

1.1.5.1 Other findings

Left ear canal

Artificial lumen	A	1	A	1	1	1	0	0	A	A	0	0	0	A	A	0	0	0	0
Blubber	A	1	A	1	1	1	0	0	0	0	0	0	0	A	A	0	0	0	0
Melanin	A	1	A	1	1	1	1	1	1	1	1	1	1	A	A	1	1	1	1
Glands (Y/N)	A	0	A	0	0	0	0	0	0	1	0	1	1	A	A	0	0	0	0
Muscle	A	0	A	0	0	0	1	1	1	1	1	1	1	A	A	0	0	0	0
Cartilage (Y/N)	A	0	A	0	0	0	0	0	0	0	0	0	0	A	A	1	1	1	1
Vascular lacunae (Y/N)	A	0	A	0	0	0	0	0	0	0	0	0	0	A	A	1	1	1	1
Nervous button (Y/N)	A	0	A	0	0	0	0	0	0	0	0	0	0	A	A	1	1	1	1
Pathology (Y/N)	A	0	A	1	1	1	1	1	1	1	1	1	1	A	A	0	0	0	0
Cellular infiltration (Y/N)	A	0	A	1	1	1	1	1	1	1	1	1	1	A	A	1	1	1	1

Right ear canal

Artificial lumen	A	A	A	A	1	A	A	A	A	A	A	A	0	A	0	0	0	0	0	A	0	0	0	0	0
Melanin	A	A	1	1	1	1	1	1	1	A	A	A	1	A	1	1	1	1	1	A	1	1	1	1	1
Blubber	A	A	1	1	1	1	1	1	0	0	0	A	0	A	0	0	0	0	0	A	0	0	0	0	0
Glands (Y/N)	A	A	0	0	0	0	1	1	1	1	1	A	0	A	0	0	0	0	0	A	0	0	0	0	0
Muscle	A	A	0	1	1	1	1	1	1	1	1	A	1	1	0	0	0	0	0	0	0	0	0	0	0
Cartilage (Y/N)	A	A	0	0	0	0	0	0	0	0	0	A	1	1	1	1	1	1	1	1	1	1	1	1	1
Vascular lacunae (Y/N)	A	A	0	0	0	0	0	0	0	0	0	A	0	A	0	0	0	1	1	A	1	1	1	1	1
Nervous button (Y/N)	A	A	0	0	0	0	0	0	0	0	0	A	0	A	0	0	1	1	1	A	1	1	0	0	0
Pathology (Y/N)	A	A	0	0	1	1	0	0	0	0	0	A	0	A	0	0	0	0	0	A	0	0	0	0	0
Cellular infiltration (Y/N)	A	A	0	0	1	1	1	1	1	1	1	A	1	A	0	0	0	0	0	A	0	0	0	0	0
																								Facial nerve	

In *Globicephalus melas* (ID 441), there were nematodes present in the pterygoid sinus. No parasites were present in the middle ear or peribullar sinus. Circular erosive lesions were noted in the soft tissue of the pterygoid sinus wall, mainly on the medial side and in the vicinity of the Eustachian tube. The parasites were identified as *Stenurus globicephalae* based on the morphological appearance and using the determination tree of Baylis and Daubney, 1925 (Zylber et al., 2002).

There was a moderate amount of nematodes present in pterygoid and peribullar sinuses in this specimen of *G. melas* (ID441). The wall presented multifocal circular slight erosive lesions. The nematodes were identified as *Stenurus globicephalus* based on morphology and morphometry (Delyamure, 1969).

Also, the innervation of the sinuses was similar to that of other species, with a the presence of several small nerve fibres in the wall. The sinus complex was very elaborate with large extensions towards dorsal and many soft tissue septa originating from the wall, which was entirely pigmented.

1.1.6 Cuvier´s Beaked whale (ID177/19)

In one beaked whale (ID429), we noted only few and small scattered lymphocytic concentrations in the papillary layer in one single section. In contrast, in the other beaked whale (ID177/19), there was a bilateral polymorphonuclear infiltration with neutrophils, macrophages, lymphocytes, and a general activation of the ECALT. Inside the inflammatory process, there were also indications of local haemosiddherophagis, although too few to conclude.

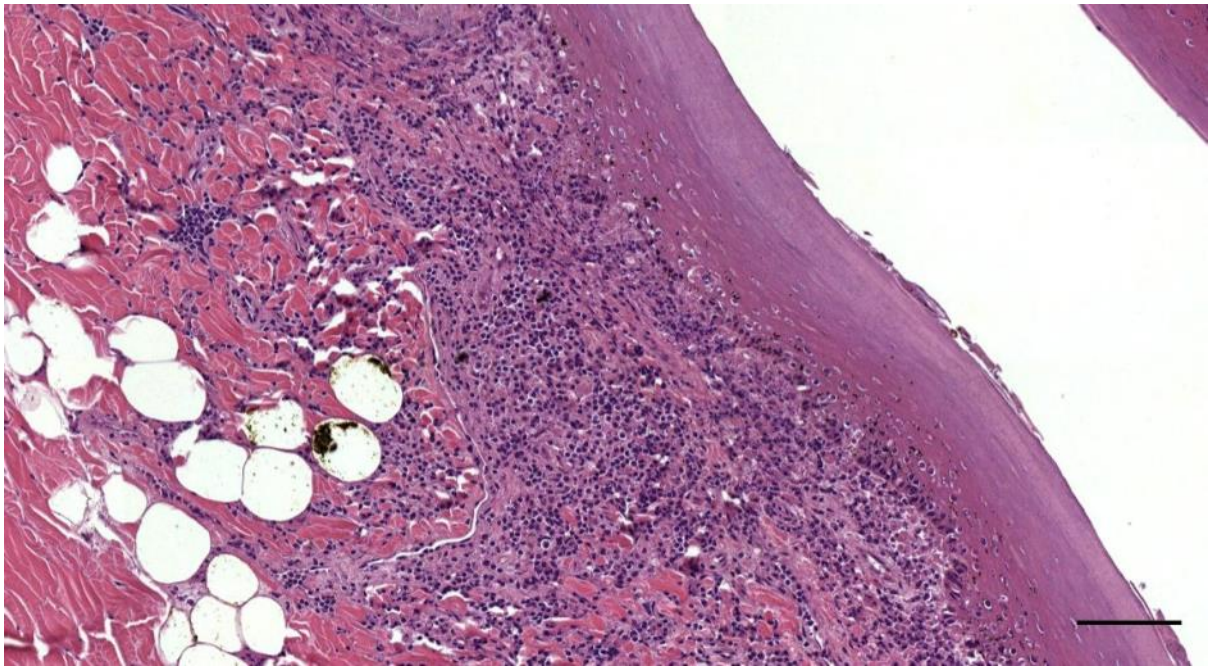

Figure 368. Histological transverse section (HE staining) through the external ear canal of a Cuvier´s beaked whale about 5.5 cm beneath the skin (ID177/19_L11). Polymorphonuclear infiltration, possible melanophages and necrosis. Scale bar 100 µm

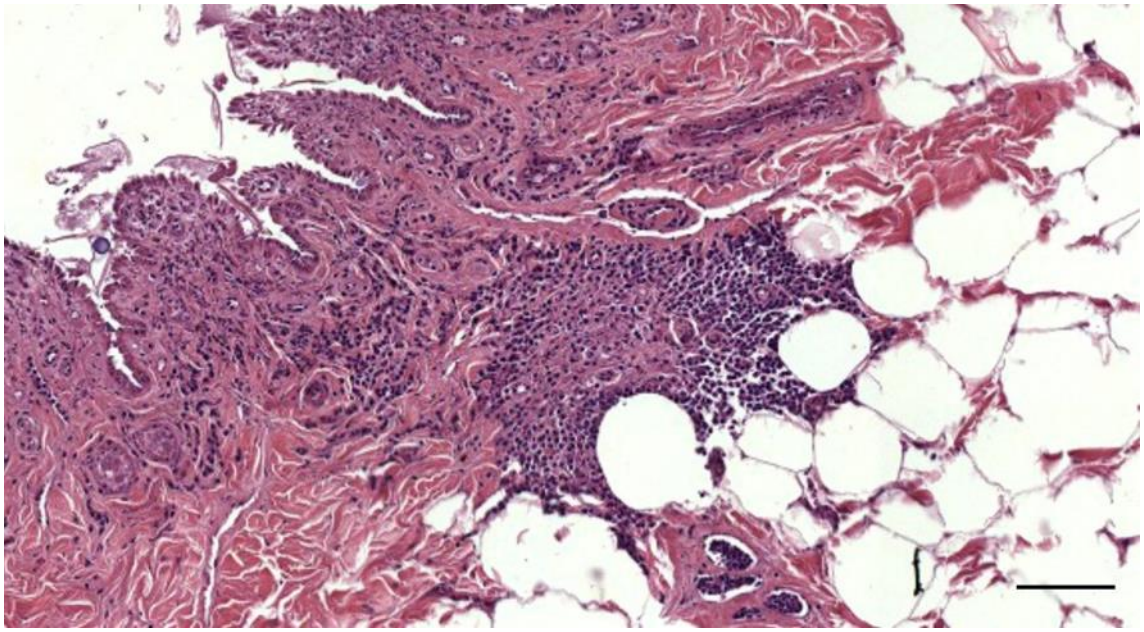

Figure 369. Histological transverse section (HE staining) of the external ear canal adnexa of a Cuvier´s beaked whale. Note the concentration of mononuclear cells at the border between ear canal subepithelial connective tissue and fat. Scale bar 100 µm

1.1.7 Harbour porpoise (UT1718)

Interestingly, there was no pathology directly associated with the external ear canal in any of the ten harbour porpoises that were subjected to the histological evaluation. The only abnormality involved a single specimen with a unilateral congestion with contracted arteries, perivascular presence (cuffing) of lymphocytic cells and macrophages and oedema between the ear canal and the cartilage in the deepest parts of the ear canal (Figure 370, Figure 371). Even though this was not considered an otitis externa, because of the very mild nature and focal occurrence in the deep ear canal, it is mentioned in this chapter because of the similarity in histopathological findings with the cases described above.

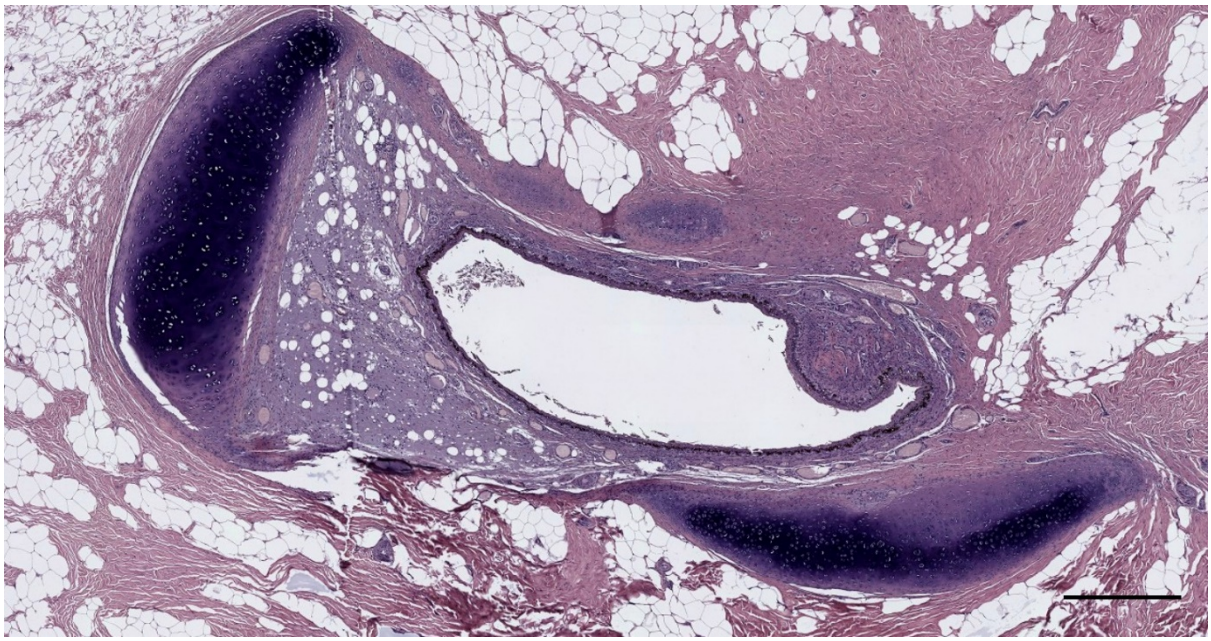

Figure 370. Histological image (HE staining) of a transverse section through the external ear canal of a harbour porpoise, about 5 cm beneath the skin (UT1718_L1402). Scale bar 500 µm

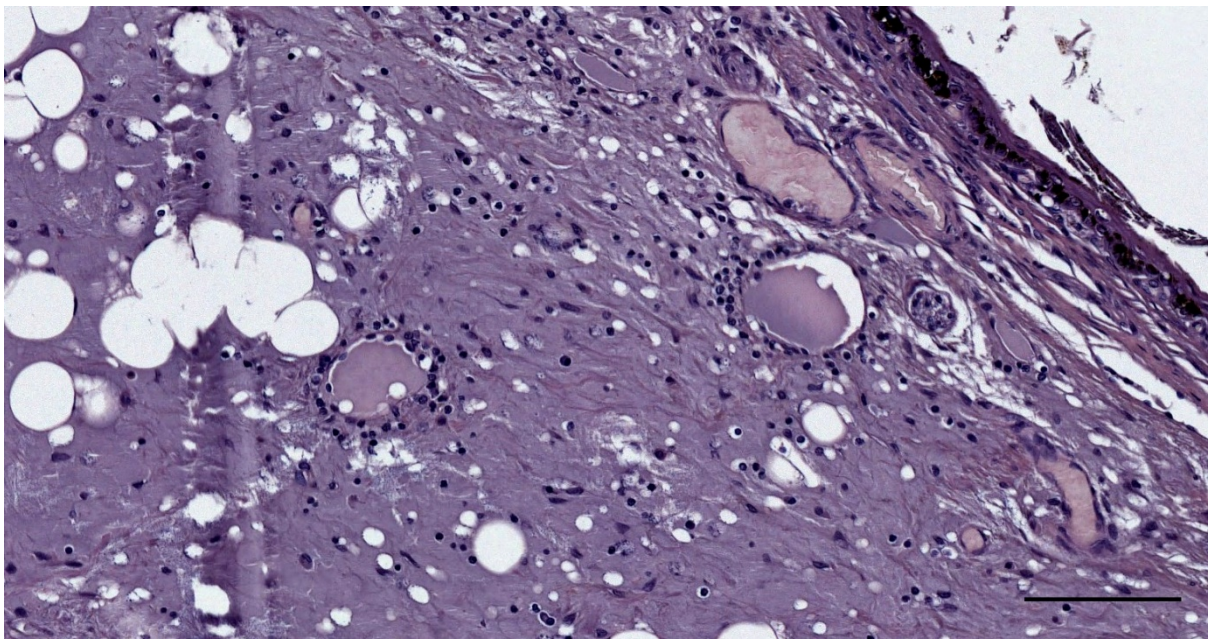

Figure 371. Detail of Figure 370. Perivascular presence (cuffing) of lymphocytic cells and macrophages; Oedema with protein leakage associated with an inflammatory process, with splitting of collagen fibres. (UT1718_L1403). Scale 100 µm

1.2 Dermatitis/panniculitis

In one case, the chronic lymphocytic inflammation (with scattered macrophages) was associated with a bacterial embolus, in its turn likely associated with a systemic infection (ID274/18). The embolus was associated with a pyogranulomatous inflammatory reaction with foci of mononuclear and multinucleated giant cells and a vasculitis (Splendore-Hoeppli phenomenon). This animal also presented bilateral lymphadenopathy, also indicative of the chronic pathological condition. All these findings directed towards a chronic pathological condition, with systemic infection of bacterial origin. These conclusions corresponded to the general necropsy findings and demonstrated the value and post-mortem analysis of the external ear canal could have and contribute to the general post-mortem assessment.

In two other striped dolphin, the inflammatory processes were associated with cachexia (ID5386, ID232/18). This might have associated with a nutritional vitamin deficiency (cfr. Soto et al., 2010), although the pathological processes not fully understood. In another striped dolphin (ID362/18), the mild inflammation was of unknown origin.

1.2.1 Striped dolphin (N274/18)

Chronic active pyogranulomatous panniculitis: On the ear canal´s course through the blubber, there was bilaterally a mild multifocal mixed infiltration of scant mononuclear cells in the subepithelial layer (Figure 499), associated with the glands (Figure 373), also in deeper sections between the ear canal and cartilage, often in a perivascular distribution, similar to the findings in a harbour porpoise (UT1718). There was also an infiltration in the more peripheral connective/adipose tissue surrounding the canal, which was more pronounced on the right side. In contrast, in the adipose/connective tissue surrounding the left ear canal, about halfway its course, on the lateral margin of the ear canal cartilage, there was a focal invasion of inflammatory cells visible as a chronically active mixed cell panniculitis (Figure 372).

There was also a round lesion of about 0.7 x 1.0 mm, with a pyogranulomatous inflammatory reaction with foci of mononuclear (eosinophils, neutrophils, macrophages) and multinucleated giant cells (Figure 374). The centre contained many neutrophils, while the borders of the lesion mainly contained macrophages. In close vicinity of this lesions, there was a vasculitis with inflammatory cells inside the blood vessel wall, active macrophages around the vessel, and neutrophils in the lumen. There were also indications of steroid (asteroid) bodies (Splendore-Hoeppli phenomenon), which is generally associated with fungi, bacteria or parasites (Gopinath, 2018; Rodig and Dorfman). Therefore, it was hypothesized that this lesion could have been a reaction to a bacterial embolus as a consequence of a systemic infection. A similar lesion was found in a harbour porpoise (Figure 375, Figure 376).

This finding was independent of the lymph/haemal node observed associated with the right ear canal.

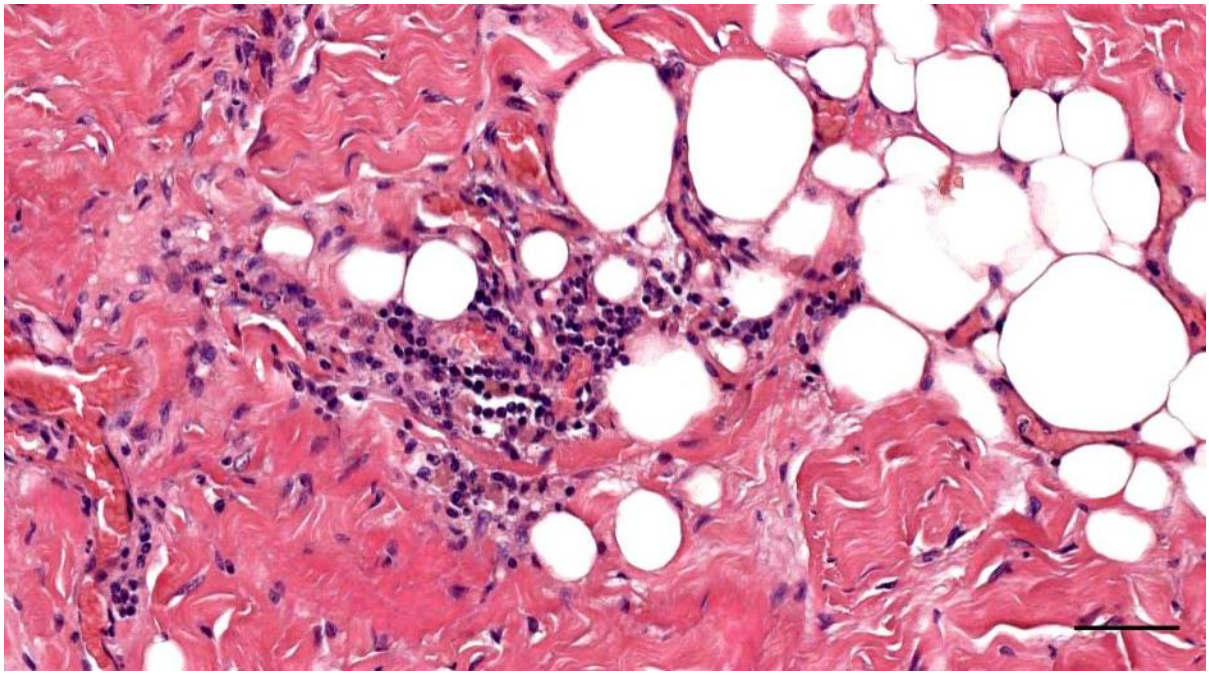

Figure 372. Histological detail (HE staining) of the chronic active mixed panniculitis (274/18_L5). Scale bar 50 µm

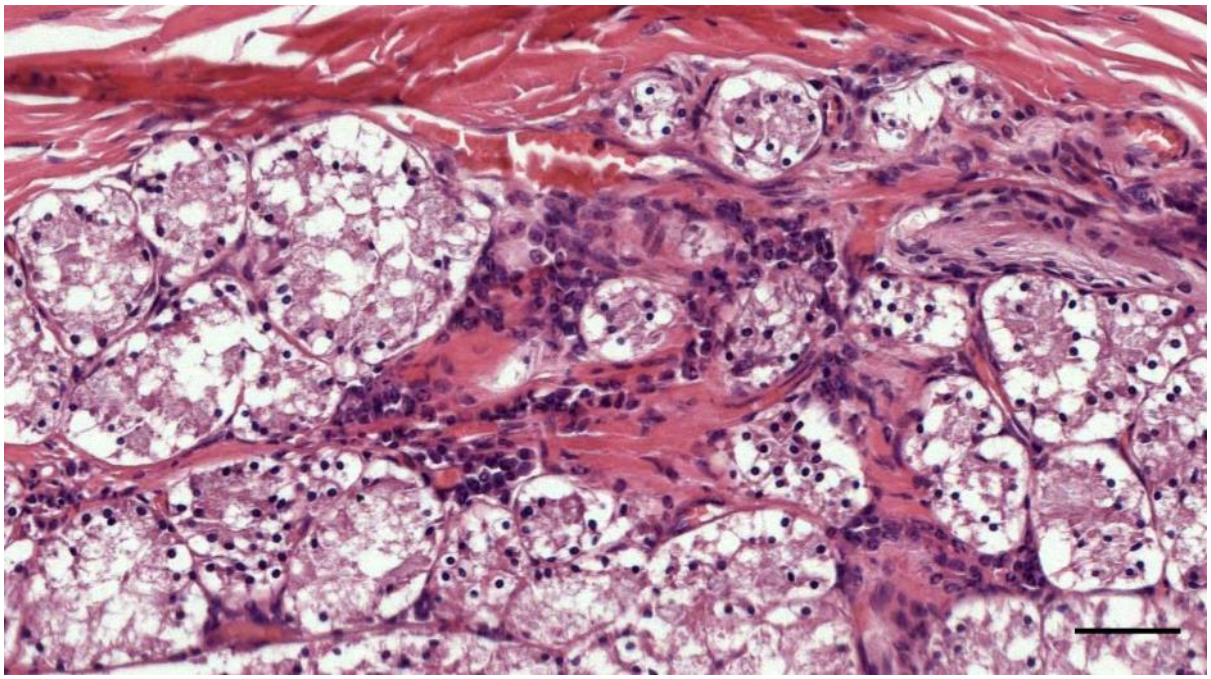

Figure 373. Histological detail (HE staining) of mononuclear cells (lymphocytes, and few plasma cells and macrophages associated with the glands in a section through the superficial ear canal. Scale bar 50 µm

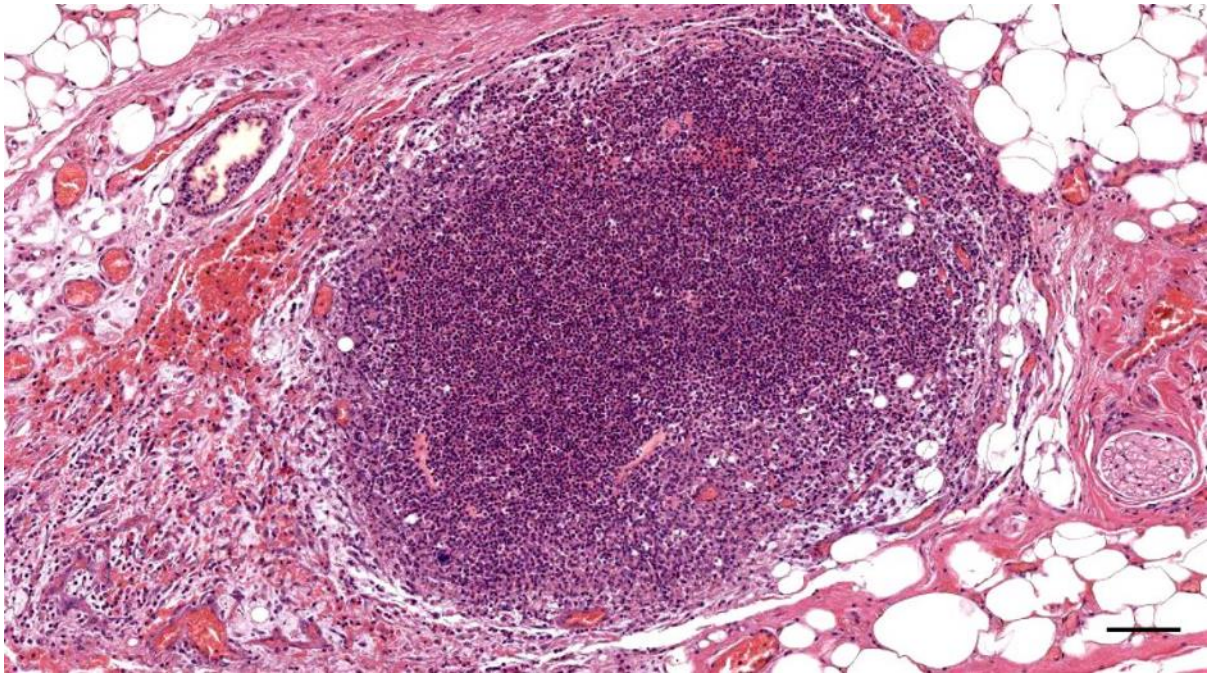

Figure 374. Histological image (HE staining) of the pyogranulomatous reaction and vasculitis in a striped dolphin. Scale bar 100 µm

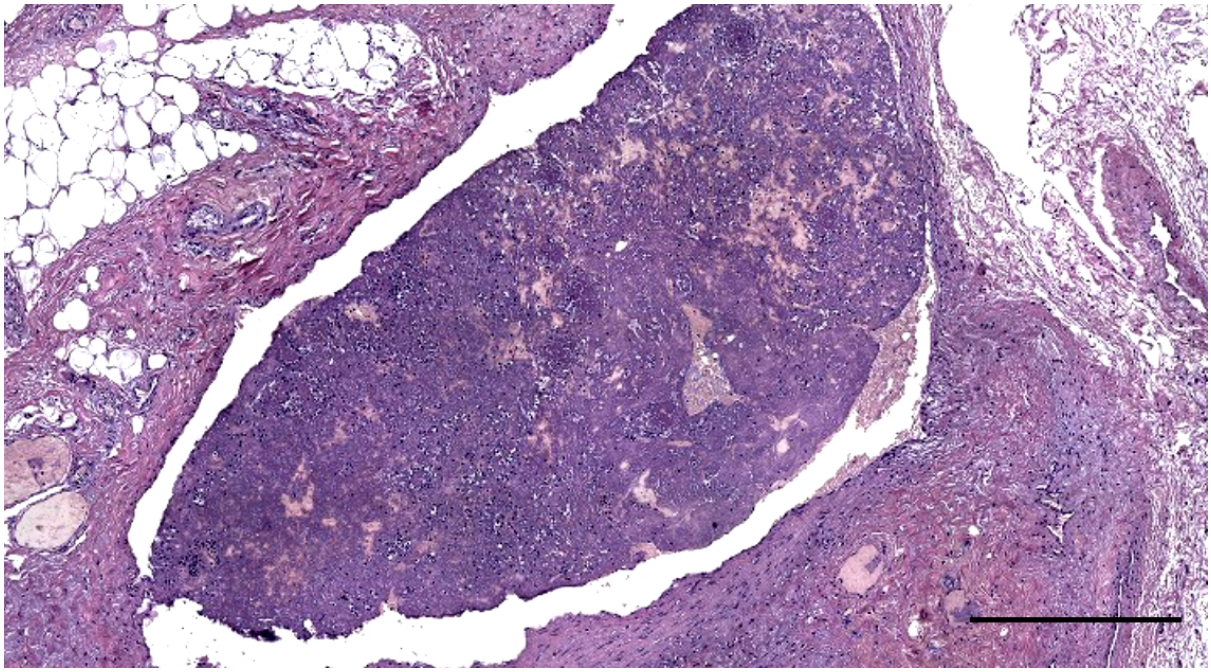

Figure 375. Histological image (HE staining) of a transverse section through the right ear canal of a harbour porpoise about 1.5 cm beneath the skin (UT1727_R16). Coagulation in a blood vessel. Scale bar 500 µm

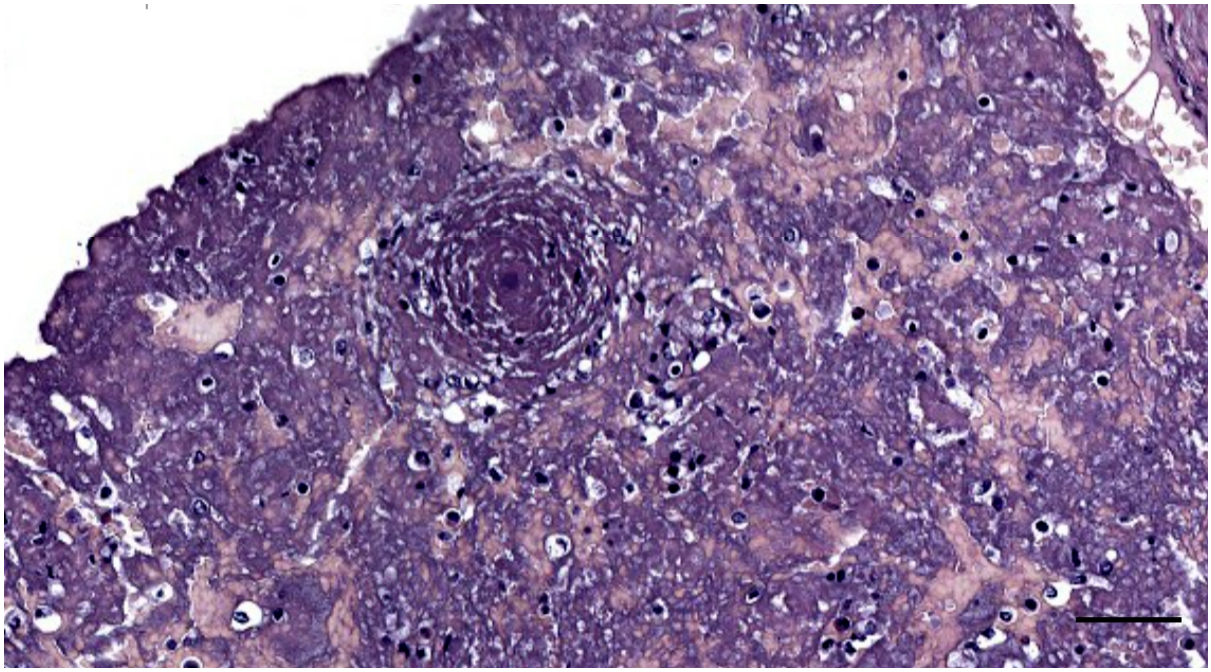

Figure 376. Detail of Figure 375. Asteroid body in the coagulation (UT1727_R16). Scale bar 50 µm

1.2.2 Striped dolphin (ID5386) and striped dolphin (ID232/18)

Artificial lumen	0	1	A	A	0	0	A	0	A	0	0	0	0
Melanin	0	0	A	A	0	1	A	1	A	1	1	1	1
Blubber	0	1	A	1	0	0	A	0	A	0	0	0	0
Glands (Y/N)	0	1	A	A	1	0	A	0	A	0	0	0	0
Muscles	0	0	1	1	1	1	A	0	A	0	0	0	0
Cartilage (Y/N)	0	0	A	A	0	1	A	1	A	1	1	1	1
Vascular lacunae (Y/N)	0	0	A	A	0	1	A	1	A	1	1	1	1
Nervous button (Y/N)	0	0	A	A	0	A	A	A	A	1	1	1	1
Pathology (Y/N)	0	0	A	1	0	0	A	0	A	0	0	0	0
Cellular infiltration (Y/N)	0	0	A	A	0	0	A	0	A	0	1	A	A
	NF												

Figure 377. Schematic representation of the left ear canal of striped dolphin ID5386

Two striped dolphins presented a microgranulomatous panniculitis in deep blubber layer (Figure 378, Figure 379). The lesions were situated in the deep blubber layer and were relatively well defined. There were multifocal microgranulomas containing macrophages associated with adipocytes. There was also more tissue between adipocytes, indicative of adipocyte atrophy. This also corresponded to the macroscopic findings of a darker colouration of the interior half of the blubber layer, associated with the presence of gelatinous appearance of the fat as a consequence of serous atrophy of the fat, and also subcutaneous oedema. To our knowledge, this pathology has not yet been reported in cetaceans, although a similar case has been reported for striped dolphin where the aetiology of the lesions was related to a vitamin E deficiency (Soto et al., 2010). There, the pathology was most probably associated with the cachectic state of the animal, which would lead to overregulation of fat consumption, the release of free radicals and a consecutive inflammatory reaction.

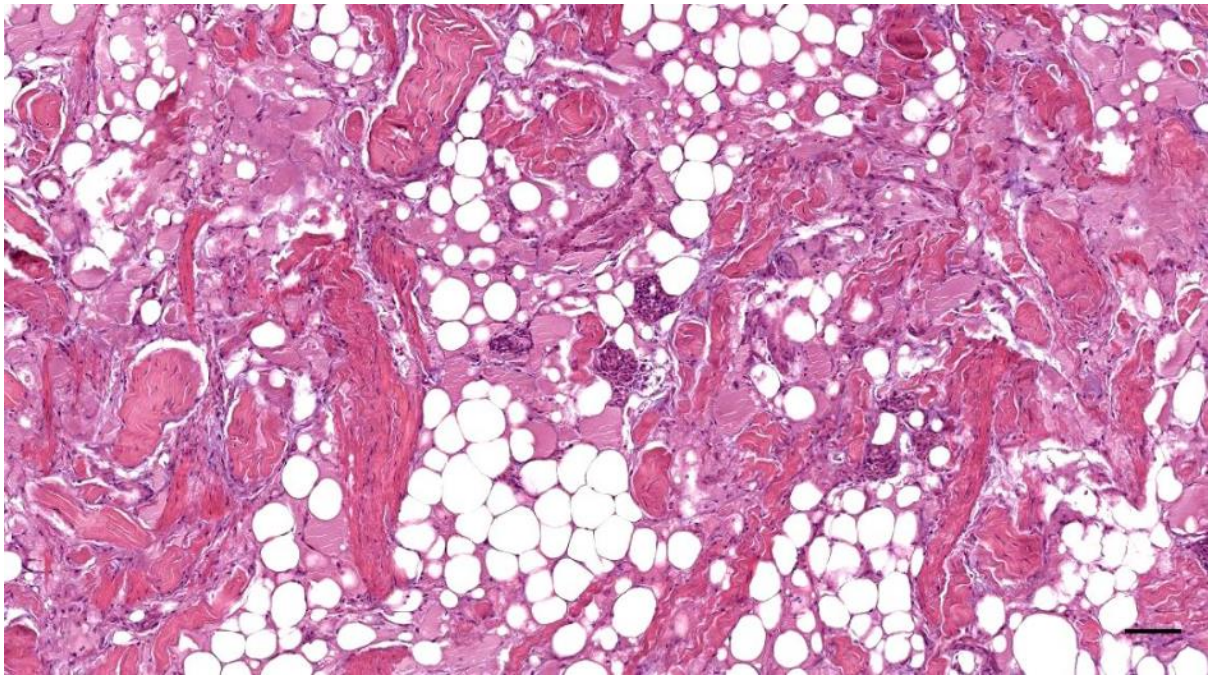

Figure 378. Histological image (HE staining) of a striped dolphin panniculitis with several microgranulomas (5386_L4). Scale bar 100 µm

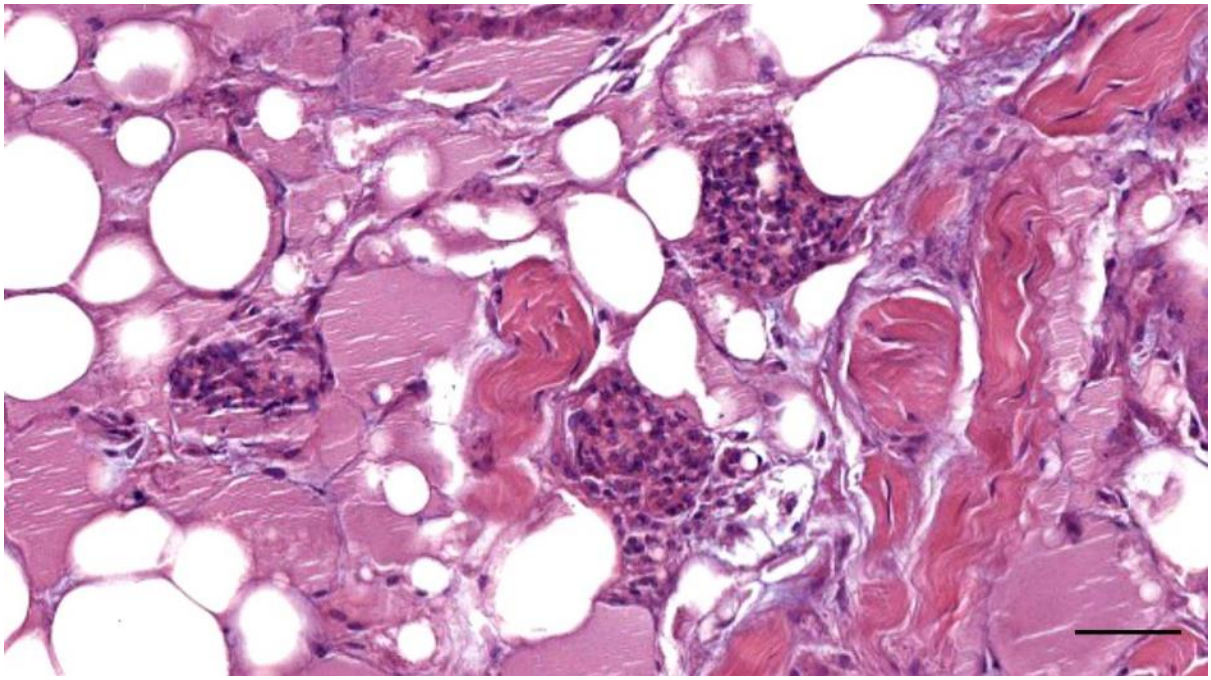

Figure 379. Detail image (Figure 378)(HE staining) of the microgranulomas in the adipoconnective tissue around the ear canal in a striped dolphin (5386_L4 HE). Scale bar 50 µm

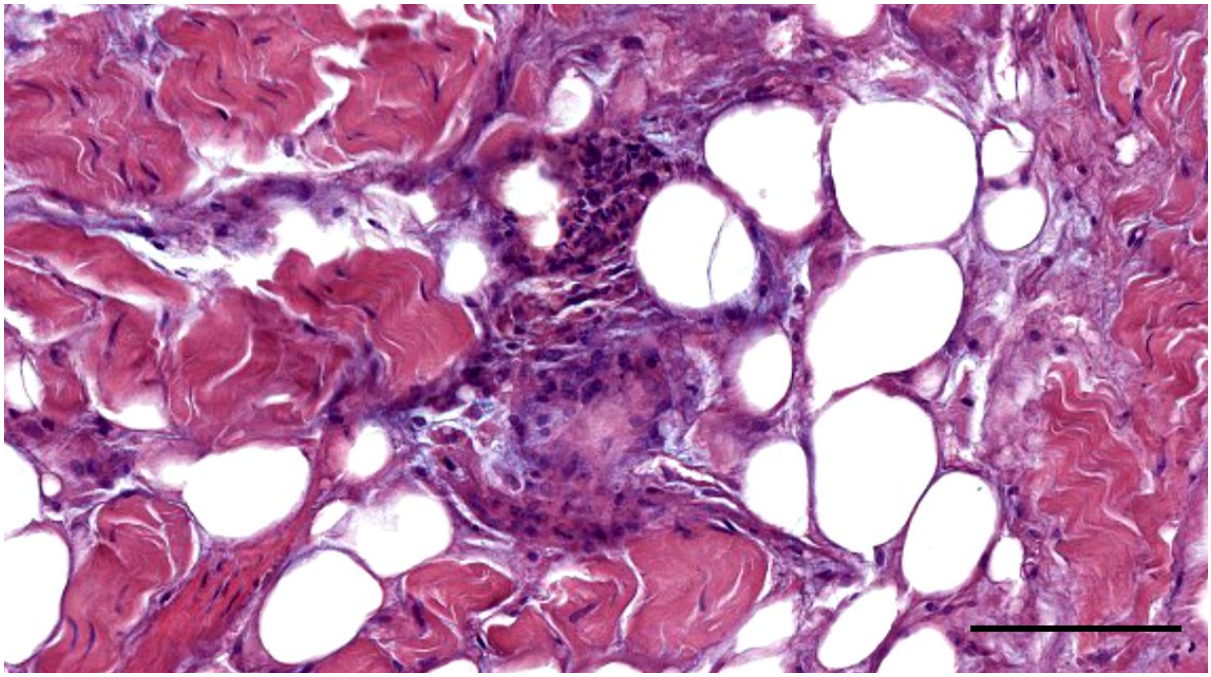

Figure 380. Detail image (Figure 378)(HE staining) of inflammatory cells associated with adipocytes. Note the presence of a possible multinucleated cell.

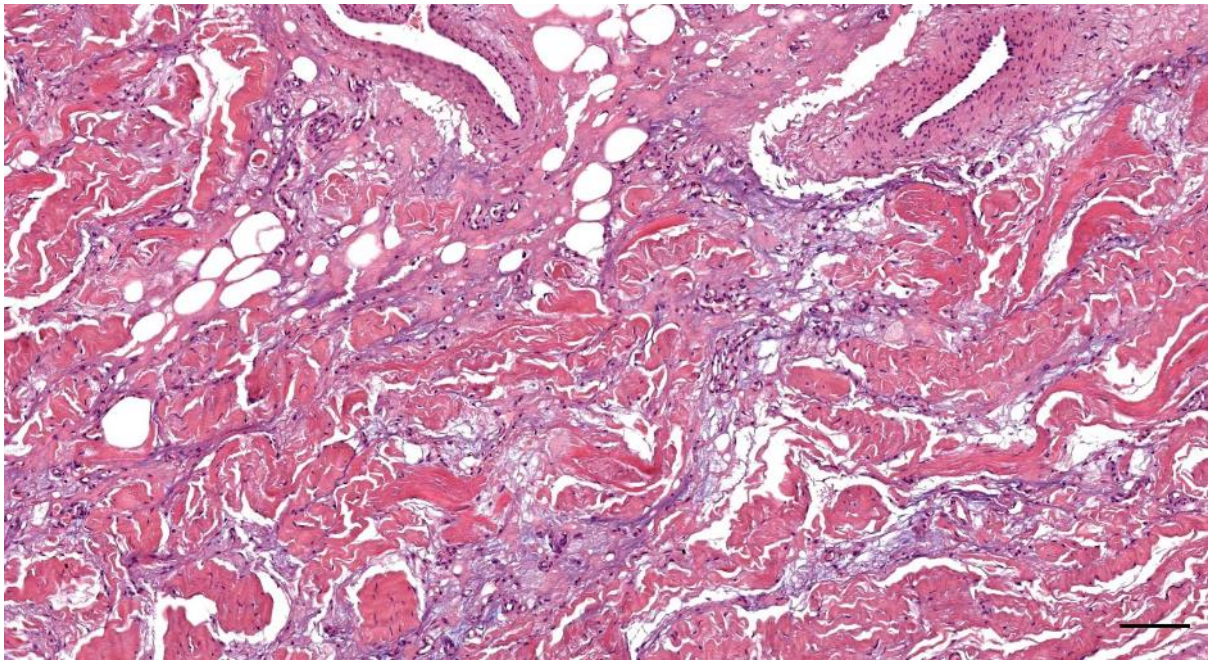

Figure 381. Histological image (HE staining) of a panniculitis associated with the ear canal in a striped dolphin (232/18_10B). There is a general proliferation of mesenchymal cells with oedema in the adipo-connective tissue (but not near the canal) with tissue degeneration (of adipocytes) and indications of invasion of mononuclear inflammatory cells (macrophages and lymphocytes) with entrapment of the connective tissue fibres. The inflammation was present in the subepithelial connective tissue, and the loose connective tissue outside the fibro-elastic tissue capsule. Scale bar 100 µm.

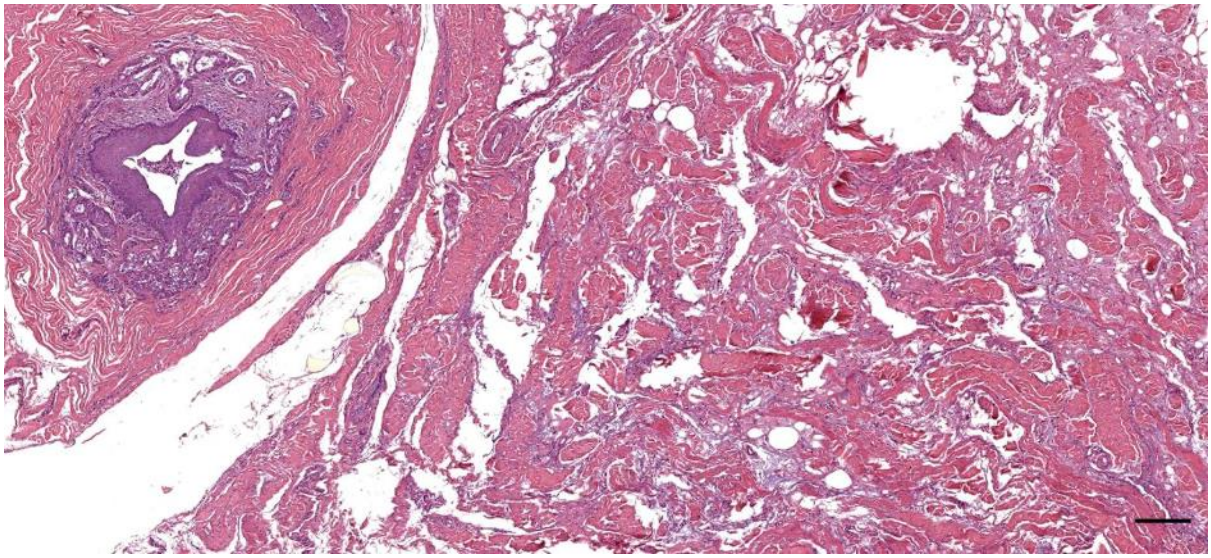

Figure 382. Histological image (HE staining) of a panniculitis associated with the ear canal in a striped dolphin (ID232/17). Scale bar 200 µm

1.2.3 Striped dolphin (ID145/18)

Artificial lumen		A		0	0	0	0	0	0	0	0	0	0	0	A	0	0
Melanin		1		1	1	1	1	1	1	1	1	1	1	1	A	1	1
Blubber		1		0	0	0	0	0	0	0	0	0	0	0	A	0	0
Glands (Y/N)		0		0	0	0	0	0	0	0	0	0	0	0	A	0	0
Muscle		0		1	0	0	0	0	0	0	0	0	0	0	A	0	0
Cartilage (Y/N)		0		1	1	1	1	1	1	1	1	1	1	1	A	1	1
Vascular lacunae (Y/N)		0		0	0	0	1	1	1	1	1	1	1	1	A	1	1
Nervous button (Y/N)		0		0	0	1	1	1	1	1	1	0	0	1	A	1	1
Pathology (Y/N)		1		0	0	1	0	0	0	0	0	0	0	0	A	0	0
Cellular infiltration (Y/N)		1		1	0	1	1	1	1	1	1	1	1	1	A	0	0

Figure 383. Schematic representation of the left ear canal and associated soft tissue from superficial (left) to deep (right)

This animal presented a mixed inflammatory reaction around the external ear opening. There were subjectively many mononuclear cells in the superficial dermis around the porus acusticus externus to at least 6 mm beneath the epidermis (Figure 384, Figure 385). It appeared as a mixed inflammatory reaction with mainly mononuclear cells in a perivascular distribution, and some neutrophils. The same inflammatory reaction was present in deeper sections (Figure 386).

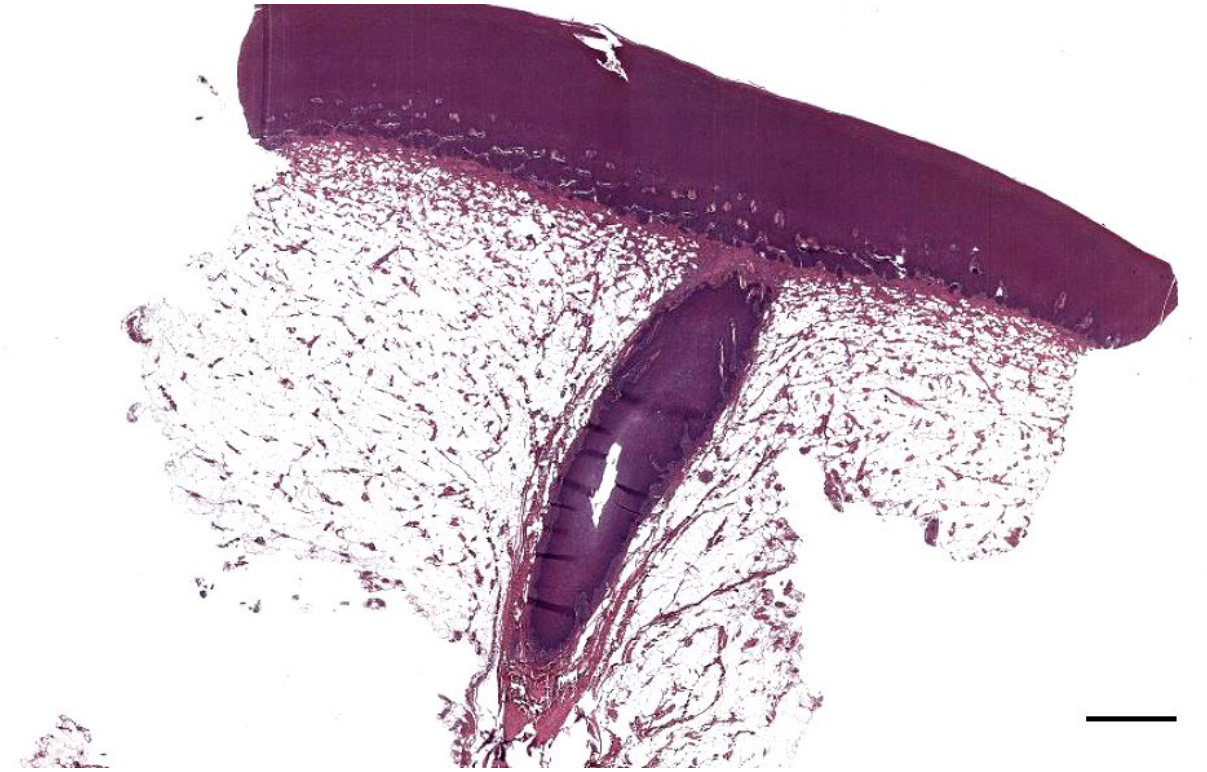

Figure 384. Histological image (HE staining) of a longitudinal section through the external ear canal in the superficial dermis (145/18_R1, HE). Scale bar 1 mm

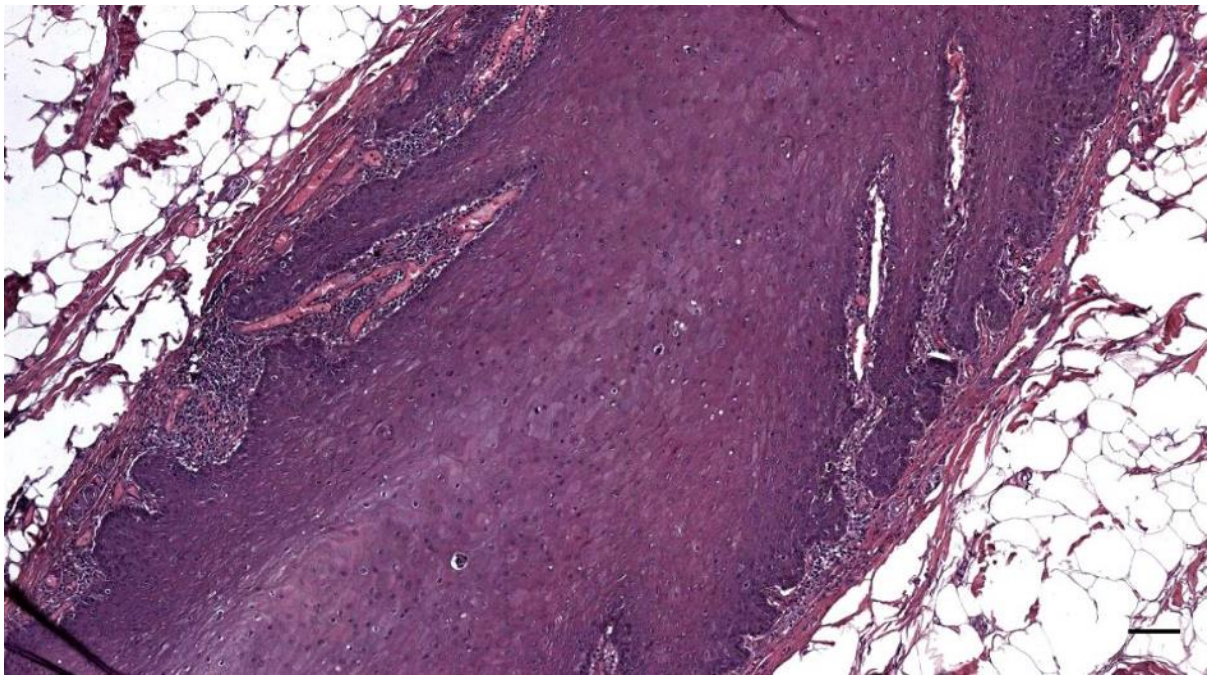

Figure 385. Histological image (HE staining) of a longitudinal section through (the wall of) the ear canal in the superficial dermis (145/18_R1, HE). There are mononuclear cells and corpuscles in the subepithelial connective tissue and dermal papillae. Scale bar 100 µm

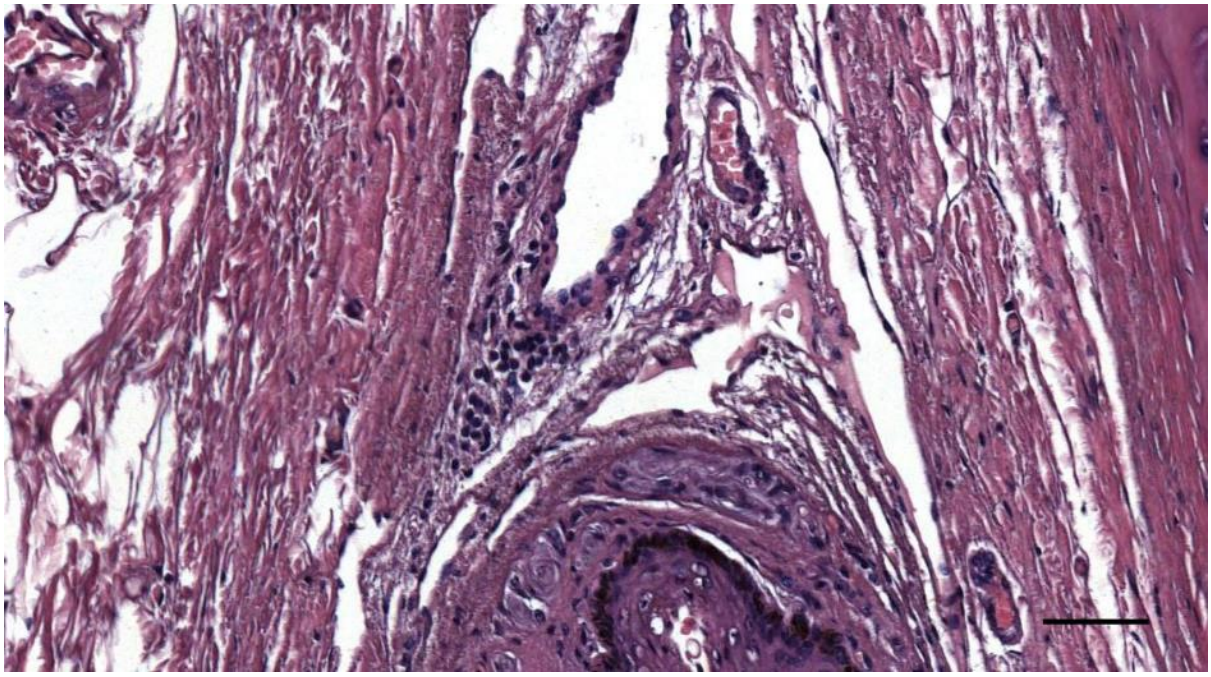

Figure 386. Histological detail image (HE staining) of mononuclear cells in a perivascular distribution close the ear canal (bottom) (145/18_R5). Scale bar 100 µm

1.2.4 Striped dolphin (ID620/17)

This animal showed the presence of inflammatory cells in the dermal papillae of the skin, and the superficial dermis of the distal end of the ear canal (Figure 387, Figure 388, Figure 389). Also, there was a multifocal presence of lymphocytes, plasma cells and macrophages around the glandular structures.

Figure 387. Histological cross-section (HE staining) of the left external ear opening in a striped dolphin (620/17_L2). Scale bar 100 µm

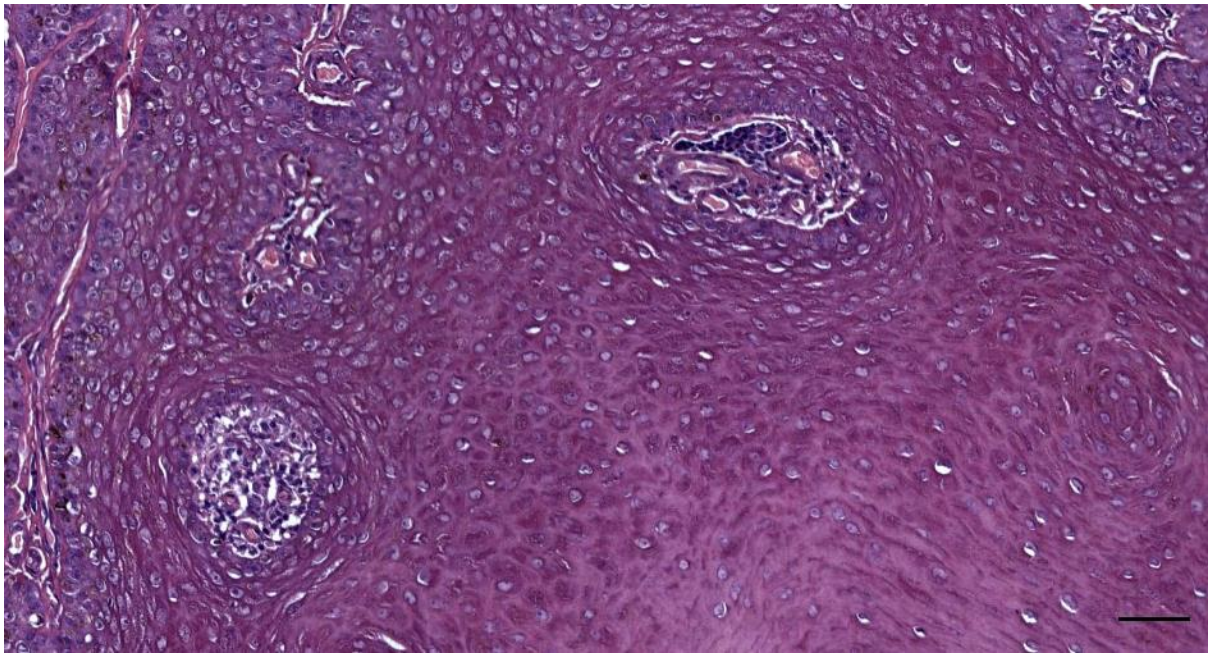

Figure 388. Detail of Figure 387 (620/17_L2_detail). Mononuclear cells in the dermal papillae around the external ear opening. Scale bar 50 µm

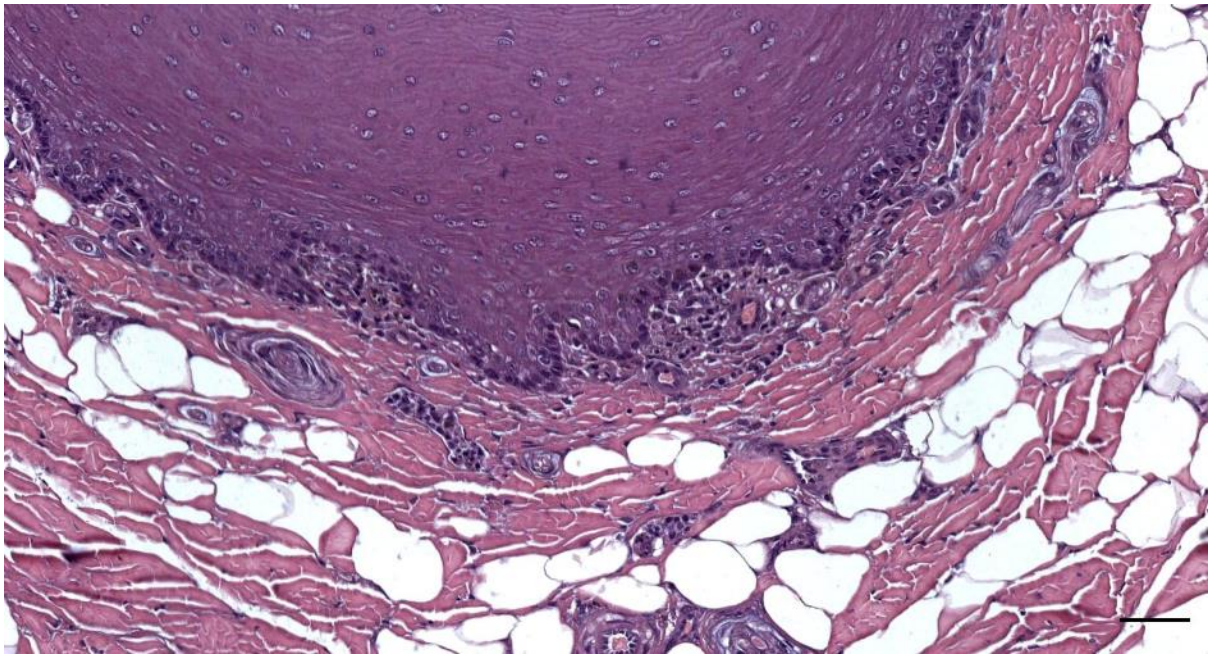

Figure 389. Histological detail (HE staining) of inflammatory cells in the subepithelial tissue of a striped dolphin ear canal (620/17_L3). Scale bar 50 µm

1.2.5 Striped dolphin (ID362/18)

This animal presented a mild interstitial panniculitis with perivascular cuffing of macrophages and lymphocytes, and thickened endothelial cells.

This individual also presented a possible cholesteatoma, a a large amount of lymphocytic cells situated between the ear canal and cartilage (possibly associated with the cholesteatoma), and nodular lymphoid tissue -> See Result, Discussion and Annex respective chapters.

rostroventral to the ear canal and on other side of cartilage, there was two large (1.2 x 2.5 mm on cross section) focal nodular concentration of mononuclear cells in the adipoconnective tissue. (Figure

715, Figure 716, Figure 717). The structure was encapsulated, but only on one side (direction of the ear canal). It was very well vascularized. The cellular content were lymphocytes and plasmacells (indicate of a viral infection), with a sinusial histiocytosis (indicating a filtering functioning, typical for bacterial infection). There was lymphoid depletion and an eosinophilic matrix (indicative of long-term activation, possibly as a reaction to Morbillivirus infection). There were also apoptotic changes. (Figure 717).

1.3 Muscle pathology

Histo-morphological changes in the striated musculature of free-ranging toothed whales is a relatively common finding. Most are degenerative changes, atrophy, and chronic lesions, with also occasional parasitic infection and inflammation of the muscle (Sierra et al., 2017). The muscle lesions in this study were identified as degenerative lesions (with regeneration and necrosis), muscle atrophy, and indications of chronic fibrosis. The degenerative lesions in this study might have been associated with capture-myopathy in few live-stranded animals, while in most cases the aetiology was not identified. The same was valid for the other lesions, for which full comprehensive studies should be performed to narrow down the possible etiologies. We did not perform any specific investigations to characterize the lesions in detail. The use of immunohistochemical markers to identify type I and II muscle fibres, and myoglobin and fibrinogen, together with other histochemical stains such as PAS, could give insight in the specific type of lesion and its possible etiologies, and differentiate between ante- and post-mortem lesions.

1.3.1 Atrophy

1.3.1.1 Cuvier´s beaked whale (ID177/19)

Muscle atrophy (Figure 390, Figure 396) besides the activation of the ECALT (Figure 368).

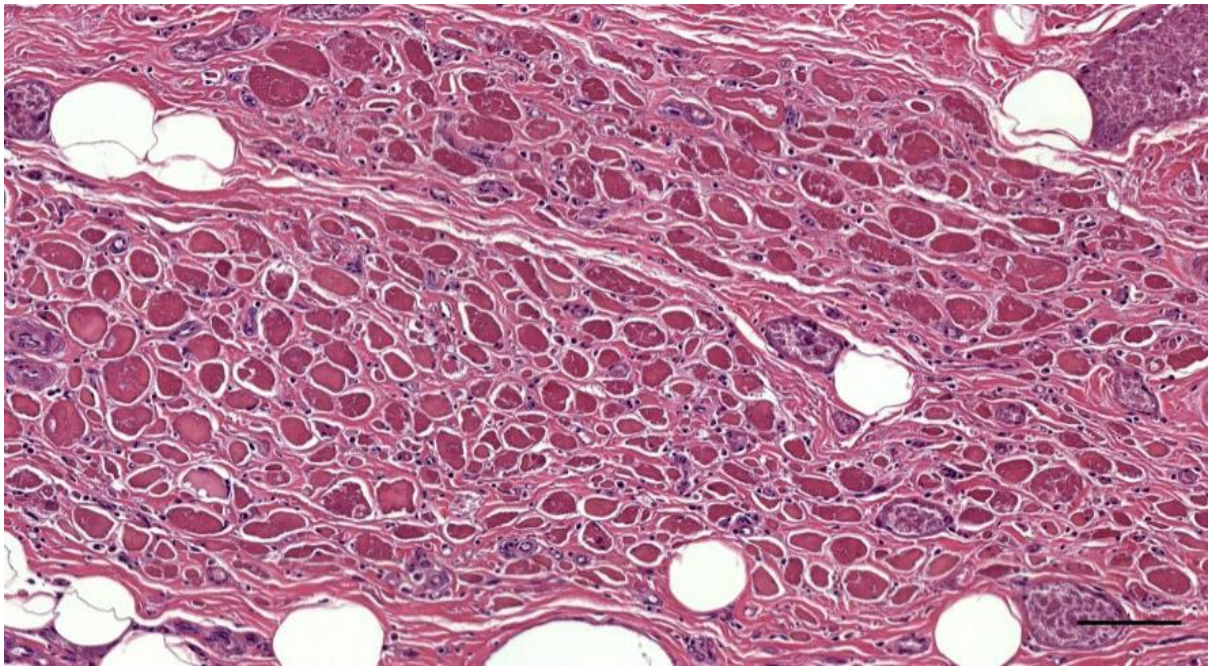

Figure 390. Histological detail (HE staining) of the muscle tissue in a transverse section through the external ear canal of a Cuvier´s beaked whale at about 2 cm beneath the skin (ID177/19_R04_01). Scale bar 100 µm

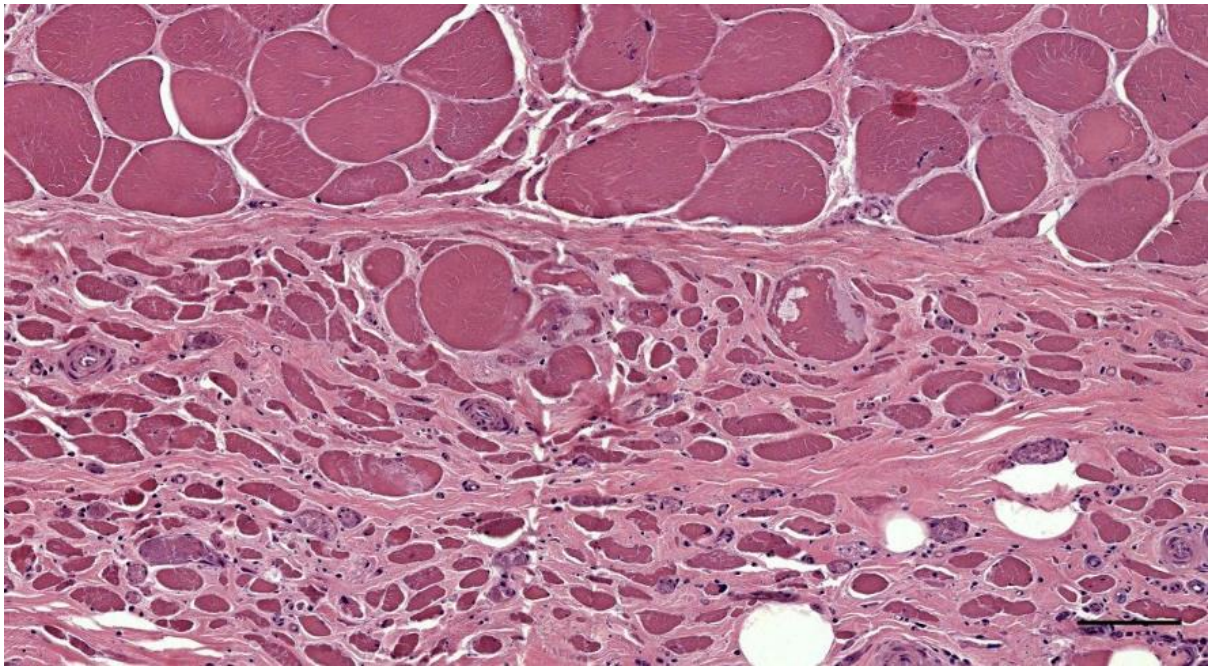

Figure 391. Histological transverse section through the external ear canal of a Cuvier´s beaked whale. Scale bar 100 µm

1.3.1.2 Striped dolphin (ID145/18)

Artificial lumen	A		0	0	0	0	0	0	0	0	0	0	0	A	0	0
Melanin	1		1	1	1	1	1	1	1	1	1	1	1	A	1	1
Blubber	1		0	0	0	0	0	0	0	0	0	0	0	A	0	0
Glands (Y/N)	0		0	0	0	0	0	0	0	0	0	0	0	A	0	0
Muscle	0		1	0	0	0	0	0	0	0	0	0	0	A	0	0
Cartilage (Y/N)	0		1	1	1	1	1	1	1	1	1	1	1	A	1	1
Vascular lacunae (Y/N)	0		0	0	0	1	1	1	1	1	1	1	1	A	1	1
Nervous button (Y/N)	0		0	0	1	1	1	1	1	1	0	0	1	A	1	1
Pathology (Y/N)	1		0	0	1	0	0	0	0	0	0	0	0	A	0	0
Cellular infiltration (Y/N)	1		1	0	1	1	1	1	1	1	1	1	1	A	0	0
	Turin															

Figure 392. Schematic representation of the left ear canal and associated soft tissue from superficial (left) to deep (right).

This animal presented a mild myofibre atrophy with focal nuclear clumps (Figure 393, Figure 394). Similar lesions have been observed in actively stranded dolphins that showed muscular denervation atrophy (Sierra et al., 2017). The specimen in our study was likely a bycaught animal, based on the necropsy findings.

There were also mononuclear cells in the superficial dermis around the porus acusticus externus to at least 6mm beneath the epidermis (Figure 384, Figure 385). It appeared as a mixed inflammatory reaction with mainly mononuclear cells in a perivascular distribution, and some neutrophils. The same inflammatory reaction was present in deeper sections (Figure 386).

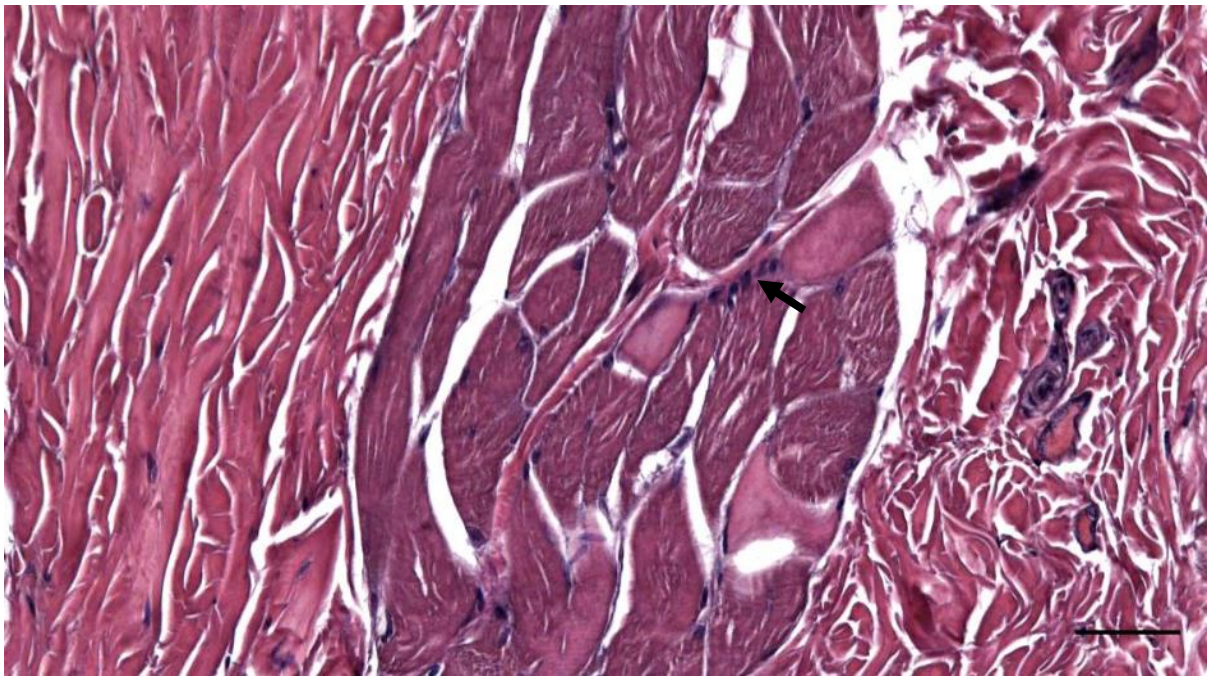

Figure 393. Histological detail image (HE staining)(145/18_R3) of a muscle with signs of mild atrophy, nuclear clumps (arrow). Scale bar 50 µm

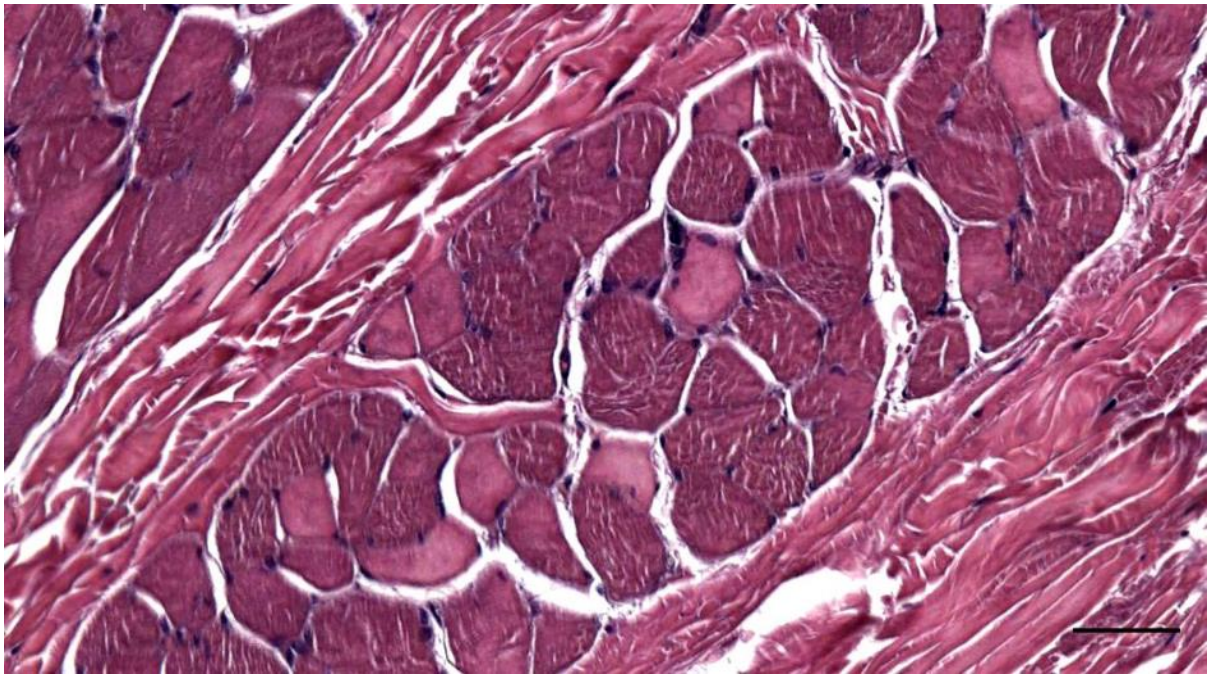

Figure 394. Histological detai image (HE staining)(145/18_R3) of a muscle with signs of mild atrophy. Scale bar 50 µm

1.3.2 Muscle degeneration, regeneration and necrosis

1.3.2.1 Striped dolphin (ID419/16)

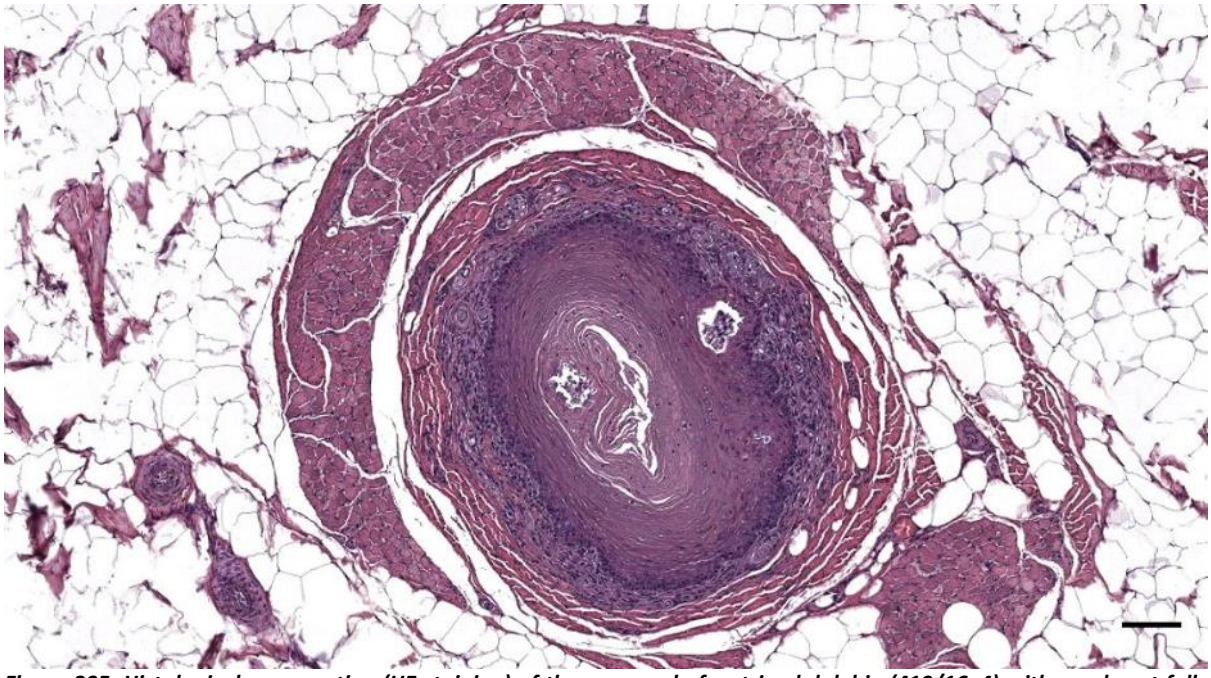

Figure 395. Histological cross-section (HE staining) of the ear canal of a striped dolphin (419/16_4) with an almost fully obstructed lumen, and two glandular excretory ducts travelling through the epithelium. Muscles with degenerated fibres. Scale bar 100 µm.

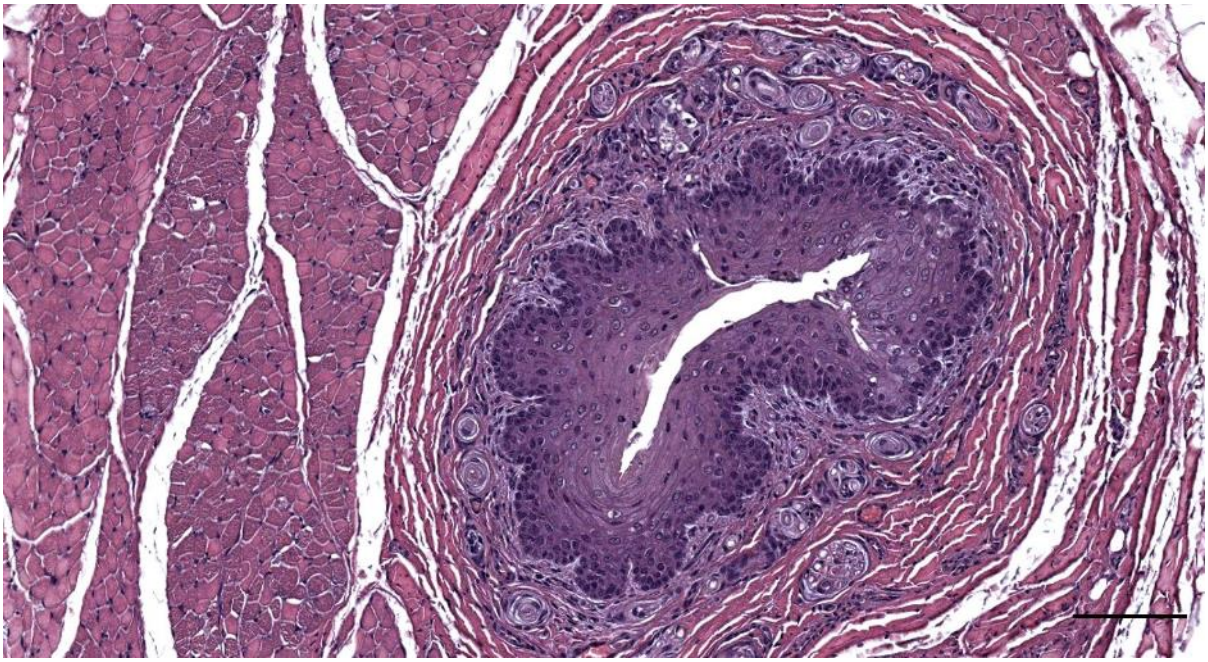

Figure 396. (419/16_4) Ear canal with abundant lamellar corpuscles in the subepithelial tissue. Muscles with degenerated fibres. Scale bar 100 µm.

1.3.2.2 Striped dolphin (ID509/17)

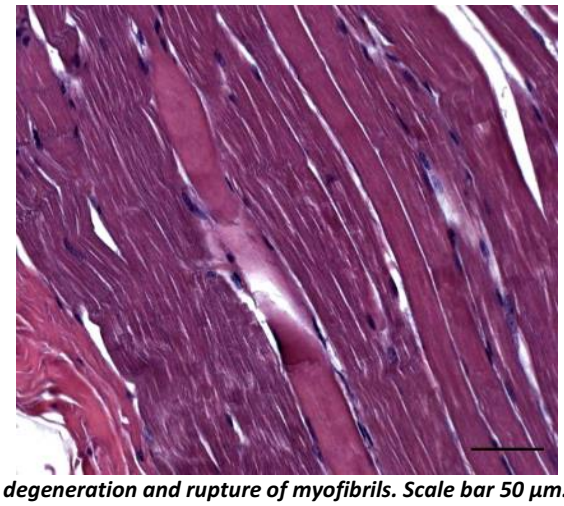

Figure 397. (509/17_L6) Muscle degeneration and rupture of myofibrils. Scale bar 50 µm.

Sample block	Left	1 - skin	2	3	4	5	6	7	8	9	10L	11	12	13	14	15	Lx1
Artificial lumen		1	1	1	0	0	0	0	A	0	A	0	0	0	0	0	0
Melanin		0	0	0	0	1	1	1	A	1	A	1	1	1	1	1	1
Blubber		1	1	1	1	0	0	0	A	0	A	0	0	0	0	0	0
Glands (Y/N)		0	0	1	1	0	0	0	A	0	A	0	0	0	0	0	0
Muscle		0	0	0	1	1	1	1	A	0	A	0	0	0	0	0	0
Cartilage (Y/N)		0	0	0	0	0	1	1	A	1	A	1	1	1	1	1	1
Vascular lacunae (Y/N)		0	0	0	0	0	0	0	A	1	A	1	1	1	1	1	1
Nervous button (Y/N)		0	0	0	0	0	0	0	A	1	A	0	A	0	0	1	1!
Pathology (Y/N)		0	0	0	0	0	0	0	A	0	A	0	0	0	0	0	0
Cellular infiltration (Y/N)		0	1	0	0	0	0	0	A	1	A	1	1	1	1	1	1
															NF		

Figure 398. Schematic representation of the right ear canal and associated soft tissues from superficial (left) to deep (right)

1.3.2.3 Striped dolphin (ID620/17)

Subacute, mild muscle tissue damage with fractured muscle fibres and necrotic degeneration with the infiltration of inflammatory cells (and likely myogenic cells)(Figure 399), and also signs of regeneration (myogenesis) (Figure 400), indicating a subacute process. There was also oedema.

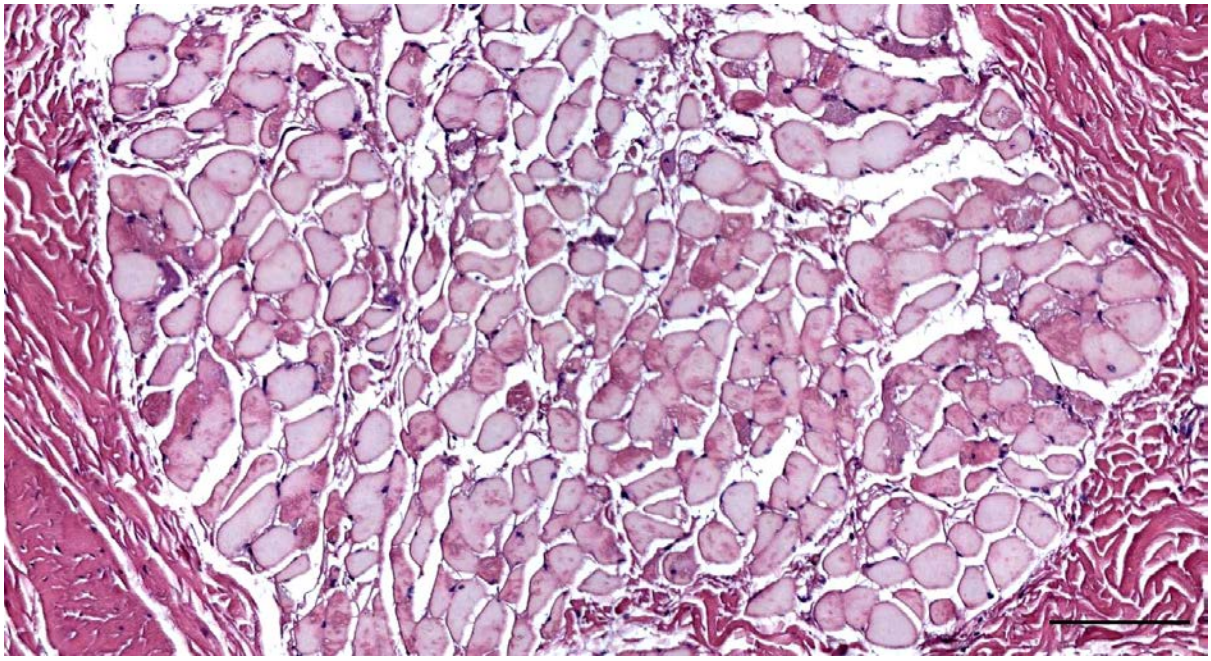

Figure 399. Muscle degeneration and necrosis with infiltration of inflammatory cells. Scale bar 100 µm.

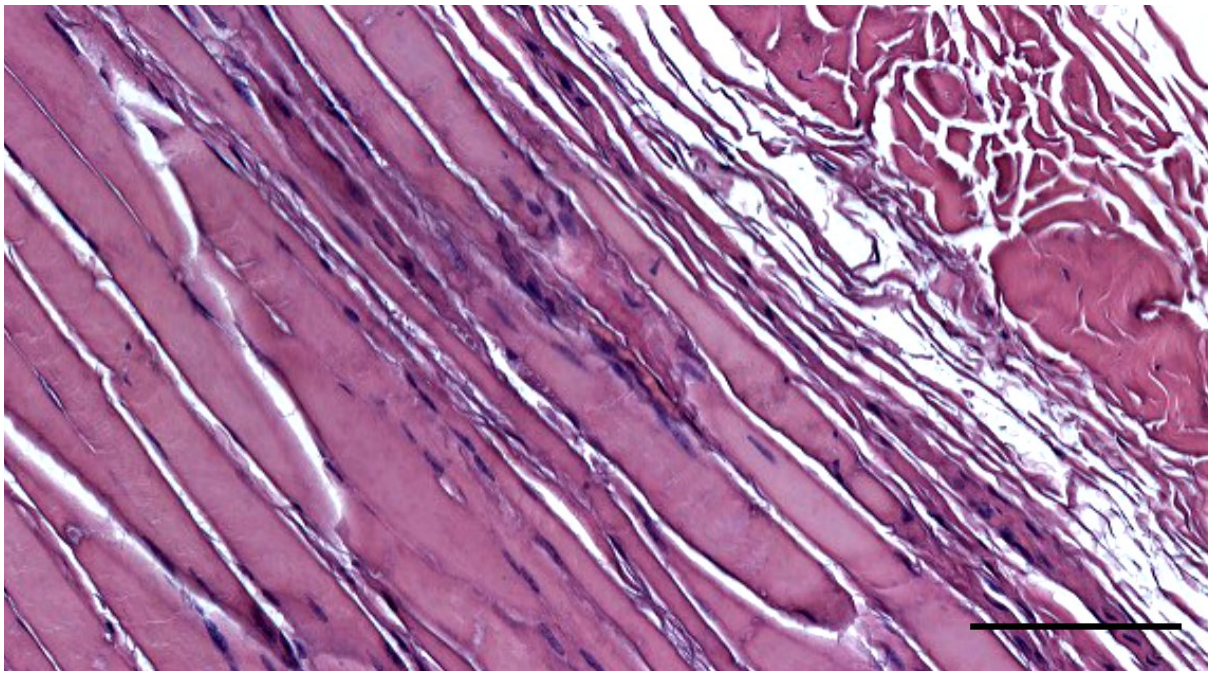

Figure 400. Detail of muscle regeneration. Scale bar 100 µm

Other findings:

- Presence of inflammatory cells in the dermal papillae of the skin, and in the superficial dermis of the distal end of the ear canal (Figure 387, Figure 388, Figure 389). Also multifocal presence of lymphocytes, plasmacells and macrophages around the glandular structures.
- Similarly, scant inflammatory cells in deeper sections between the ear canal and cartilage.
- Glands
    - the ducts contained apparent secretory cells (See Results)

- The glands contained a mineralized content, likely due to a prolonged stay of secretory product within the lumen. The epithelium was not glandular, but a stratified squamous non-keratinized epithelium. It is unsure if this could be a form of metaplasia, or that the tissue is a non-secretory excretory duct (See Results).
- Glandular structures showed signs of degeneration, and pyknotic nuclei

- There were signs of starvation visible in the adipoconnective tissue surrounding the ear canal, with the large variability in size of the fat cells, a decrease in ratio fat/connective tissue, and an infiltration of inflammatory cells with the scant presence of macrophages that often contained lipid droplets.
- Subacute, mild muscle tissue damage with fractured muscle fibres and necrotic degeneration with the infiltration of inflammatory cells (and likely myogenic cells)(Figure 399), and also signs of regeneration (Figure 400), indicating a subacute process. There is also oedema.

These findings are likely associated with the live stranding of the animal. The regeneration of the muscle fibres would not, but could be explained by the nervous symptoms the animal showed before stranding as it might have bruised itself before the stranding event.

1.3.2.4 Other striped dolphin cases with muscle degeneration

Animals: ID292/18, ID145/18, ID362/18.

1.3.2.5 Harbour porpoise (UT1709)

Acute necrosis of a scant amount of the muscular fibres around the ear canal (without the presence of inflammatory cells), together with the presence of oedema (Figure 401). This, together with the finding of contracted arteries, indicated a live stranding event, which corresponded to the information provided of this animal.

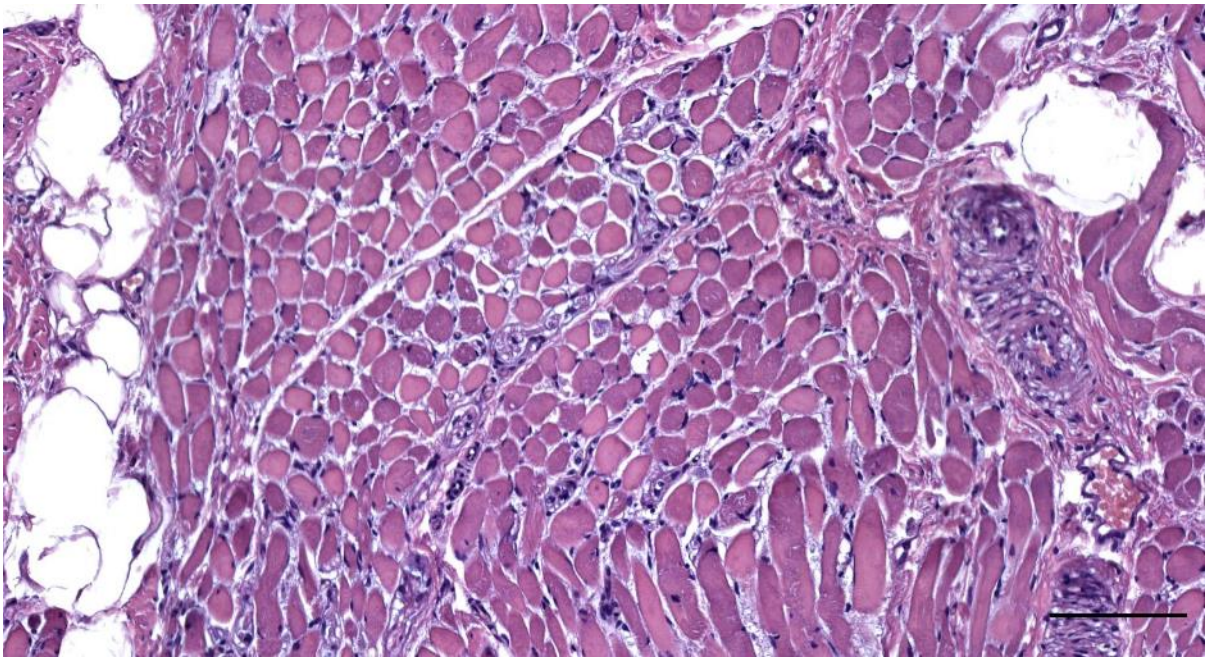

Figure 401. Histological image of the musculature around the ear canal in a harbour porpoise (UT1709_06). Acute muscle necrosis. Scale bar 100 µm.

1.3.2.6 Bottlenose dolphin (ID457)

Mild muscle degeneration (Figure 402)

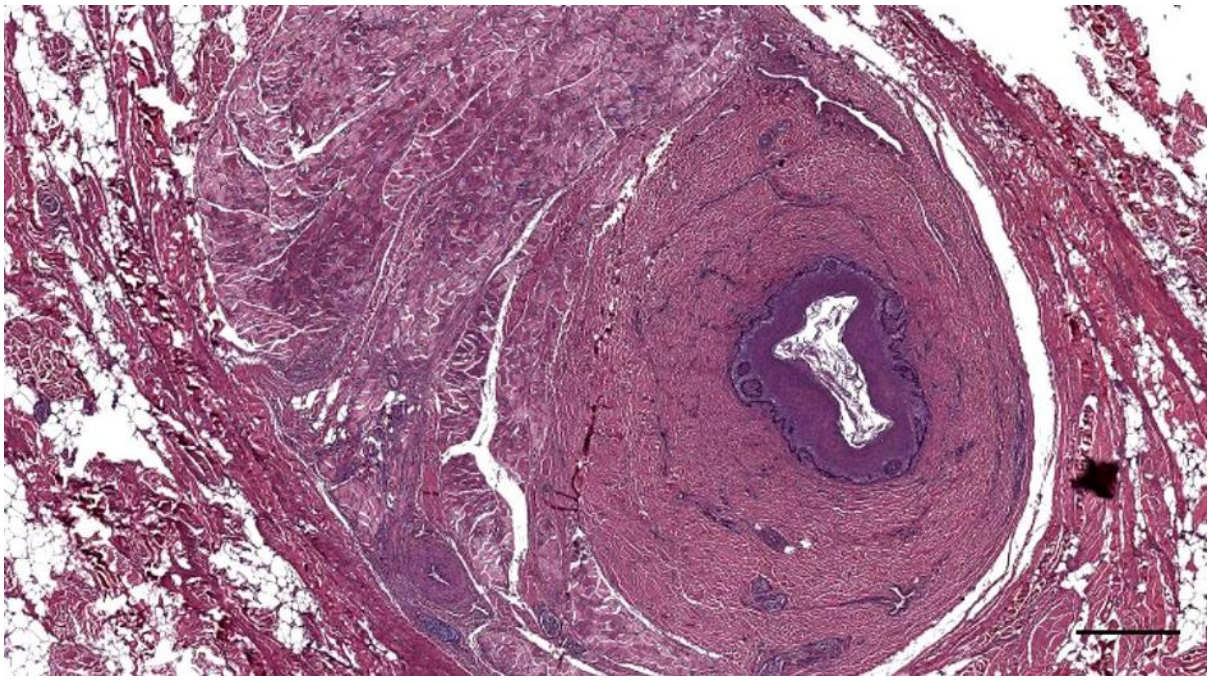

Figure 402. (457_R5) The ear canal, and degenerated muscles. Scale bar 500 µm

Artificial lumen	1	1	1	1	0	0	0	0	0	0	0	0	0	0	0	0	0	0
Melanin	0	0	1	1	1	1	1	1	1	1	1	1	1	1	1	1	1	1
Blubber	0	1	1	1	1	0	0	0	0	0	0	0	0	0	0	0	0	0
Muscle	0	0	0	1	1	1	0	1	1	1	0	0	0	0	0	0	0	0
Glands (Y/N)	0	0	0	0	0	1	0	0	0	0	0	0	0	0	0	0	0	0
Cartilage (Y/N)	0	0	0	0	0	0	1	1	1	1	1	1	1	1	1	1	1	1
Vascular lacunae (Y/N)	0	0	0	0	0	0	0	0	0	0	0	1	1	1	1	1	1	1
Nervous button (Y/N)	0	0	0	0	0	0	0	0	1	1	1	1	1	1	1	1	1	1
Pathology (Y/N)	0	0	0	0	0	1	1	0	0	0	0	0	0	0	0	0	0	0
Cellular infiltration (Y/N)	0	0	1	1	1	1	1	0	0	0	0	0	0	0	1	1	1	1
														NF				

Figure 403. Schematic representation of the tissue of the ear canal that were investigated, each column represents a tissue block.

1.3.3 Muscle fibrosis

1.3.3.1 Bottlenose dolphin (ID444)

There was one bottlenose dolphin with indications of mild endomysial fibrosis, an increase in the amount of fibrous tissue between muscle fibres (Figure 404)

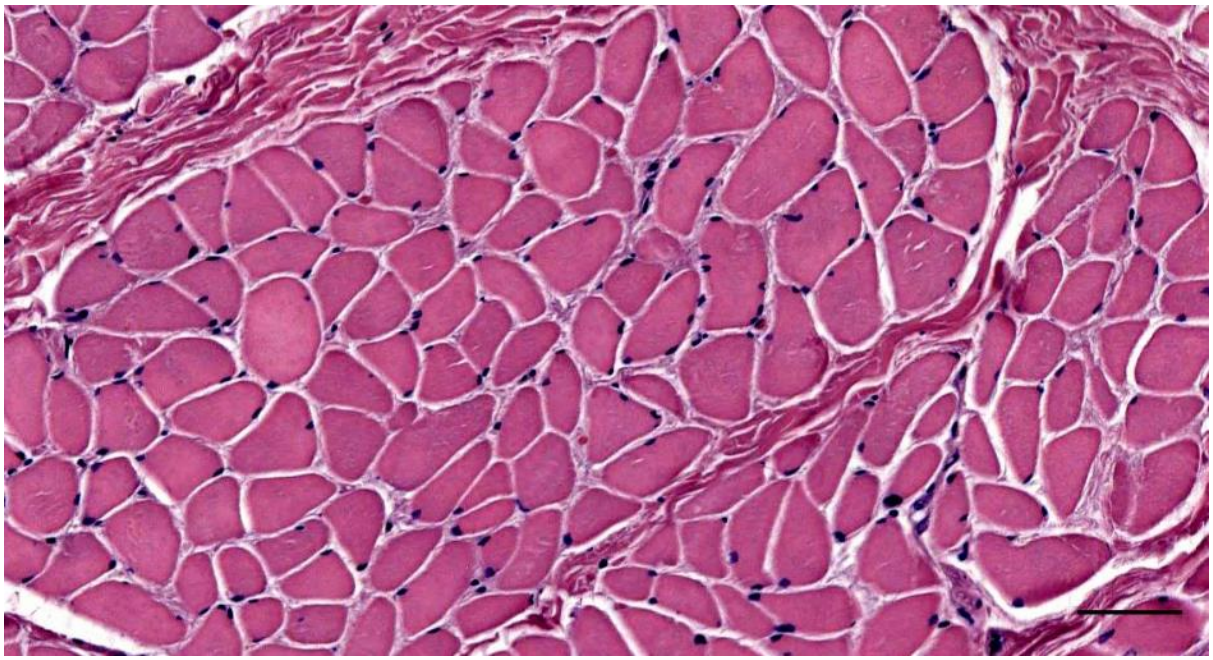

Figure 404. Histological image (HE staining) of a transverse section through a striated muscle in a bottlenose dolphin (444_L5). There is possibly a mild endomysial fibrosis. Scale bar 50 µm

1.4 Adipose tissue – effects of starvation

1.4.1 Striped dolphin (ID620/17)

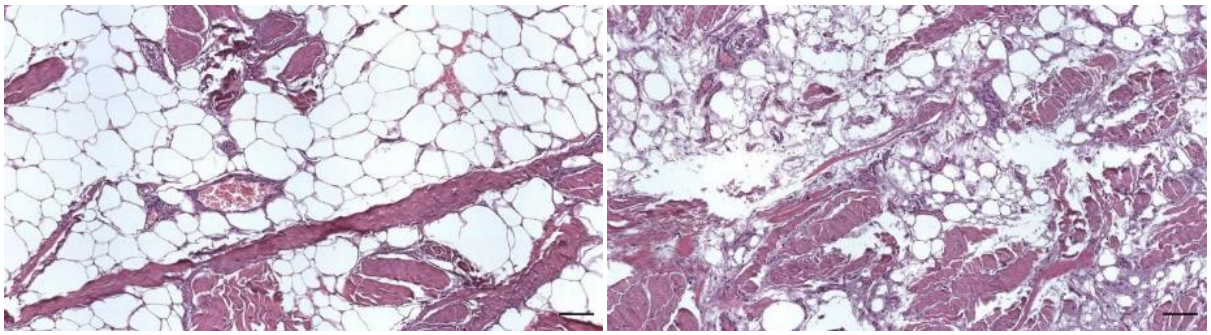

Figure 405. Comparison of two areas of the adipoconnective tissue in the same histological section (HE) around the ear canal in a striped dolphin (ID620/17-L6) Left: seemingly healthy adipoconnective tissue. Right: effects of starvation, with shrinkage of the fat cells and a decrease of the ratio fat/connective tissue. There is a marginalisation of inflammatory cells, with scant macrophages with lipid droplets in the cytoplasm. Scale bars 100 µm.

1.4.2 Cuvier's beaked whale (ID177/19)

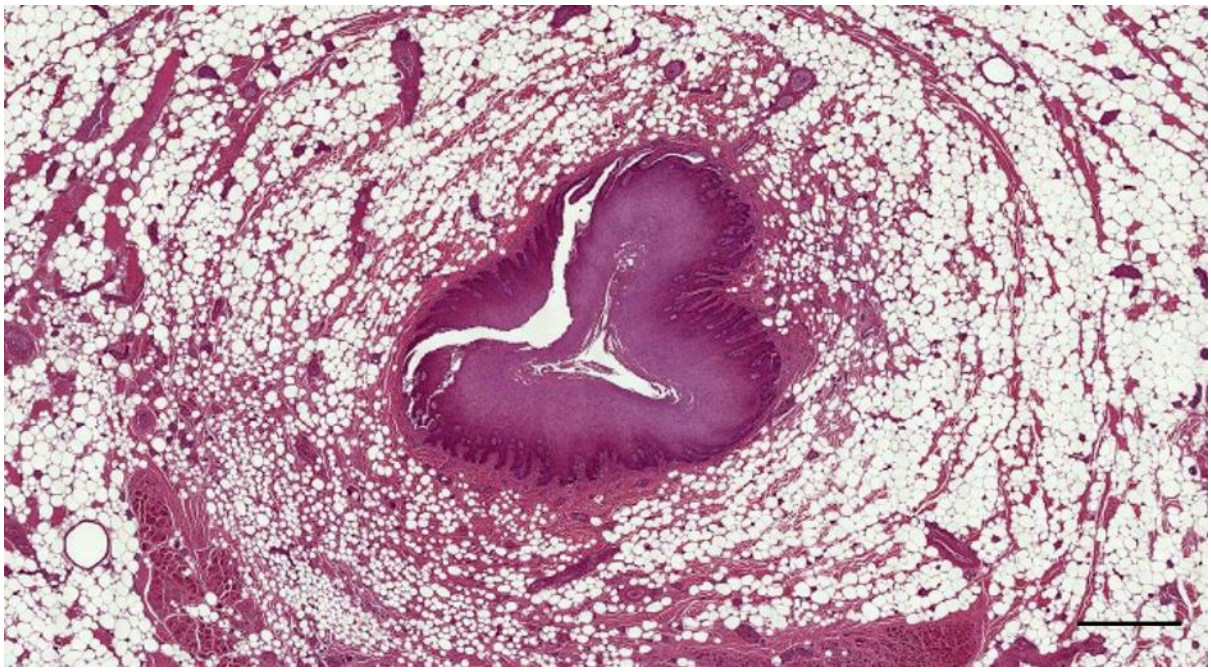

Figure 406. Histological transverse section (HE staining) through the external ear canal of a Cuvier´s beaked whale about 2 cm beneath the skin (ID177/19_R04_03). Note the variation in size of the fat cells. Scale bar 1 mm

1.5 Epithelial cyst and cholesteatoma

The difference between striped dolphin case ID362/18 with the possible cholesteatoma and the case with a likely epithelial cyst (ID44/17) is not entirely clear. Both animals presented a round structure next to the ear canal at the level of the cartilage, lined by a stratified squamous epithelium. The content of the structures seemed different in that the cyst contained desquamated epithelial cells and necrotized keratin, while in the other case there were likely cholesterol clefts. Future research is needed to characterize both cases, and to compare with any mineralized content as was sometimes seen in glandular structures. It is unknown if these findings were benign and if they could have any impact on the animal.

A cholesteatoma of the external ear canal is a destructive and expanding growth of the squamous epithelium of the canal, forming a cystic accumulation of keratin. It occurs without a specific cause (congenital or spontaneous), or secondary to inflammation, surgery, radiation, or trauma (Holt, 1992; Owen et al., 2006). It has been described in the human ear canal, although uncommon and more commonly encountered in the middle ear (Heilbrun et al., 2003; Aswani et al., 2016). When in the external ear canal, the most common symptoms (if any) are otalgia and otorrhea. It should also be distinguished from *keratosis obturans*, the accumulation of large keratin plugs inside the ear canal, accompanied by acute, severe pain and loss of hearing (Piepergerdes et al., 1980). The cases described here, do not present any types of inflammation, or bulging into the ear canal, let alone bone erosion, as described for cholesteatoma (Pernick, 2020). Based on the current histological results, it cannot be stated with certainty that it is indeed a cholesteatoma, for that, an immunohistochemical investigation would be needed to characterize the cellular nature and possibly the proliferative indexes of the cells (e.g. using various cytokeratin antibodies, and anti-Ki67)(Banco et al., 2014).

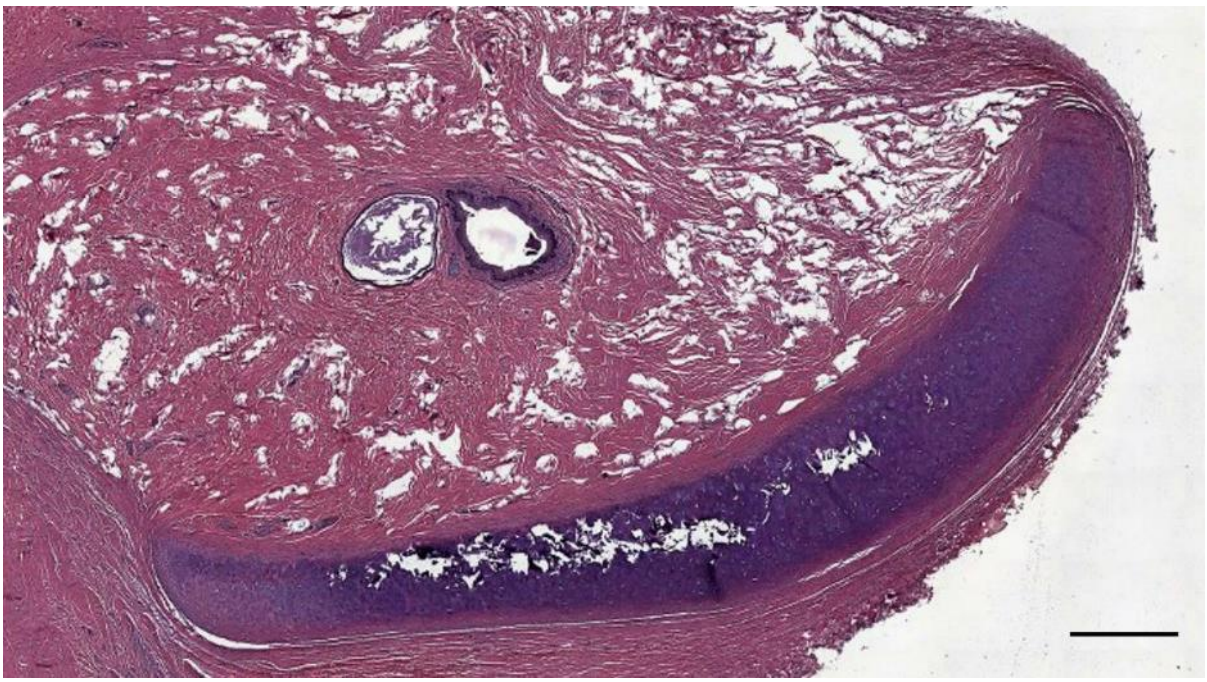

Figure 407. Histological image (HE staining) of a cross-section through the ear canal and cartilage in a striped dolphin at about 3 cm beneath the skin (44/17_R8). Note the ear canal, cartilage and possible epithelial cyst. Scale bar 500 µm

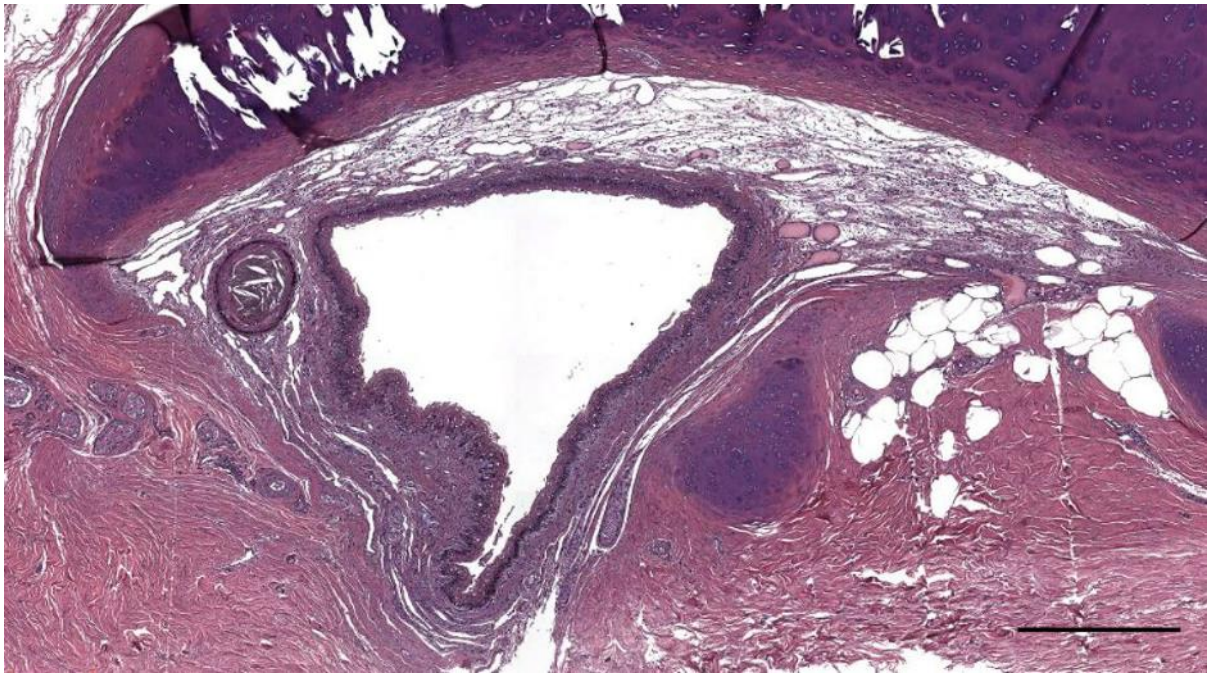

Figure 408. Histological image (HE staining) Ear canal and cartilage in a striped dolphin (362/18_L13). Note the presence of a possible cholesteatoma. Scale bar 0.5 mm

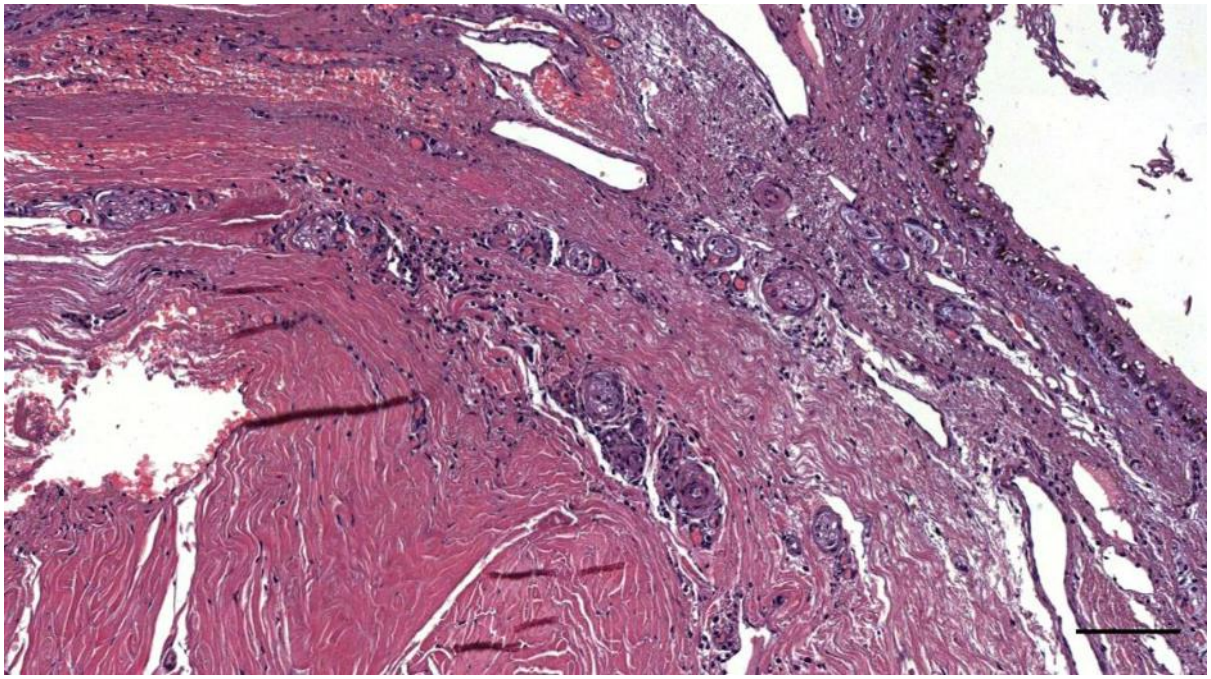

Figure 409. Histological image (HE staining) of the ear canal adnexa of a striped dolphin (362/18_L14). Note the presence of mononuclear cells (lymphocytes) in the connective tissue in the same location as the cholesteatoma but in a section that is less than 5 mm deeper. Scale bar 100 µm

1.6 Overview of pathology associated with the external ear canal in terrestrial mammals

Below is a schematic classification of otitis externa as described in terrestrial mammals, sorted according to the cause (infectious/reactive) and the presentation (acute/chronic) of the inflammation.

Presentation

- Acute
    - diffuse otitis externa (usually bacterial)
    - localised otitis externa (furunculosis)
- Chronic otitis externa

Cause

- Infectious
    - Bacterial
        - Furunculosis

Furunculosis is an infection of the apopilosebaceous unit of the hair follicle, which can lead to abscess formation (with pus and necrotic tissue). The aetiology is often associated with Staphylococcus sp. bacteria. It can be presented as a painful well-circumscribed erythematous pustule around the hair. Since there are no hairs and no associated sebaceous glands, this does not occur in toothed whales.

        - Diffuse

This process involves a diffuse involvement of the ear canal wall. It might be caused by a trauma to the meatal skin, or associated with bacterial pathogens (Pseudomonas / Staphylococcus sp.). It involves two phases: in the acute phase, the discharge is initially serous and transition into purulent, with debris that accumulates in the canal that can lead to a decreased hearing. In the chronic phase, there is scanty or no discharge, while hypertrophies of the surrounding tissue can cause occlusion of the meatus (i.e. stenotic otitis externa).

        - Malignant

The complications that could be associated with persistent inflammation of the ear canal include, perichondritis and cellulitis caused by Staphylococcus; stenosis of the ear canal: post chronic otitis externa due to fibrosis and adhesions; perforation of the tympanic membrane; and the development to malignant otitis externa. Malignant otitis externa or necrotizing otitis externa is a rare complication that commonly occurs in elderly with diabetes and less often also immunosuppressed individuals (Nussenbaum, 2020). The leading cause is *Pseudomonas aeruginosa*, although it can also occur in association with *Staphylococcus* sp., and even *Aspergillus*. The otitis externa progresses into osteomyelitis of the temporal bone, and a characteristic finding is the presence of granulation tissue at the bottom of the ear canal, at the osteocartilaginous junction. From the temporal bone, it can spread to base of the skull, dura mater, intracranial structures, and can even cause facial nerve paralysis (due to neurotoxins of Pseudomonas).

- Fungal (Otomycosis)

Most commonly caused by *Aspergillus niger/fumigatus* or *Candida albicans* (Ismail et al., 2017)

- Viral
  - HZ Oticus

Virus: Varicella zoster, involves the VII and VIII nerve; Neuralgia (Aka Ramsay Hunt syndrome)

- Haemorrhagic otitis externa and bullous Myringitis

This inflammation is associated with infection with Influenza or Mycoplasma and can lead to hemorrhagic bullae on the tympanic membrane and in the skin of the deep ear canal, associated with severe pain and a serosanguinous discharge.

- Reactive
  - Eczematous otitis externa

Eczematous otitis externa is consequential to an allergic reaction to topical agents (e.g. neomycin, hair spray, shampoo), and is often is presented with vesicles on the pinna and external ear canal with irritation and oozing of any content.

- Seborrheic otitis externa

Often associated with seborrheic dermatitis of the scalp of the head

- Neurodermatitis

This inflammation is associated with psychological factors that cause a compulsive scratching of the skin and/or outer ear.

- Radiation-induced otitis externa

This type of inflammation is a very rare complication that can occur after radiotherapy.

Other pathologies of the external ear, besides inflammation, include cystoma, many types of neoplasia, and pathologies of the pinna including diseases of the skin and associated with the cartilage (e.g. haematoma, cellulitis and (peri)chondritis, erysipelas, recurrent polychondritis), and external canal cholesteatoma (see specific case), among others.

2 Evaluation of techniques – assessment of the methodology

Table 19. Overview of the variety of techniques applied in this study

CHAPTER	OBJECTIVE	TECHNIQUE	COMMENTS/RESULTS	SUCCESS/FAIL
SAMPLING NETWORK	Species Sc (5) and Tt (5) Other species	National network Italy	Sc: 6, Tt: 2; Other species: Zc: 1, Gm: 1,	S (except Tt) S
	Species Sc (5) and Tt (5)	Local network Barcelona	Sc: 13; Tt: 0; Other species: Dd: 1; Zc: 1	S (except Tt) S
	Other cetacean species	International network	Utrecht University: L. IJsseldijk: *Phocoena phocoena: 10*	S
	Comparison terrestrial mammals		Roe deer, cow, northern giraffe (and mouse, failed because of fixation)	S
	Pinniped species	International network	ULg, T. Jauniaux U.Hannover, U. Siebert Expressed interest in collaboration; NEEDS FOLLOW-UP	F
SAMPLING PROTOCOL	Sample collection	Sampling protocol + dispersion	Italian stranding network + International spread through annual necropsy workshop ULg (Belgium)	S S
	Publication and recognition	ACCOBAMS/ASCOBANS	No attempt was made for official publication	F
TISSUE FIXATION	For histology/IHC	10% neutral buffered formalin		S
	For EM	Karnovsky's fixative		S
	Other	Paraformaldehyde	Mouse samples sent by the University of Köln. Not usable for tissue processing at the lab at BCA	F
GROSS ANATOMY AND PATHOLOGY	Gross necropsy and macroscopic evaluation	Camera Olympus + Camera cellphone +	(Type: Olympus DSLR 550D)Necropsy reports, pictures and descriptions; Type: Google Pixel 3a;	S
	Textures 3D rendering	Camera cellphone + Image processing + Texture files	Type: Google Pixel 3a; ImageJ[2]; Materialize[3]	S S S
	Gross morphology	CT-/MRI-scan	Need for a fresh, not frozen head; CT of fresh harbour porpoise (provided by Utrecht University)	F Ongoing
MICROSCOPIC ANATOMY AND PATHOLOGY	Identification of tissues of primary and secondary interest	HE-stain	Tissues of primary and secondary interest have been identified	S
	General tissue assessment	HE-stain	HE is useful for the general assessment of morphology and pathology	S
	Elastic fibres	Weigert´s elastic stain Acid Orcein Giemsa	Both techniques worked, but AOG was easier to interpret because of tissue contrast	S S

[2] Rasband, W.S., ImageJ, U. S. National Institutes of Health, Bethesda, Maryland, USA, https://imagej.nih.gov/ij/, 1997-2018.
[3] http://boundingboxsoftware.com/materialize/

CHAPTER	OBJECTIVE	TECHNIQUE	COMMENTS/RESULTS	SUCCESS/FAIL
	Detection/Exclusion of parasites in the ear canal lumen	PAS-stain & Pan-CK IHC		S
	Detection and identification of bacteria in the ear canal lumen	GRAM 1 GRAM 2	Results were indicative but non-conclusive	F F
	Identification vascular lacunae	IHC vWf		S
	Unambiguous identification and of sensory nerve formations + potential for automatic identification and segmentation	Luxol Fast Blue; Spaethe´s silver stain; Palmgren´s silver stain; Bielschowksy´s stain IHC; Masson´s trichrome (Aniline blue / Goldner)	Only IHC proved successful, but it was too expensive to apply on a large scale	F F F F S F
	Detailed morphology of lamellar corpuscles	HE	Good for general description	S
		IHC S100	Modified protocol: Dilution 1:2k + Casein blocking agent	S
		IHC NSE	Modified protocol: Dilution 1:250 + Casein blocking agent	S
		IHC NF	Standard protocol	S
		IHC PGP9.5	Modified protocol including melanine bleaching 1min + Ab dilution 1:500-1:2k + Casein blocking agent	S
		All alternative histochemical stains mentioned above	This technique did not provide additional information	F
		Confocal microscopy	Using NF, S100, PGP9.5 and Dap1	Work in progress
	Identification of other SNF	IHC PGP9.5	Good technique – Needs more evaluation in other tissues (e.g. vibrissae)	S
		IHC NF	Can show free nerve endings	F
		IHC NSE	Provided no additional information	F
		IHC S100	No other SNF were found using anti-s100	F
				S
	Pathology	Histological techniques	Succesfulness depended on the type of findings, tissue quality etc.; E.g. purulent otitis externa in striped dolphin has not yet been fully understood; Further investigations and appropriate techniques are considered to be used in the future.	S/F
MICROSCOPY MATERIAL	General microscopic assessment	Olympus BX41 (Olympus Italia S.r.l., Milan, Italy)		S

CHAPTER	OBJECTIVE	TECHNIQUE	COMMENTS/RESULTS	SUCCESS/FAIL
	Slide digitization	- D-sight (A. Menarini Diagnostics, S.r.l., Florence, Italy);	Semi-automatic (full automatic gave bad results); Limited to 5 slides; Output: .jp2 or online access Telepathology (Web-D-sight+)	S
		- Scanscope XT (Aperio, Vista, CA, USA)	Fully automatic scanning; batches up to 200 slides; output: .SVS	S
	Server-based access to slides (tissue assessment + images for publication + image sharing with external partners)	Server: Telepathology (Visia Imaging S.r.l., San Giovanni Valdarno (AR), Italy		S
	Detailed pictures	Leica DMD108 (Leica Microsystems CMS GmbH, Milan, Italy)	Magnification up to x100. Successful with HE stainings; other stainings need more evaluation for a correct adjustment of the image parameters	S
3D RENDERING FROM HISTOLOGY	Image File conversion	Gdal translate; Aperio Imagescope[4] (Leica Biosystems S.L.U.)	Jp2 -> Tif (with possible resolution adaption): batch processing; .SVS -> tiff. (with possible resolution adaption): manual processing	S S
	Image processing (area of interest; size and resolution; colour matching; etc)	ImageJ + general image processing software		S
	Image alignment	ImageJ Register Virtual Stack slides[5] ImageJ TrakEM2[6]	Automated registration, with adjustment of parameters; Successful on a small Scale bar with little variation in the image; Manual rigid registration;	S S
	Digital tissue classification (Masson´s trichrome stained slides)	General image processing software	Colour channel separation: technique works, but does not provide results needed for true tissue segmentation; Good and promising results; not as flexible as ILastik;	S S
		ImageJ Trainable Weka segmentation[7]; Ilastik[8] (v1.4.0)	Good results; best software for this purpose.	S

[4] https://www.leicabiosystems.com/digital-pathology/manage/aperio-imagescope/
[5] http://imagej.net/Register_Virtual_Stack_Slices
[6] https://imagej.net/TrakEM2
[7] https://imagej.net/Trainable_Weka_Segmentation
[8] Berg, S., Kutra, D., Kroeger, T., Straehle, C. N., Kausler, B. X., Haubold, C., et al. (2019). ilastik: interactive machine learning for (bio)image analysis. Nat Methods 16, 1226–1232

CHAPTER	OBJECTIVE	TECHNIQUE	COMMENTS/RESULTS	SUCCESS/FAIL
	Segmentation and modelling	3D Slicer		S
	3D Rendering	Blender (v 2.79 – 2.82)[9]		S
		Amira 6.0 software (FEI, France)	A comprehensive software that includes the image processing and tissue classification and 3D rendering all in one. A test version proved very promising, but a budget should be made to acquire the full version software.	F

[9] Community, B. O. (2018). *Blender - a 3D modelling and rendering package*. Stichting Blender Foundation, Amsterdam. Retrieved from http://www.blender.org

2.1.1 *Sampling protocol delphinid head: external ear canal*

It is recommended to have a specific person dedicated to the dissection of the head. As such, the head should be separated from the body as soon as possible (e.g. after sampling of the cerebrospinal fluid).
If not possible to have a specific person dedicated to this task, for whatever reason, samples can be taken in a gross matter, kept in formalin, and trimmed down to smaller sizes for further fixation.
If sampling the individual tissues is not possible, the entire head can be stored frozen at -20°C.

- External ear canal and surrounding tissues.

  The lower jaw can be removed for easier access, but it is recommended to leave it intact in order not to produce any accidental damage to the soft tissues of the ear canal.

  If possible, the external ear canal and surrounding soft tissues (radius of 1-2 cm) should be sampled together with the tympanoperiotic complex (TP complex) as a whole. If the TP complex will not be removed, the soft tissues of the ear canal should be dissected as far medial as possible.

1. Locate the external ear opening: small indent few cm caudal and slightly ventral to the lateral commissure of the eye (See Figure 410, Figure 411).
2. Mark a rectangle around the opening with sides of about 1,5 cm in length
3. Insert the blade through the dorsal and caudal side of the rectangle in a straight angle to the longitudinal axis of the body, down to the level of the bone, and remove the soft tissues dorsal and caudal to the rectangle.
4. Insert the blade through the ventral and rostral side of the rectangle in a straight angle to the longitudinal axis of the body only as deep as the height of the blubber layer, and remove the skin and blubber ventral and rostral to the rectangle. (See Figure 412)
5. On the rostral side, insert the blade deeply in a straight angle. As such, you will touch the lateral side of the body of the mandible (*corpus mandibulae*). Retreat the blade and direct it slightly more caudally. Do this until the blade passes the caudal margin of the mandible. Next, dissect the tissues towards caudal. Reinsert the blade at the same location and cut through the soft tissues following the arch formed by the mandible, the squamosal and the exoccipital bone, i.e. from rostral to rostrocaudal to caudal to caudoventral direction (See Figure 413, and Figure 414)
6. Further dissect any remaining soft tissues and the TP-complex (Figure 415): separate protocol available at http://www.zoology.ubc.ca/files/Ear_extraction_and_fixation_protocol_UBC.pdf
7. Store samples in 10% neutral-buffered formalin (to be refreshed after 24h).

Contact: Steffen De Vreese - steffen.devreese@lab.upc.edu / steffen.devreese@studenti.unipd.it
Laboratori d'Aplicacions Bioacústiques (LAB) - Universitat Politécnica de Catalunya (UPC)
Dipartimento di Biomedicina Comparata e Alimentazione (BCA) - Università degli Studi di Padova (UniPD)

Figure 410. Left lateral view of the eye and external auditory opening of a striped dolphin. Note the location of the external auditory opening, ±4 cm caudoventral to the caudal commissure of the eye. In striped dolphins the opening is sometimes marked with a pigmentation that continuous as a very fine line in the direction of the angle of commissure of the mouth (see also Figure 411. Detail of Figure 410. Left lateral view of the external auditory opening with marked linear pigmentation).

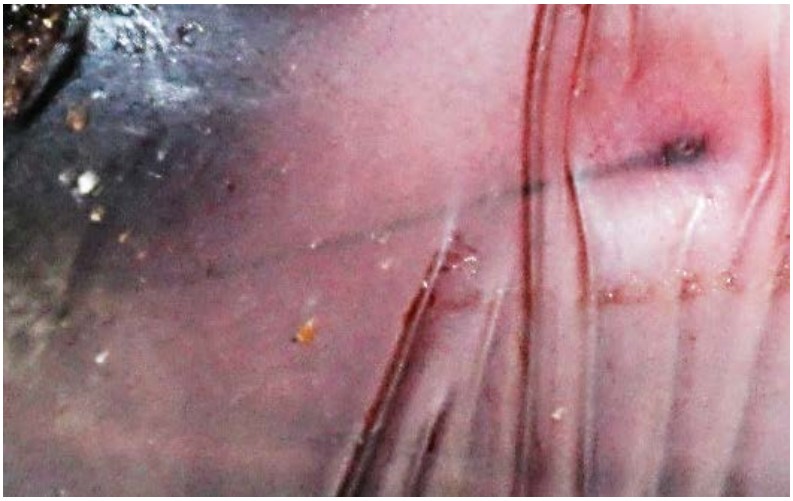

Figure 411. Detail of Figure 410. Left lateral view of the external auditory opening with marked linear pigmentation

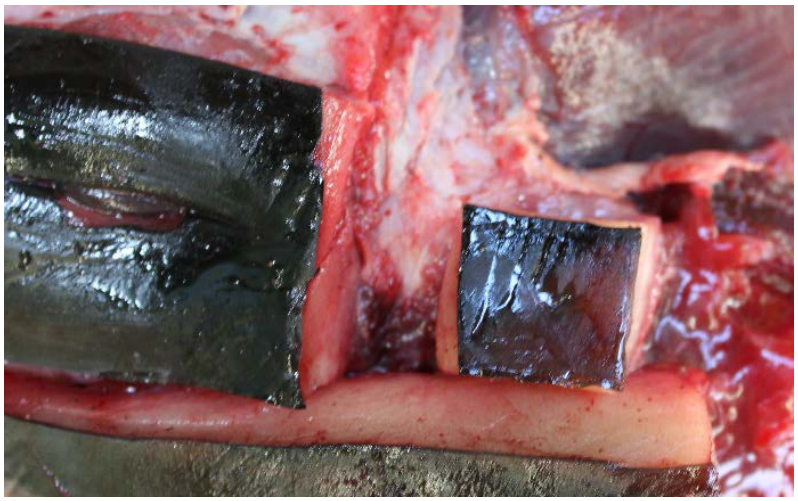

Figure 412. Left lateral view of the external ear opening in the centre of the rectangle with the soft tissues removed around it.

Contact: Steffen De Vreese - steffen.devreese@lab.upc.edu / steffen.devreese@studenti.unipd.it
Laboratori d'Aplicacions Bioacústiques (LAB) - Universitat Politécnica de Catalunya (UPC)
Dipartimento di Biomedicina Comparata e Alimentazione (BCA) - Università degli Studi di Padova (UniPD)

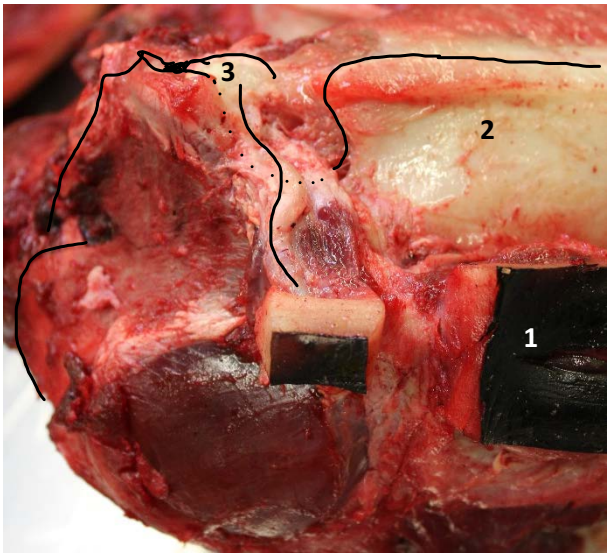

Figure 413. Left lateral view of the external ear canal from the external opening to the tympano-periotic complex. Note the spiralling course starting (from external to internal) in caudoventral direction, then in rostroventral direction, then back in caudoventral direction (±45°) and reaching the tympanic bone in a horizontal manner. The canal enters the paraotic cavity in the caudodorsal margin of the trench (dotted line) created by the caudal ramus of the mandible (2) rostrally, the retrotympanic and reotrarticular (postglenoid) process of the squamosal dorsally, and the lateral margin of the exoccipital bone caudally. 1. Eye, 2. Mandible, 3. Bulla tympanica.

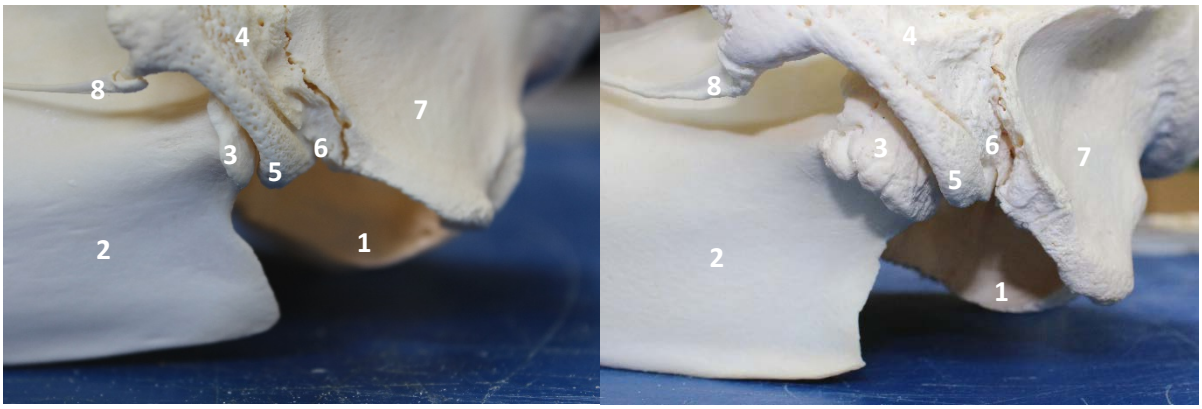

Figure 414. Left lateral view of a close-up of the ear region in the skull of a striped dolphin (left) and a bottlenose dolphin (right). Note that the tympanoperiotic complex is missing, therefore, the basioccipital bone (1) is visible; 2. Mandible with condyle (3) situated in the mandibular fossa of the squamosal (4) and part of the temporomandibular joint with the latter; 5. Retroarticular process of the squamosal; 6. Retrotympanic process of the squamosal; 7. Exoccipital; 8. Jugal bone.

Contact: Steffen De Vreese - steffen.devreese@lab.upc.edu / steffen.devreese@studenti.unipd.it
Laboratori d'Aplicacions Bioacústiques (LAB) - Universitat Politécnica de Catalunya (UPC)
Dipartimento di Biomedicina Comparata e Alimentazione (BCA) - Università degli Studi di Padova (UniPD)

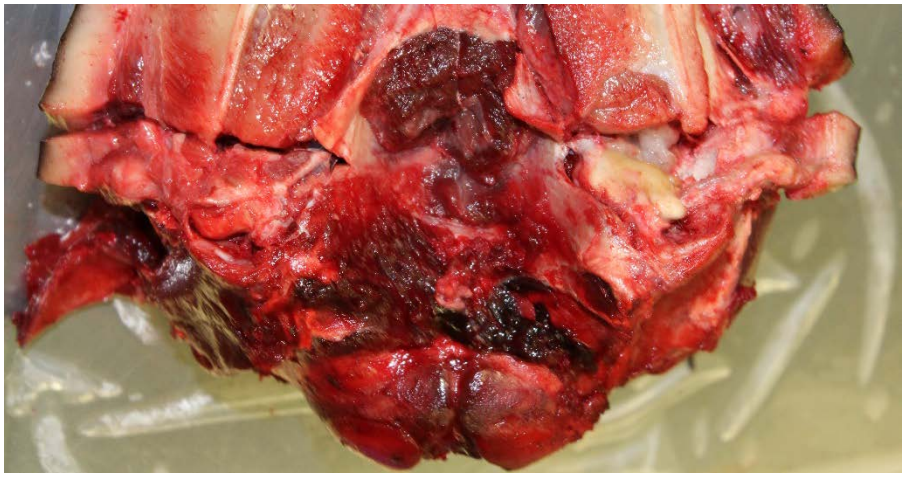

Figure 415. Ventral view of a double-sided dissection of the ear canal and TP-complex. On the left side of the picture is the preparation as described in this protocol, while on the right is the ear canal and TP-complex exposed for educational purposes.

OTHER TISSUES

Other tissues of interest are included in the following list, and below you can find a form to fill in any details.

- Intramandibular fat body: complete transverse section of at the level of the pan bone.
- Extramandibular fat body: complete transverse section (caudo)lateral to the mandible
- Wall of the ventral sinus system (pterygoid and peribullar sinus)
- Blowhole (anterior and posterior lips)
- Nasal sac system (separate protocol will be sent with future updates)
- Ocular region: transition of skin to mucosa
- Skin of the most rostral part of the muzzle, both lower and upper jaw.
- Skin of the nose, rostrolateral to the melon: vibrissal crypts
- Belly skin
- Urogenital fold
- Skin on ventral and dorsal side of the fluke

Baleen whales: If possible, please collect the entire head (stored frozen), or take specific samples of all tissues related to sound reception, with primary focus on the external ear canal, the tympanoperiotic complexes, and any fat bodies if present.

Other species: Pinnipeds: Sample of the external ear canal from the external opening to as close to the tympanic membrane as possible.

Contact: Steffen De Vreese - steffen.devreese@lab.upc.edu / steffen.devreese@studenti.unipd.it
Laboratori d'Aplicacions Bioacústiques (LAB) - Universitat Politécnica de Catalunya (UPC)
Dipartimento di Biomedicina Comparata e Alimentazione (BCA) - Università degli Studi di Padova (UniPD)

ADMINISTRATIVE DATA							
DATE		**EXECUTOR**					
ANIMAL ID		**SPECIES**			**LOCATION**		
AGE		**SEX**		**WEIGHT**		**LENGTH**	
EUTHANIZED	**Y / N**	**METHOD**					
TIME BETWEEN DEATH AND NECROPSY				**CONDITION CONDE**			

SAMPLING		
FOR HISTOLOGY		COMMENTS
External ear canal		
Lateral fat body		
Intramandibular fat body		
Extramandibular fat boy		
Paraotic sinus system		
Peribullar sinus		
Blowhole anterior		
Blowhole posterior		
Ocular region + Eye		
Skin rostral muzzle (tip)		
Vibrissal crypts		
Belly skin*		
Mammary gland		
Urogenital folds		
Anus		
Penis / Clitoris		
Pectoral fin ventral*		
Pectoral fin dorsal*		
Fluke ventral + dorsal		
Nasal sac system		
Oral commissure		

Contact: Steffen De Vreese - steffen.devreese@lab.upc.edu / steffen.devreese@studenti.unipd.it
Laboratori d'Aplicacions Bioacústiques (LAB) - Universitat Politécnica de Catalunya (UPC)
Dipartimento di Biomedicina Comparata e Alimentazione (BCA) - Università degli Studi di Padova (UniPD)

* Mark location on the back side

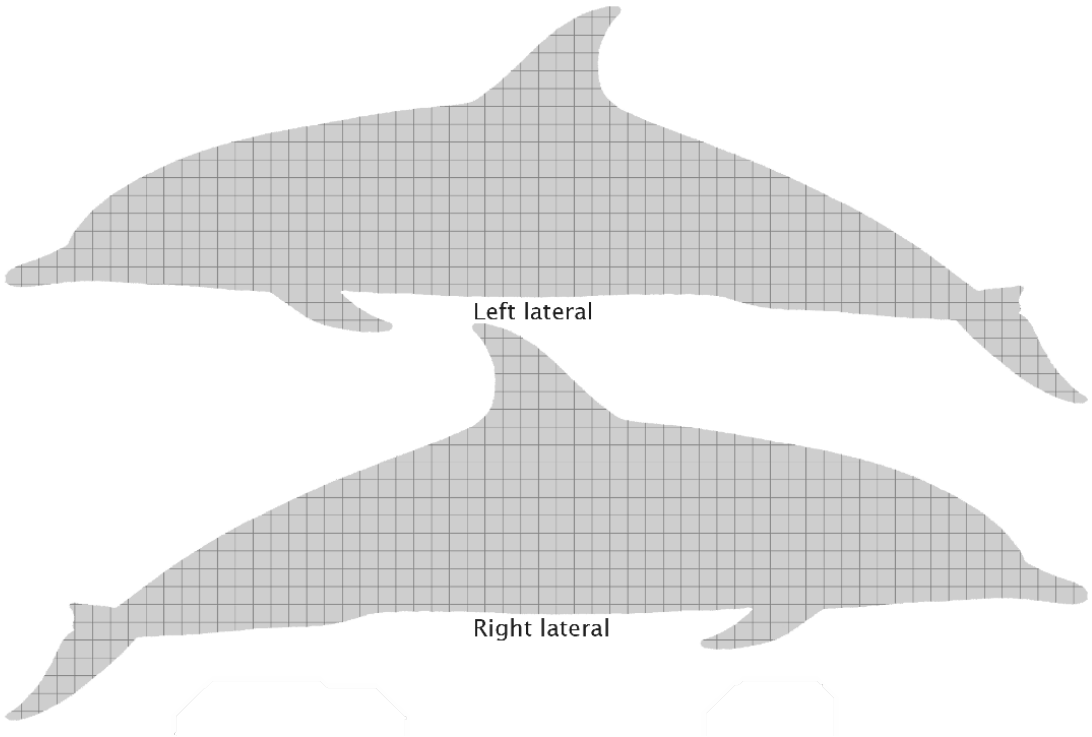

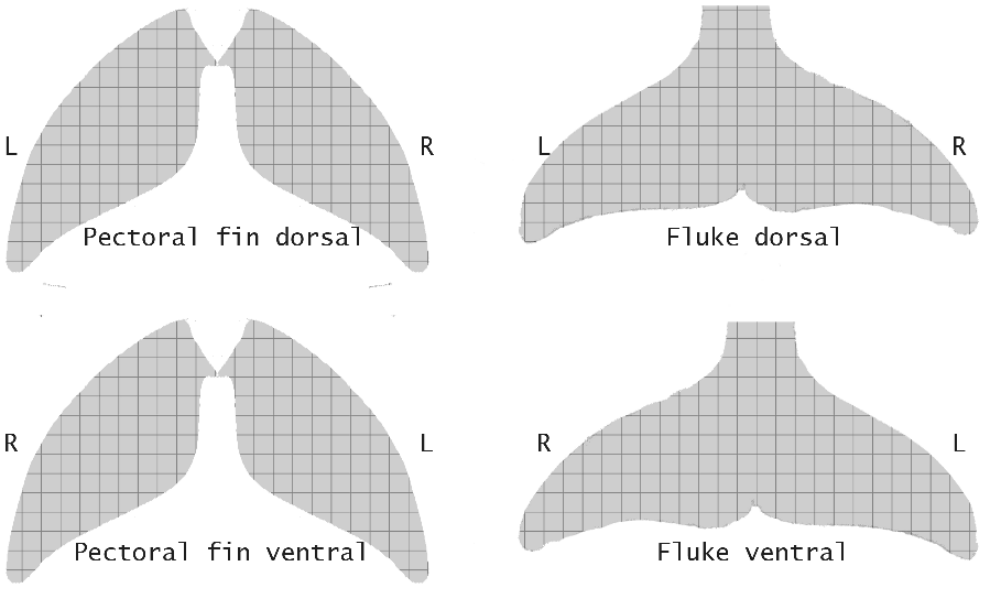

Contact: Steffen De Vreese - steffen.devreese@lab.upc.edu / steffen.devreese@studenti.unipd.it
Laboratori d'Aplicacions Bioacústiques (LAB) - Universitat Politécnica de Catalunya (UPC)
Dipartimento di Biomedicina Comparata e Alimentazione (BCA) - Università degli Studi di Padova (UniPD)

The sampling protocol was developed for the objectives of the research while taking into account the logistical limitations. Of course, the best option would be to be able to have access to fresh samples and fixate them immediately, but this was seldom achievable in practice. The post-mortem conservation **codes** (2-3, and 4 in case of a Cuvier´s beaked whale and long-finned pilot whale) proved useful for the various studies as mentioned in the sampling protocols itself, although did complicate a full anatomopathological assessment in some cases (some examples, see Figure 419, Figure 422, Figure 423, Figure 424).

We also looked at the effects of the process of freezing and defrosting on the morphology of the tissues: The impact of the freezing process alone did not have a severe impact on the identification or general morphology in any of the tissues of observed. Although the process did create some artefacts in the histological sections, all types of tissues, including nervous tissue with lamellar corpuscles, had a similar appearance as in the freshly fixated samples. In the ear canal, the main artefacts included the presence of spaces in the epithelial layers, a detachment of the superficial layers of the epithelium, and the presence of spaces in the dermis caused by a separation between connective tissue fibres, and a disruption of the cell membranes of adipocytes. Moreover, there was clear homogenization of both vascular and glandular content and glandular cells in all sections. Other artefacts that were present, were a disruption of the cell membranes of adipocytes.

The impact of the defrosting process was a lot more severe, as it created many artefacts in all layers of the tissue, and made the histological analysis of morphological and pathological features impossible in most cases, even if the animal had a relatively good conversation status (See e.g. Figure 416). As such there was a great loss of detail in all tissues associated with the external ear canal, particularly visible at magnifications of 200x and higher. There was a homogenous content in vascular and glandular structures, the muscle tissue showed vacuolization and rupture among the fibres, and so did the epithelium. However, when samples were taken from a completely frozen head and placed directly into the fixative to let defrosting take place within the container with fixative at room temperature, then the artefacts were far less severe. There were still artificial spaces in the epithelium and surrounding tissue but far less prominent and all structures, including glandular cells and lamellar corpuscles could still be identified, although not useful for detailed morphological studies.

The tissue fixation in commercial formaldehyde 10% neutral buffered proved useful for all techniques, except for TEM for which the sample underwent a double fixation in Karnovsky´s fixative (with paraformaldehyde). The state of the tissues associated with conservation code above 1, sampled and fixed as soon as possible, demonstrated post-mortem changes as:

- Degeneration of the glandular structures
- Bacteria in blood vessels (cocci and rods) (Figure 418)

- Destroyed epithelial cells and the presence of epithelial layers in the lumen, detached from the basement membrane (E.g. Figure 422) and separation of epithelium and subepithelial tissue
- The impact on the muscle tissue was not clear as there was often some kind of degeneration, likely not always due to a premortem process.
- Vacuoles in nerve fibres, possibly complicating the distinction with Wallerian degeneration (Figure 417)

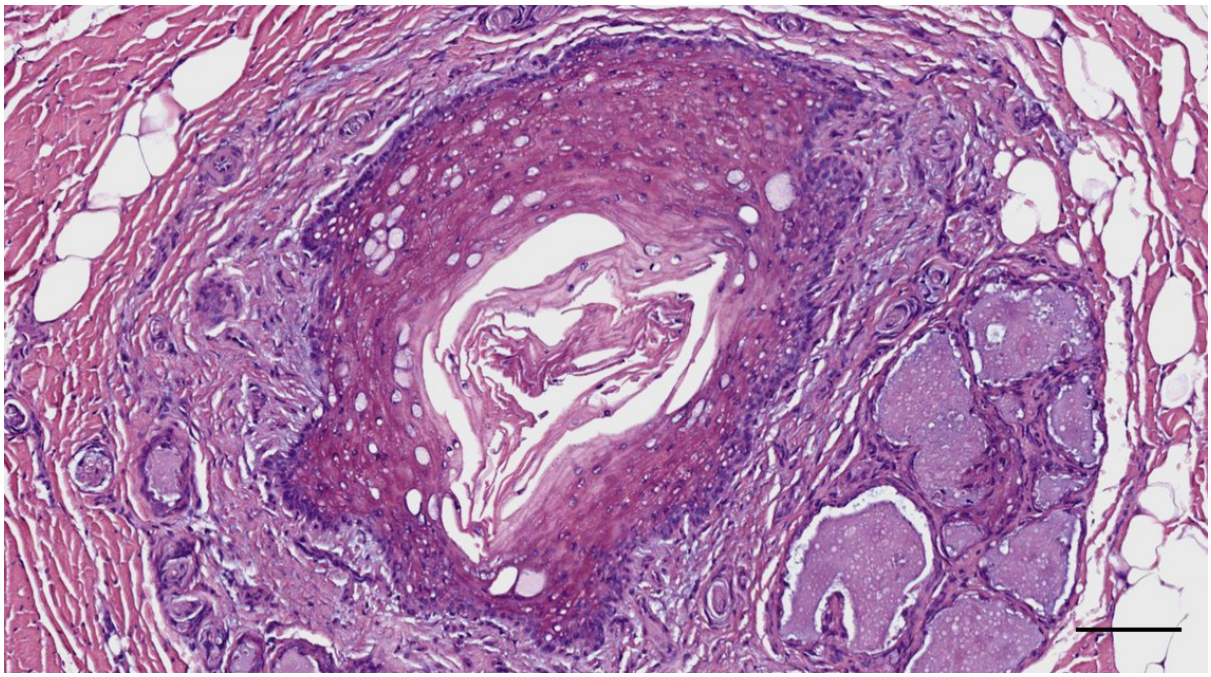

Figure 416. Histological image (He staining) of a cross-section through the external ear canal of a striped dolphin (5386_EAML_2) at about 1 cm below the surface. Note the effects of the freezing and defrosting processes as explained in the text. Scale bar 100 µm

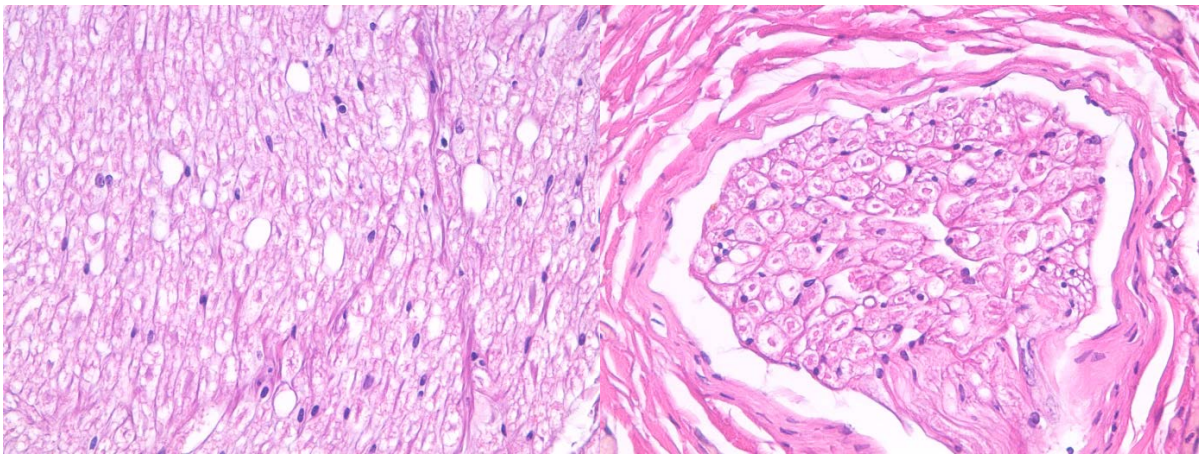

Figure 417. Histological images (HE staining) of a longitudinal and transverse section through nerve fibre (HE staining). Notice the circumaxonal vacuoles.

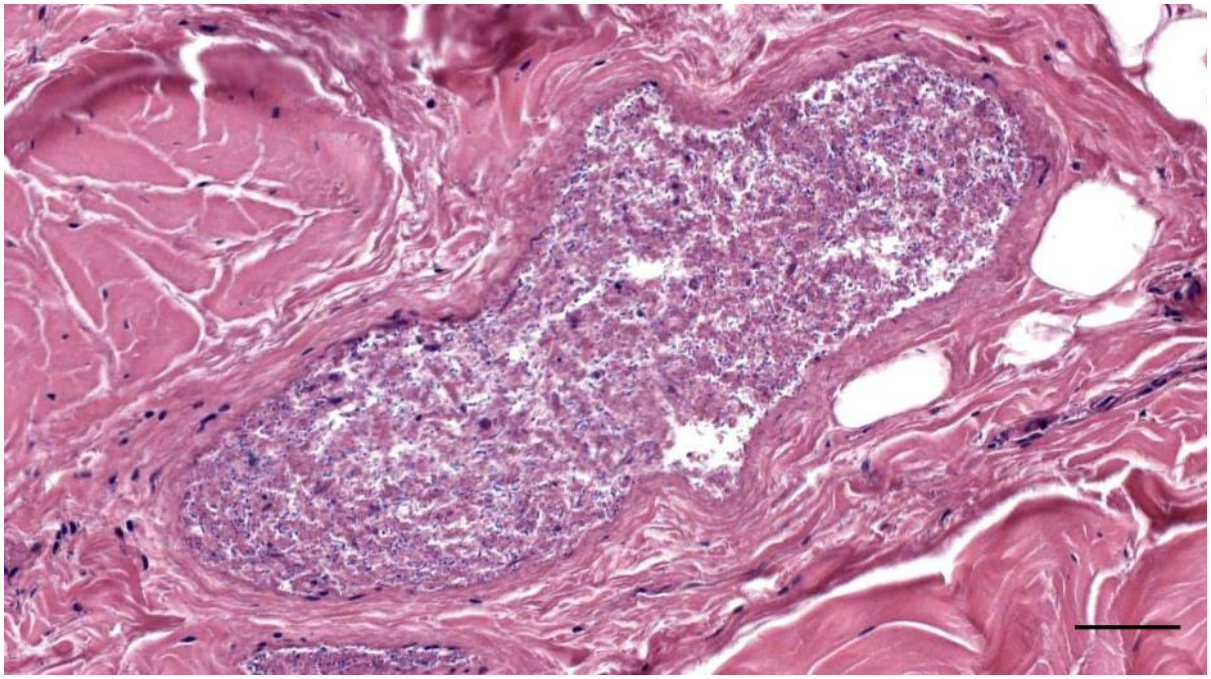

Figure 418. Histological image (HE staining) of bacteria in a blood vessel of a long-finned pilot whale (considered a post mortem). Scale bar 50 µm

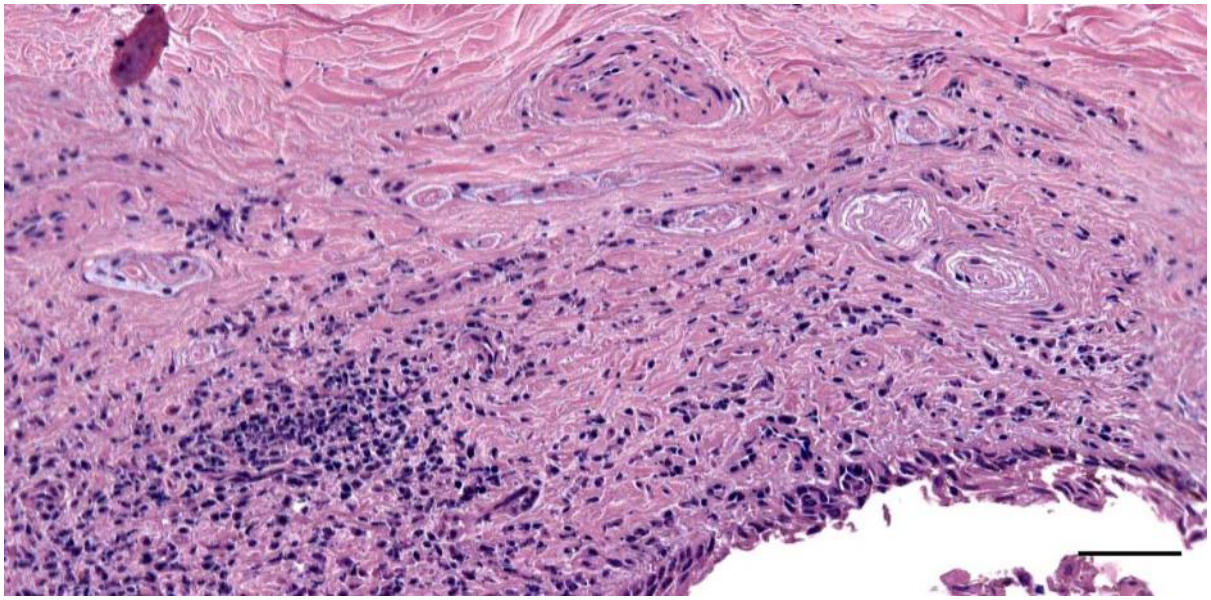

Figure 419. Histological image (HE staining) of corpuscles and small nerves in the subepithelial tissue of the ear canal of a long-finned pilot whale (ID441_L11). The distinction among nervous structures is not clear in HE sections due to the preservation state of the tissue. Scale bar 50 µm

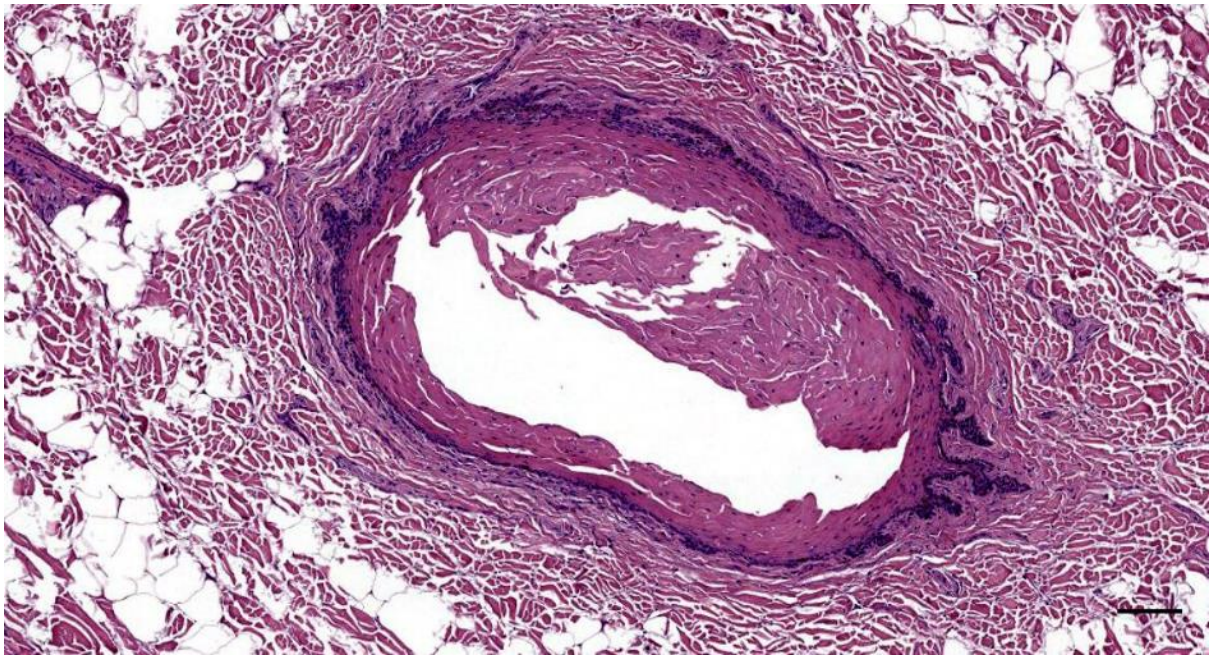

Figure 420. Histological image (HE staining) of the ear canal in a bottlenose dolphin, at about 0.5 cm beneath the skin (444_L2). It is difficult to assess to what extent the space in the ear canal epithelium is artefactual. Scale bar 100 µm

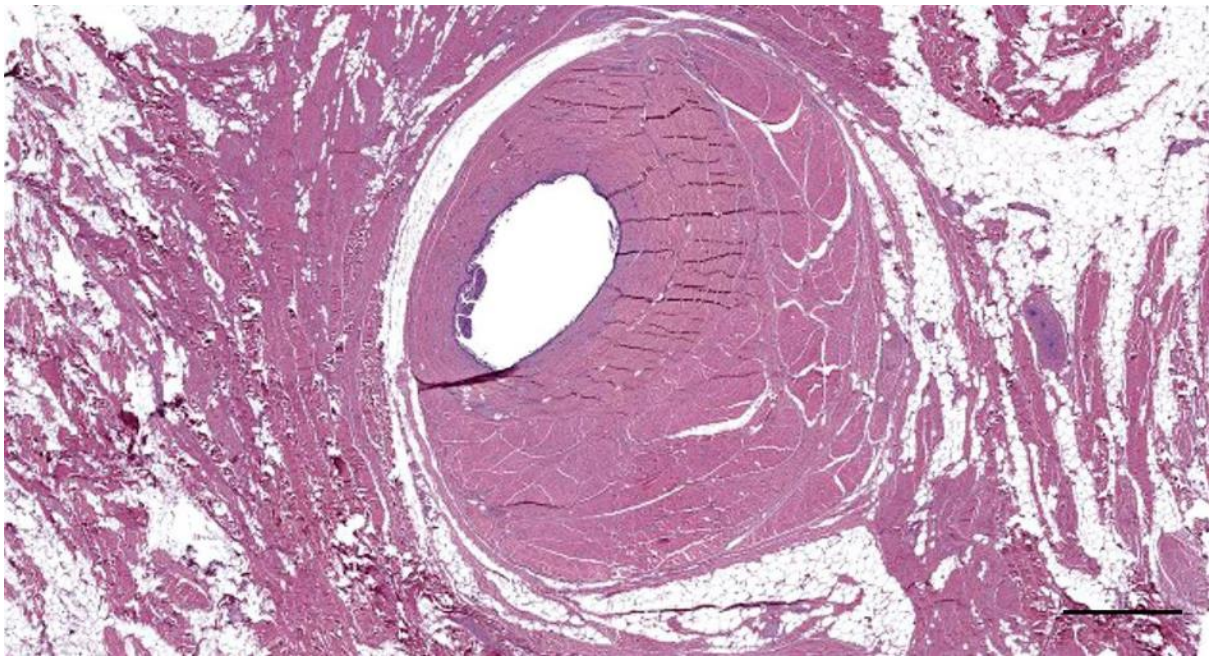

Figure 421. Histological image (HE staining) of the ear canal in a bottlenose dolphin, at about 2 cm beneath the skin (ID444_L5). Ear canal with mild multifocal chronic inflammation with lymphoplasmacytic infiltrate and melanocytes subepithelially indicating an interruption of the basal membrane (See below). Scale bar 1 mm

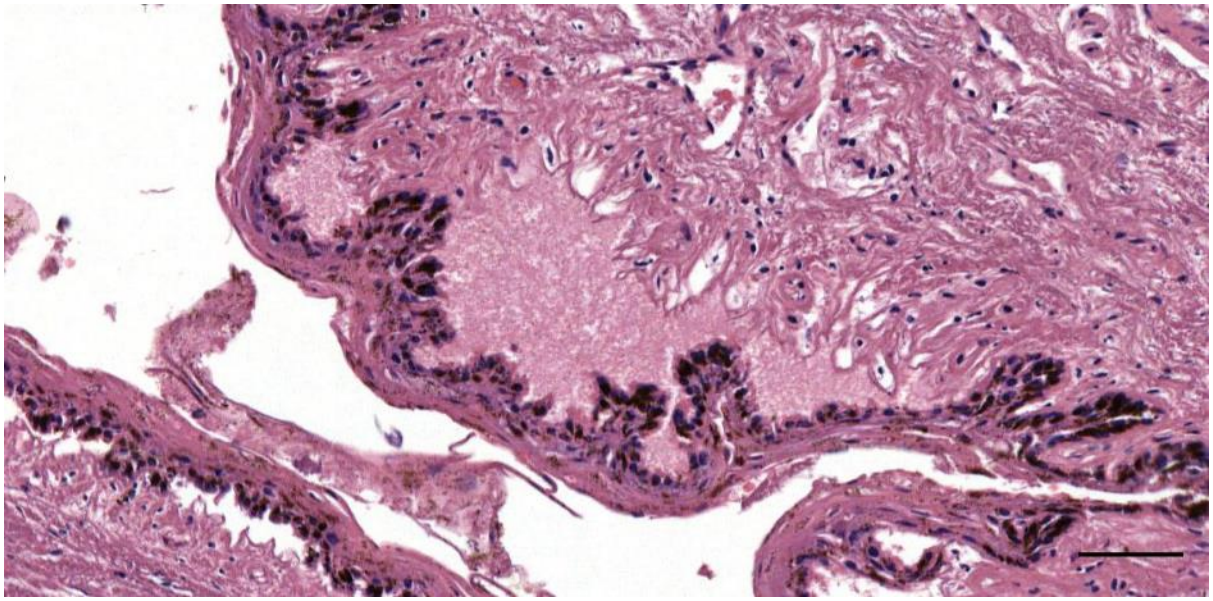

Figure 422. Detail of a detachment of the epithelium from the subepithelial tissue in the ear canal of a long-finned pilot whale (441_L16). This was considered a post-mortem finding. Scale bar 50 µm

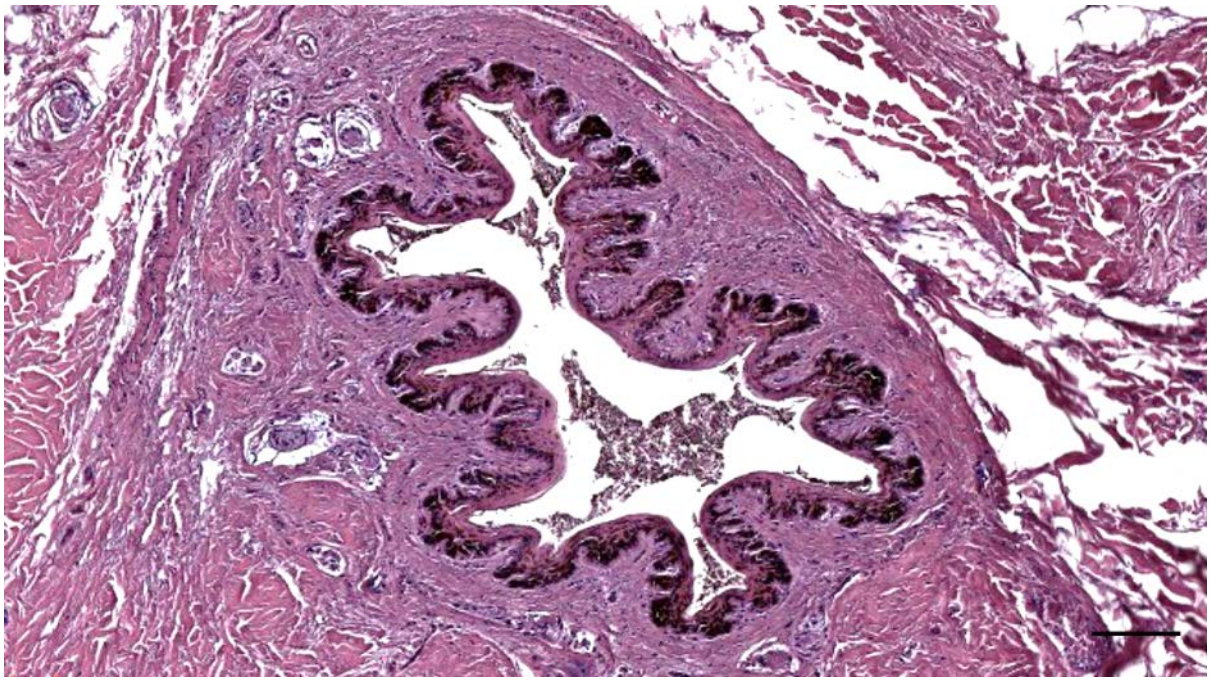

Figure 423. Histological image (HE staining) of the ear canal and corpuscles of a long finned pilot whale (441_R15) in bad preservation state. Scale bar 100 µm

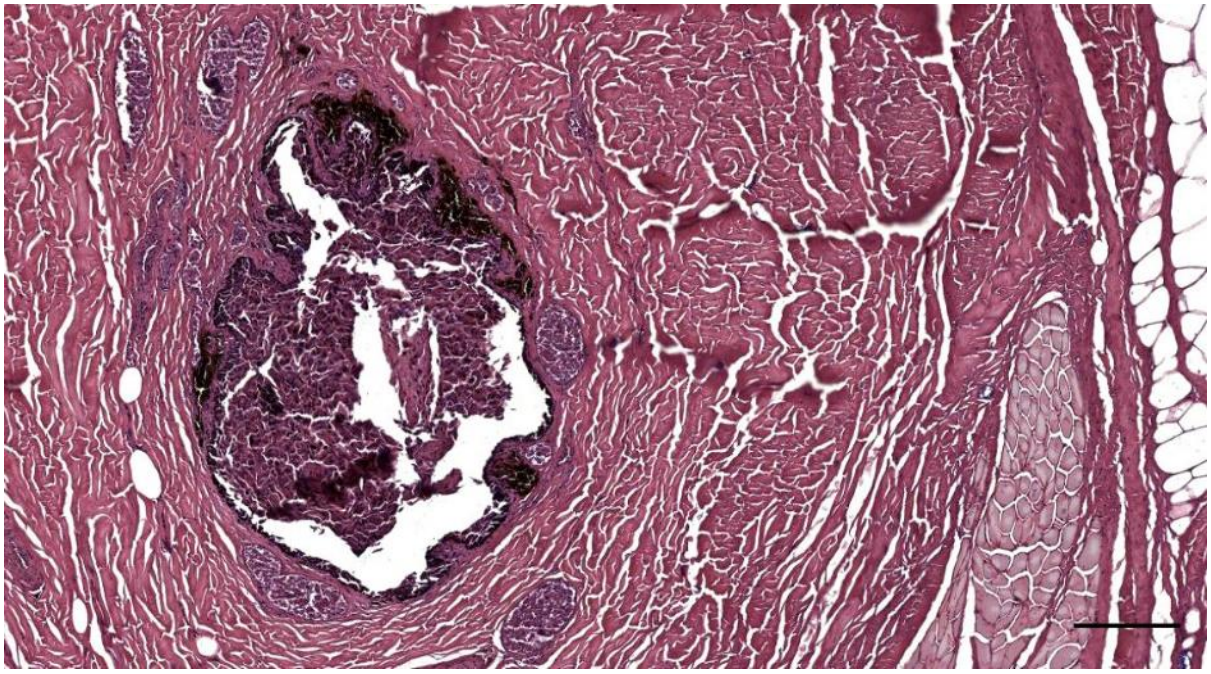

Figure 424. Histological transverse section of the external ear canal of a long-finned pilot whale (441_R6), about 3cm beneath the skin, showing the tissue in bad conservation state. Scale bar 200 µm

2.1.2 Macroscopic anatomy

Macroscopic necropsy – images with camera and macroscopic dissection proved successful for the macroscopic evaluation of tissues. More samples would be needed for comparative studies of the musculature and the macroscopically visible nerve fibres in specific.

Sihler's whole mount staining (Mu and Sanders, 2009) for the visualization and tracking of macroscopically visible nerve around the ear canal in several odontocete species proved unsuccessful in that the tissue, and specifically the fatty tissue, severely degenerated in the process and rendered the result invalid for the analysis.

2.1.3 Histology: Tissue preparation

The tissue handling and preparation for histology, from tissue block to histological slide, presented difficulties associated with the experience of the handler, the state of the tissue, and the tissue content (Figure 425, Figure 426). The physical handling and tissue preparation such as tissue orientation and the use of the microtome improved rapidly and, after the preparation of hundreds of slides, the problems could be anticipated and avoided. The state of the tissue and the tissue content did not provide many alternatives for avoiding artefacts. E.g. degenerated fat tissue is difficult to prepare in paraffin blocks and hot water baths before putting the tissue on the glass slide, and the tissue blocks containing bone (and sometimes also in the case of cartilage), had to be decalcified before cutting the slides. The decalcification protocols were kept as short and in as low concentrations as possible to maintain the integrity of the soft tissues while allowing sufficient time for the hard tissue to be cut with a microtome.

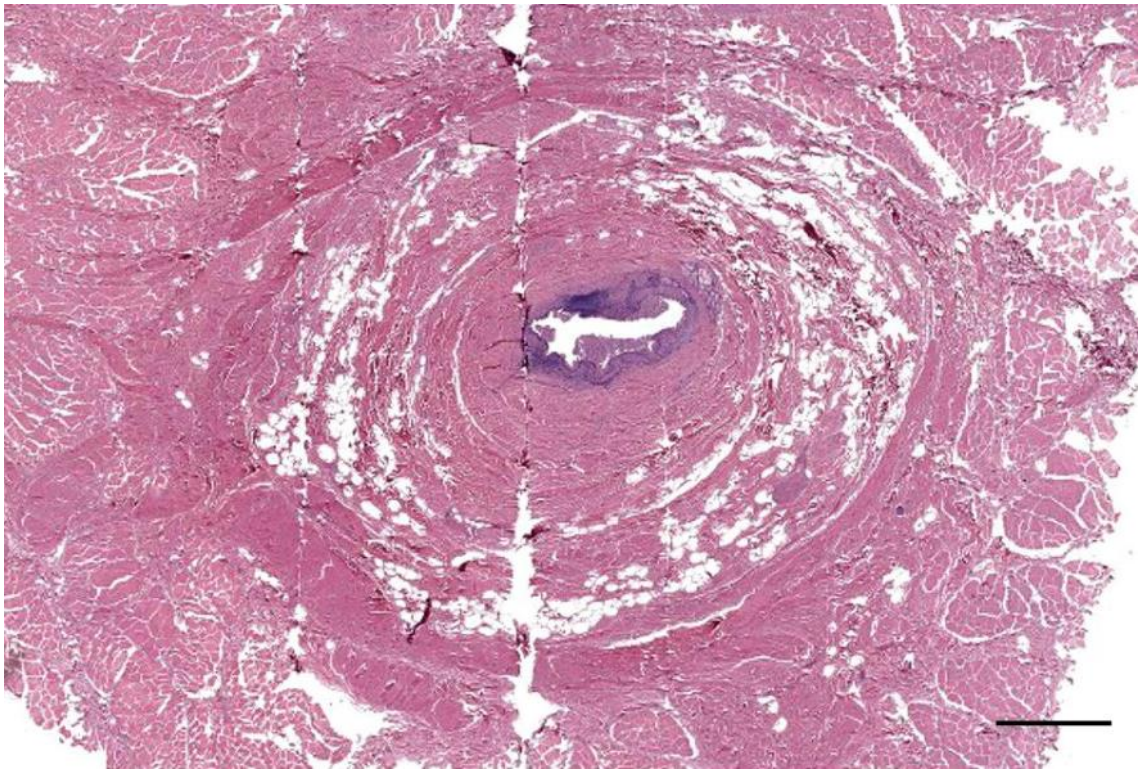

Figure 425. Histological image (HE staining) of the ear canal and adnexa in a long-finned pilot whale (441_L12). Artefact of the tissue preparation caused a vertical break line through the tissue. Scale bar 1 mm

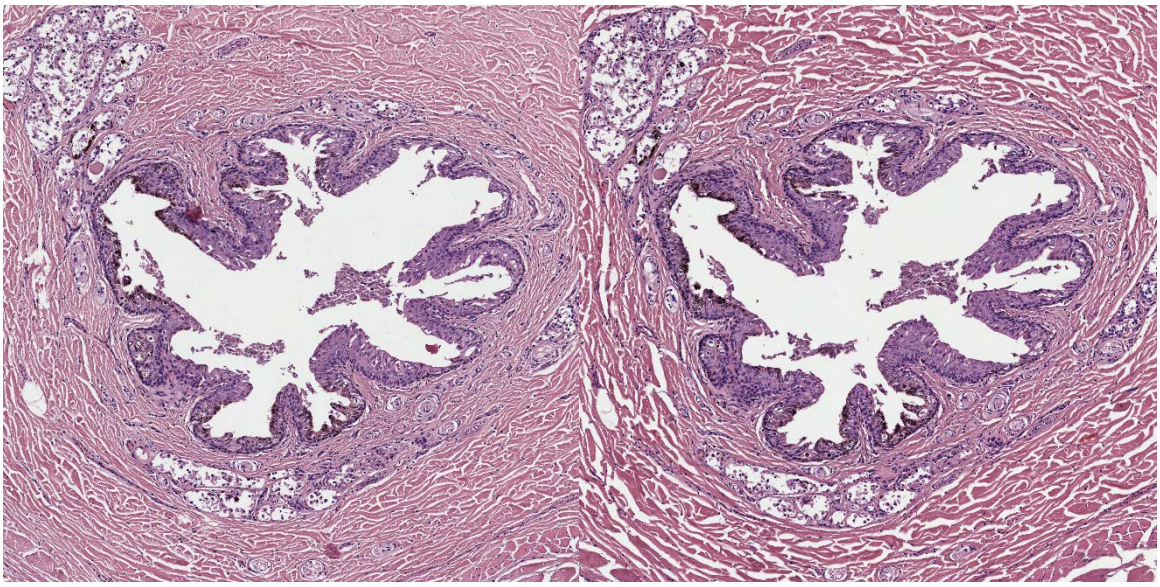

Figure 426. Two histological images (HE staining) of consecutive slides of the ear canal and glands in a striped dolphin. The influence of time spent in the warm water bath during processing of consecutive sections on the same glass slide (4 µm thickness). The right section has spent slightly more time (about 1s more) in the warm water bath because it was situated at the bottom so it entered first and came out later. Notice that there are more artefacts in the right section with more clear spaces between the connective tissue fibres around the ear canal. These two images are representative of all sections prepared in this manner.

There were several cases that presented red blood cells in the soft tissues around the ear canal, although without any tissue reaction and always situated as the border of the sample (e.g. Figure 427). These were regarded as artefacts of the tissue preparation in which there was contact with blood during the necropsy. The same counted for the presence of scant red blood cells in the lumen and the external ear opening (Figure 428).

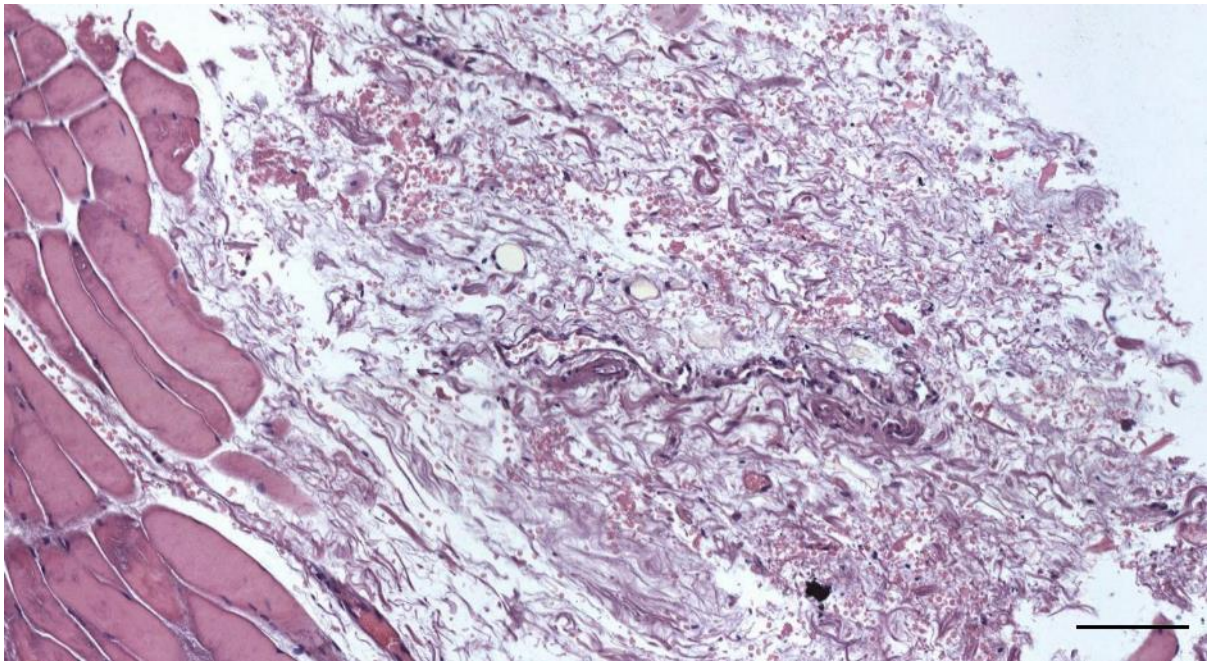

Figure 427. 620/17_L8. Red blood cells in the adipoconnective tissue associated with the external ear canal. Scale bar 100 µm

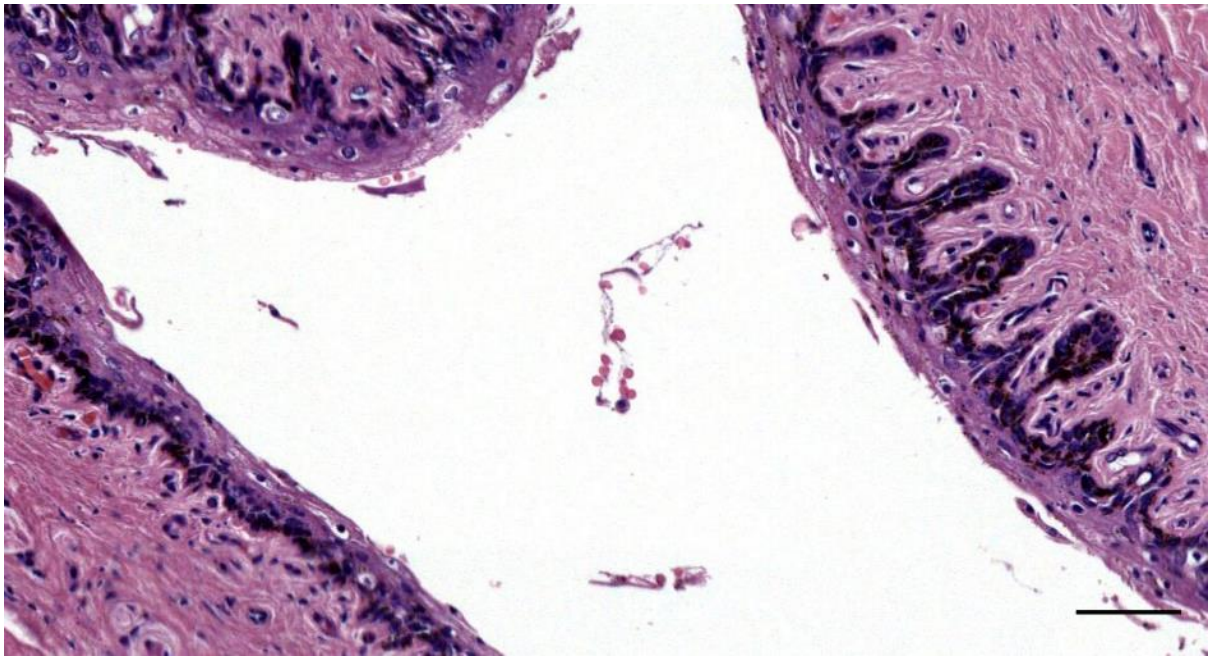

Figure 428. Ear canal with red blood cells in the lumen. Scale bar 50 µm

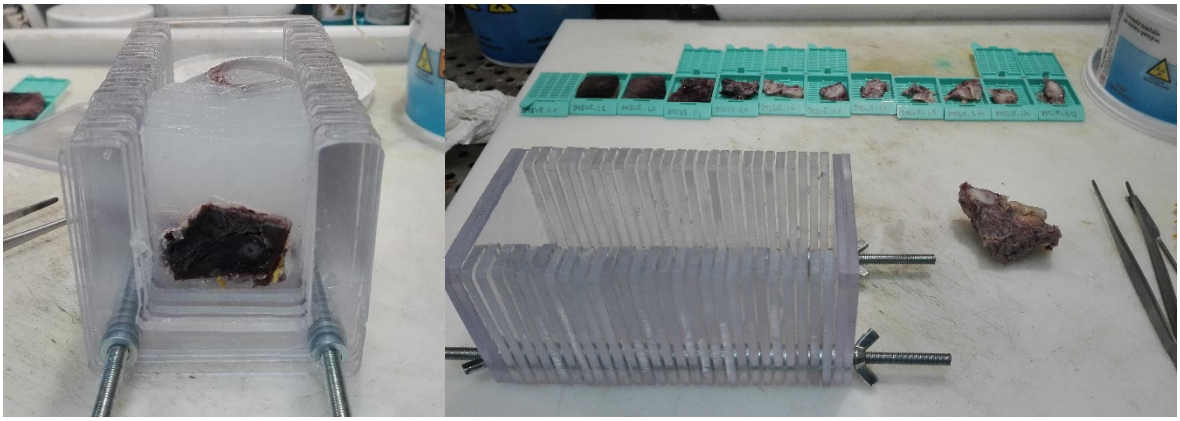

Figure 429. Antithetic slicer (5mm tissue blocks)

2.1.4 Histological stains

2.1.4.1 HE

The objective of an overall assessment of the soft tissues associated with the external ear canal has been attained, together with the identification of the tissues of primary and secondary interest (after comparison with IHC techniques, at least in fresh and well-fixed samples. The HE stain also proved useful for a preliminary study on the nervous tissue network surrounding the ear canal, although an unambiguous identification of small nervous structures was not possible (Figure 430, Figure 431, Figure 432). For the latter, other techniques have been tested, see below.

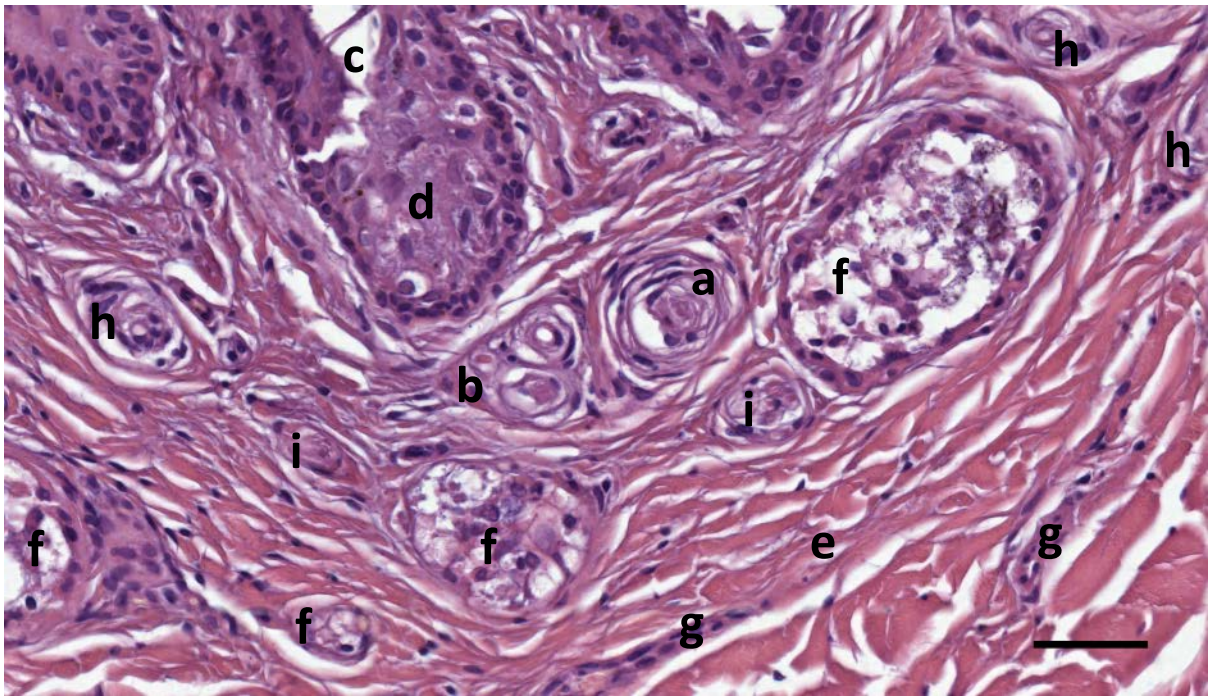

Figure 430. Detail of several nervous structures in the subepithelial tissue of the ear canal of a striped dolphin (Sc1 – block 1)(HE staining). Note the corpuscles in the centre of the image with a larger simple lamellar corpuscle (a) on the right separated by collagen fibres from a corpuscle complex (b) consisting of what are likely two corpuscles and a blood vessel or even three corpuscles. We consider all of the white areas, except for the ear canal lumen to be artefacts. Ear canal (c), epithelium (d), connective tissue (e), glandular structure (f), blood vessel (g), other simple lamellar corpuscles (h), unknown structure (i). Scale bar 100 µm.

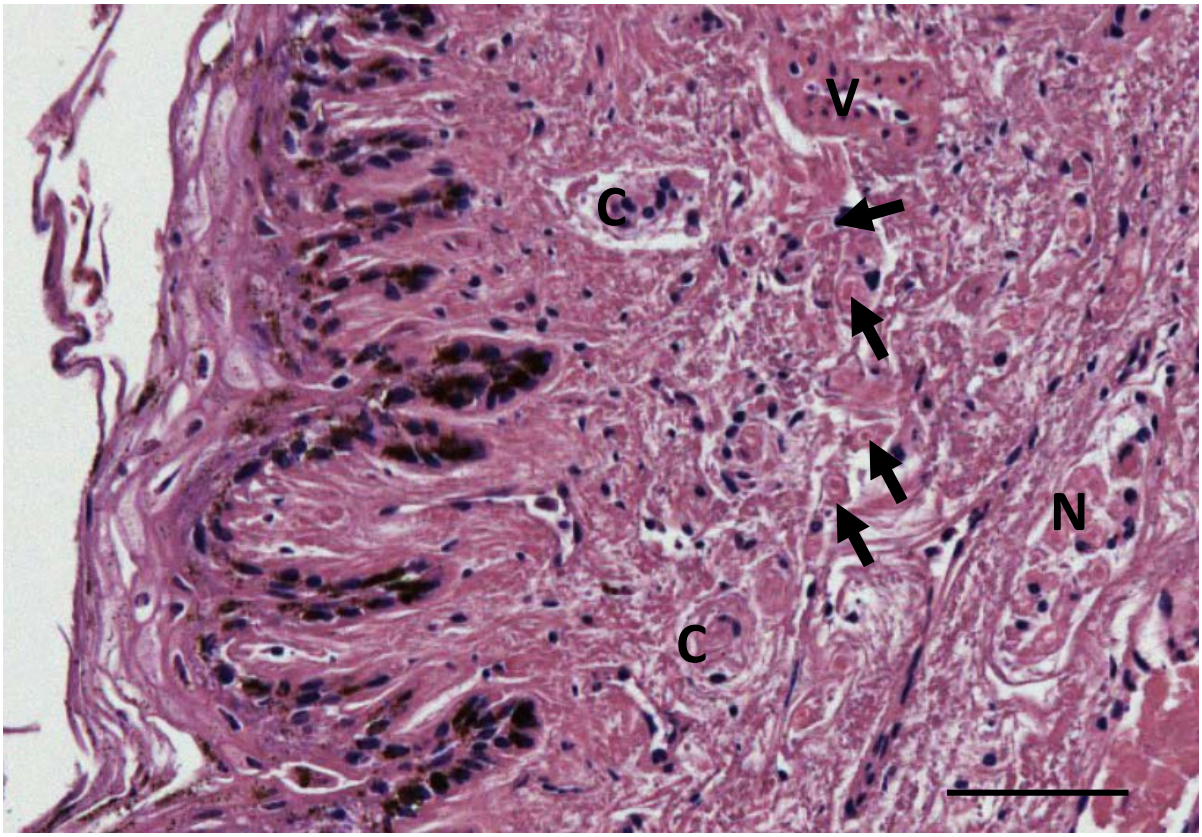

Figure 431. HE stain of the subepithelial tissue in a striped dolphin ear canal. This tissue is very richly innervated although it does not seem so at first impression with HE stain, due to the bad preservation state. Likely structures: N: nerve; C: corpuscle; V: vascular structure; Arrows: axons. Scale bar 50 µm

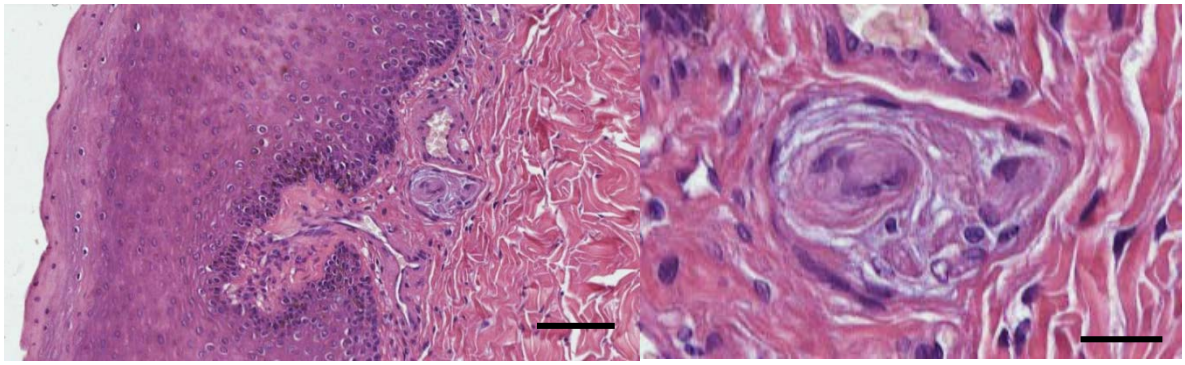

Figure 432. Possible lamellar corpuscle and small nerve embedded within the same capsule in the superficial dermal layer of the ocular commissure of a Cuvier´s beaked whale. Scale bar 100 µm left, 25 micron right

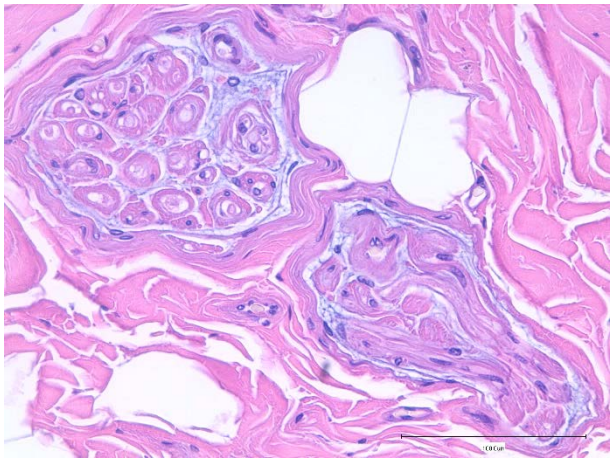

Figure 433. Section through small nerve fibres in a Cuvier´s beaked whale (HE staining). Scale bar = 100 µm

2.1.4.2 Masson's trichrome (with Aniline blue)

Masson´s trichrome stained the following:

- Nuclei and gametes — Black
- Cytoplasm, keratin, muscle fibres, acidophil granules — Red
- Collagen, mucus, basophil granules of hypophysis — Blue
- Delta cells granules of hypophysis — Blue
- Erythrocytes — Yellow

(Newly formed collagen stains blue to reddish[10])

The epithelium (incl endothelium) stained red, with a more dark red stain in the basal layer due to overlapping melanin pigment. The adnexa consisted mainly of blue stain connective tissue, and non-stain fat cells, with the ratio depending on the depth of the section through the canal.

The content of the vascular lacunae stained pinkish, indicating a mix between red and yellow, not likely pure blood. Nerve fibres stained in a normal fashion (Figure 436): the epineurium consisted of an outer, fibrous, blue layer similar and an inner, cellular, greyish blue layer with flattened fibroblasts (flattened nuclei), with all fibres arranged in a circular fashion surrounding the entire nerve. The perineurium stained blue, consisting of dense irregular connective tissue, also the endoneurium stained blue with the axon stain reddish pink. The hyaline cartilage stained blue around the lacunae with reddish trabeculae in between (Figure 434, Figure 439). The lamellar corpuscle lamellae stained a mix of red and blue (Figure 437).

This stain was chosen for the automatic tissue segmentation using machine learning techniques, because of the well-defined differentiation among the variety of soft tissues, and the relatively distinct colour pattern of nervous structures (red+blue), see 3D reconstruction of the ear canal.

Masson´s Trichrome Goldner stained similarly, although with green instead of blue.

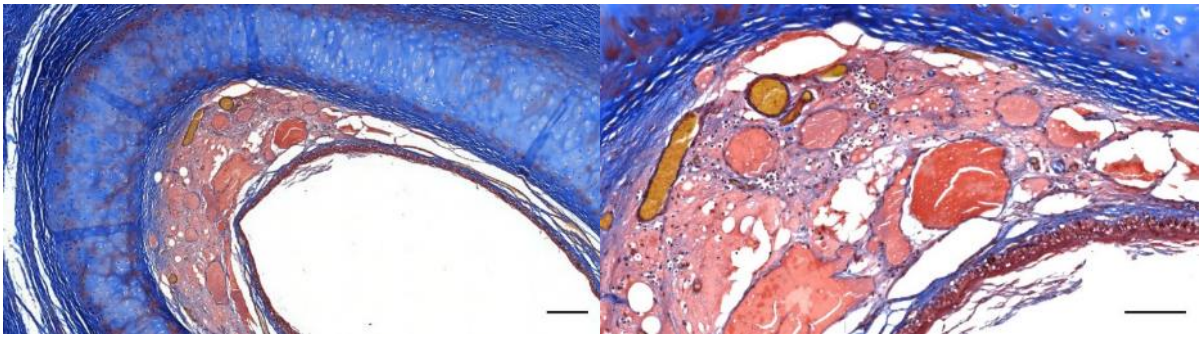

Figure 434. Striped dolphin ear canal vascular lacunae situated between the lumen (bottom right) and the cartilage (top left)(Masson´s trichrome). There are blood vessels with erythrocytes stain yellow. The endothelium and epithelium stain red, and so do the nuclei of all cells. The white spaces are fat cells, empty vascular lacunae, or artefacts. Scale bars 200 and 100 µm.

[10] (Guo et al., 2016)

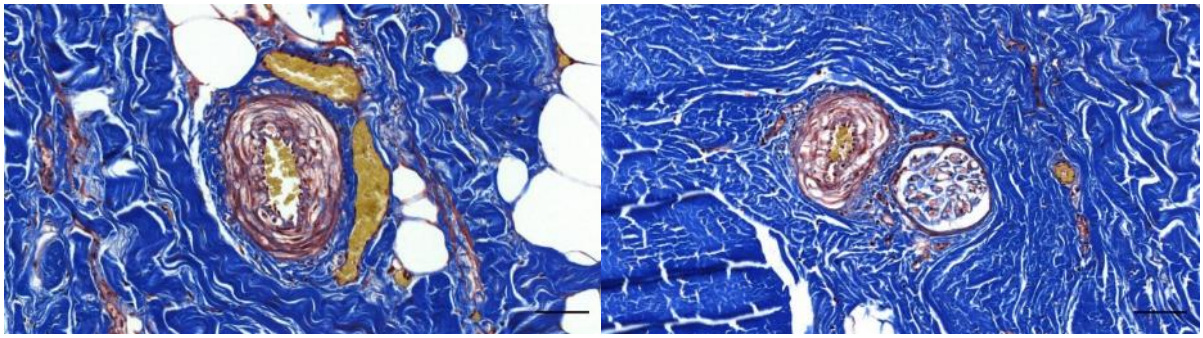

Figure 435. (Striped dolphin, Masson´s trichrome) Artery, veins and nerve fascicle. Scale bars 50 µm

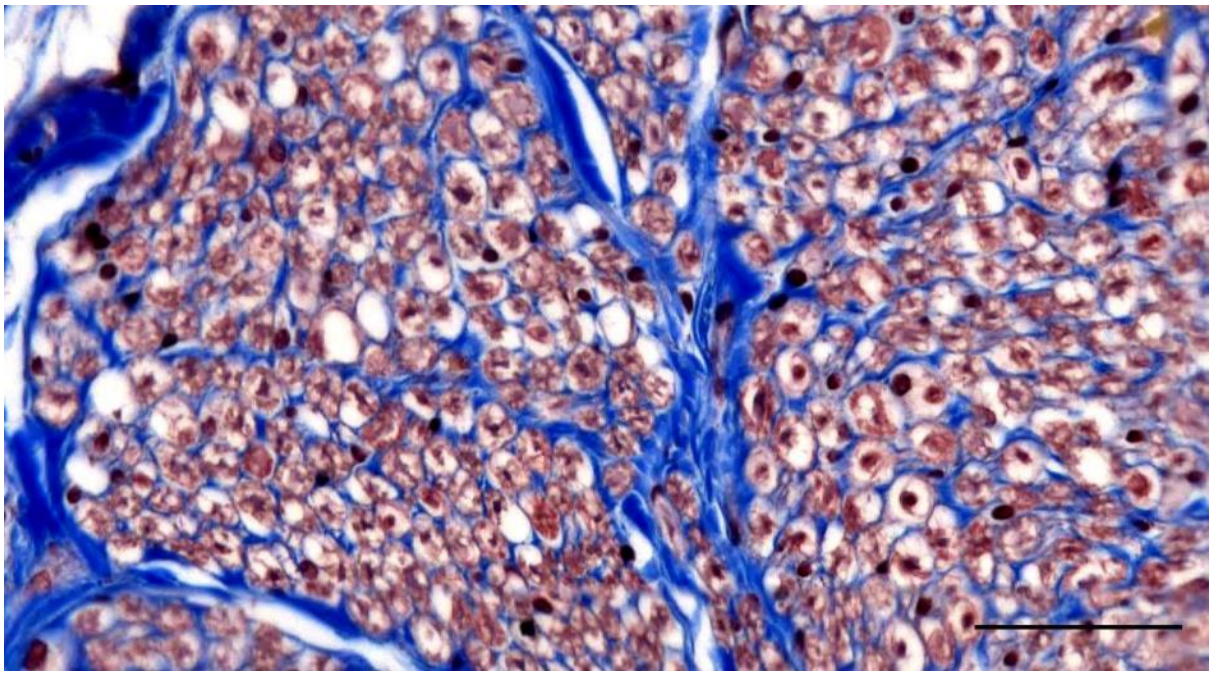

Figure 436. (Striped dolphin, Masson´s trichrome)Detail of the facial nerve in cross-section. Scale bar 50 µm

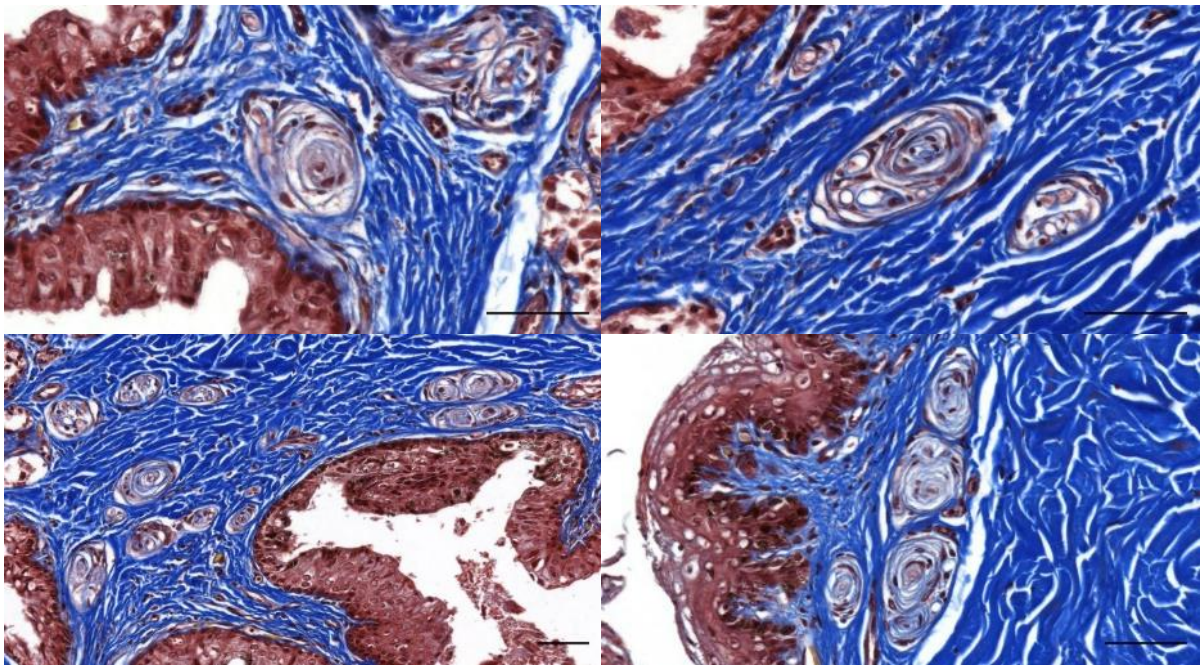

Figure 437. (Striped dolphin, Masson´s trichrome) Single and complex lamellar corpuscles around the ear canal. Scale bars 50 µm

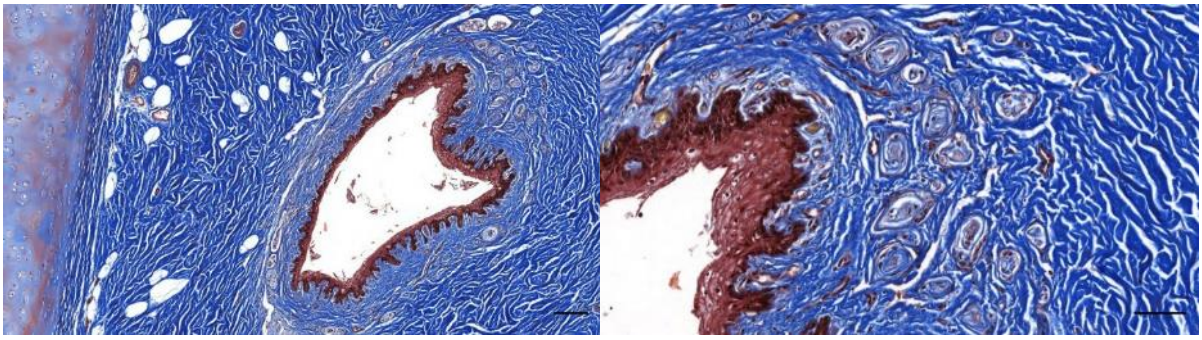

Figure 438. (444_12) Ear canal and cartilage. Note the nervous tissue ridge with a concentration of lamellar corpuscles and small nerves. Scale bars 100 and 50 µm

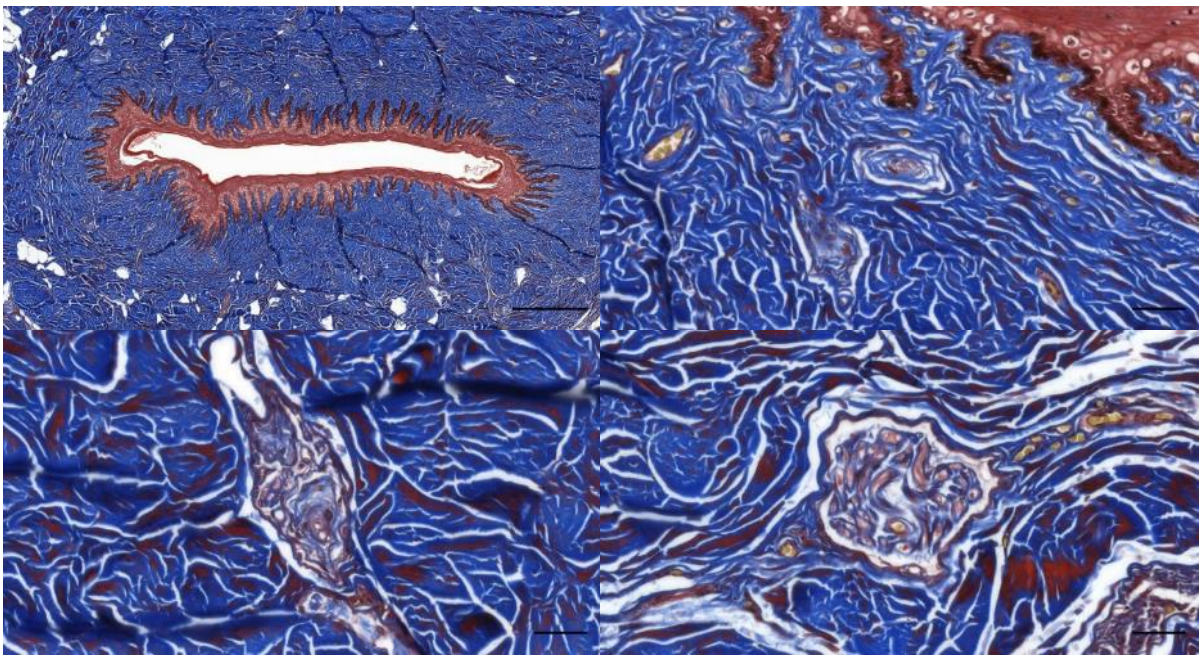

Figure 439. (429_14B) The ear canal, corpuscles and nerves. Scale bars 500 (top left) and 50 µm (other three))

2.1.4.3 Silver stains

The various silver stains did not prove successful for the unambiguous identification of sensory nerve formations and small nerve fibres.

2.1.4.3.1 Palmgren's Silver Stain (modified version)

We experimented with the standard and modifications of Palmgren´s method for staining nerves axons in paraffin-embedded material (Palmgren, 1960). The modifications included variation in tissue thickness (4 vs 8 µm), and time in the Silver stain solution (12/15/20 min), of which the 4 µm thickness and 15 min step provided the best tissue differentiation. However, it was not useful for the differentiation of small nervous structures (Figure 440), even though there was an indication of a small axon in a dermal papilla (Figure 441). On the other hand, this technique showed an interesting difference between the connective tissue close to the ear canal and more peripheral.

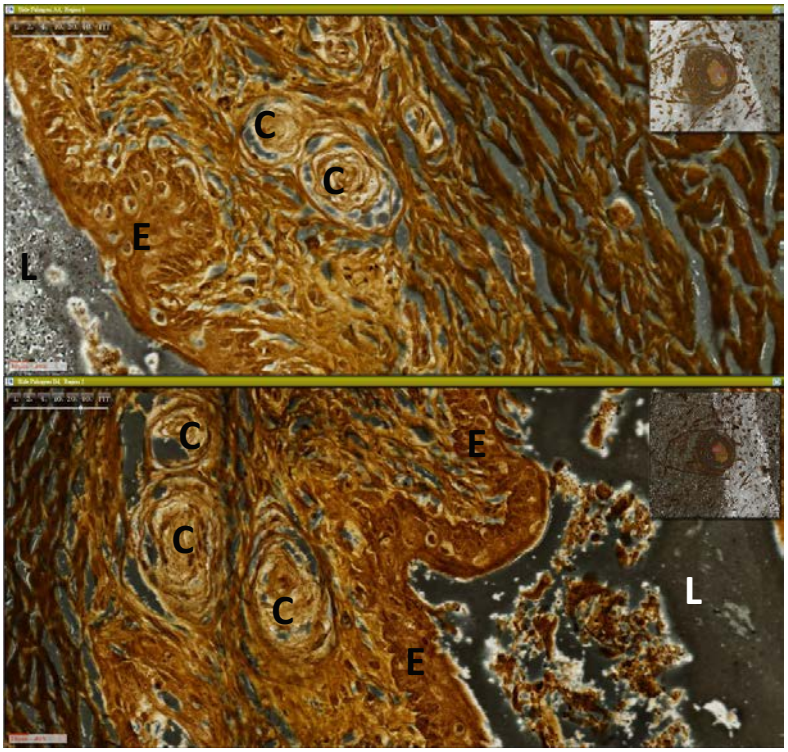

Figure 440. Detailed histological image (Palmgren's stain) of lamellar corpuscle in the subepithelial tissue of the ear canal in a striped dolphin. L: lumen; E: epithelium; c: corpuscle

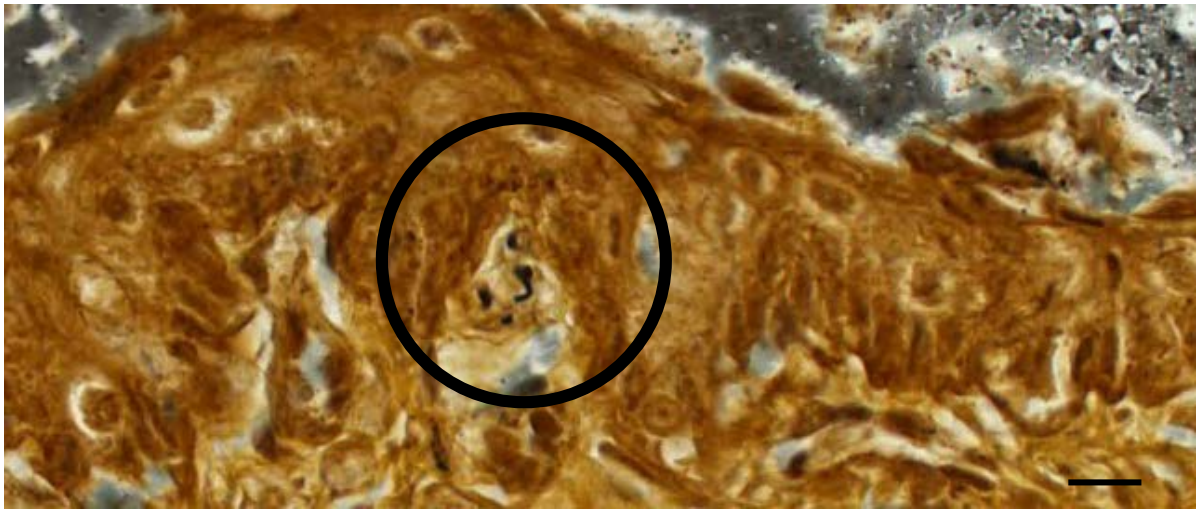

Figure 441. A4. Palmgren´s silver stain. Possible axon in the papillary layer. Scale bar 10 µm

2.1.4.3.2 Bielschowsky´s silver stain

Similar to Palmgren´s stain, although less obvious, there was a difference in the connective tissue of the subepithelial layer and further away from the ear canal (Figure 442). It also did not provide an adequate visual distinction of small nervous structures, nor additional information on the SNF morphology (Figure 443).

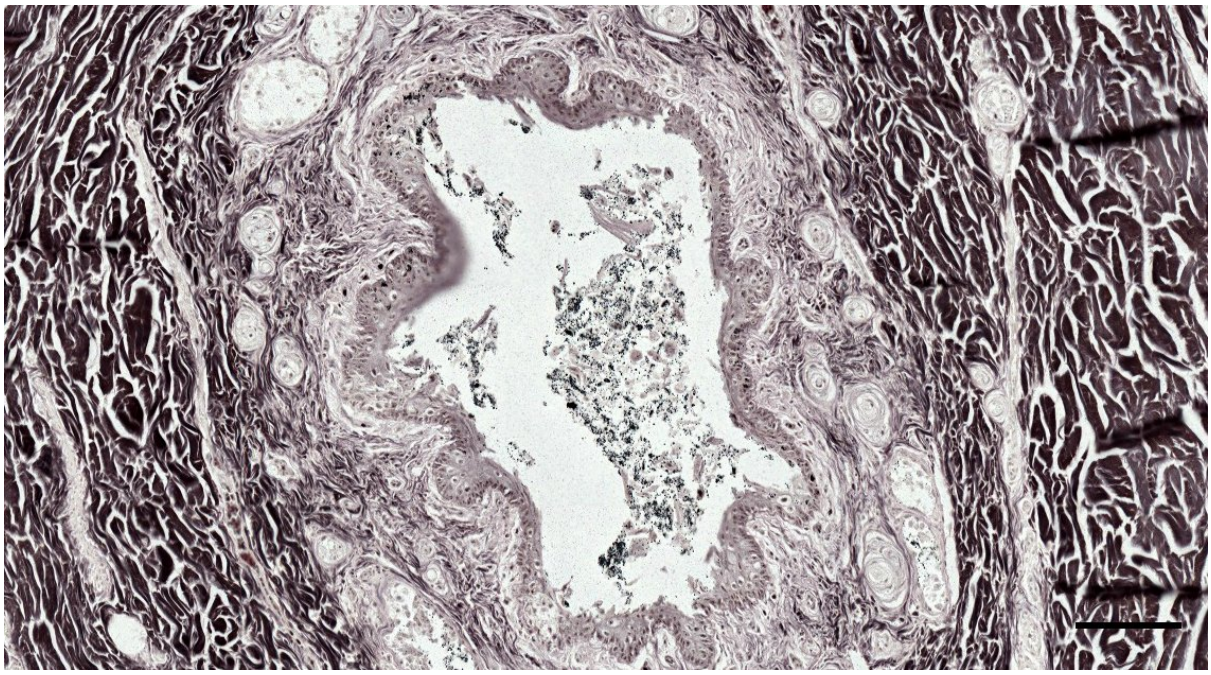

Figure 442. Histological section (Bielschowsky´s staining) of a transverse section of the ear canal of striped dolphin.

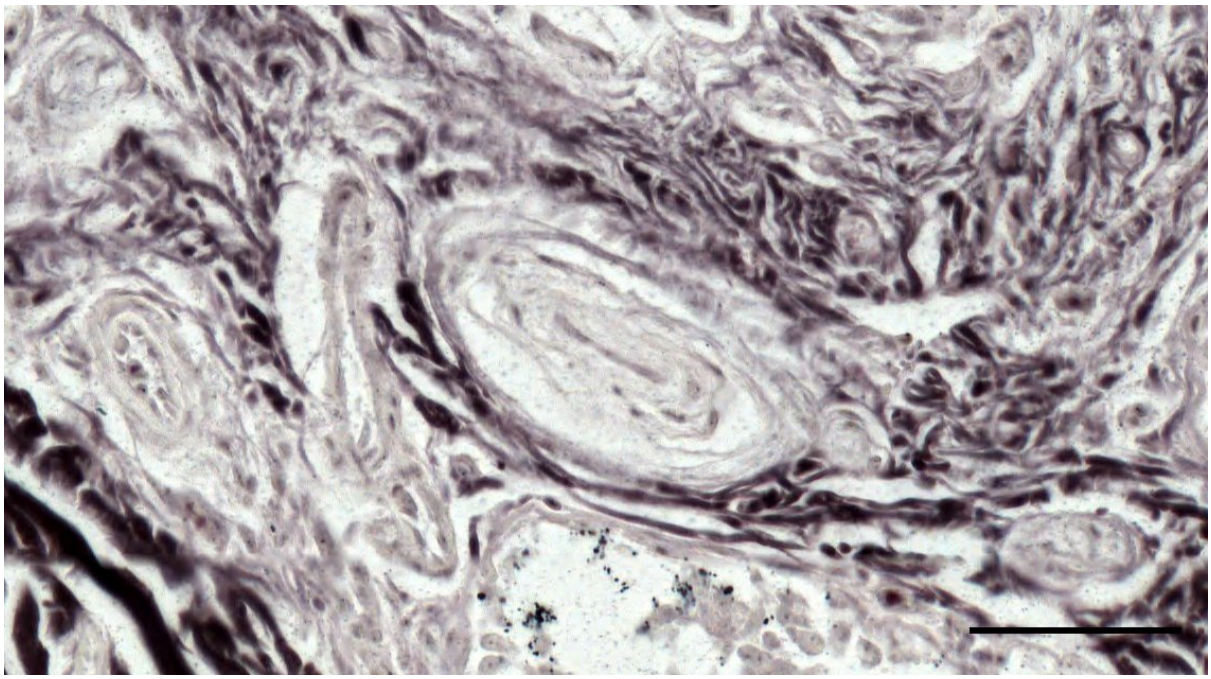

Figure 443. Oblique section through a lamellar corpuscle (Bielschowsky´s staining). Scale bar 50 µm

2.1.4.3.3 Luxol Fast Blue/Cresyl violet

This staining, which is used for staining myelin, provided no clear identification of nervous structures, and no additional information on the lamellar corpuscle composition (Figure 444). For both staining

times, there was also no positive reaction in any of the nerves, which might be indicative that the staining protocols used were not adequate for this tissue.

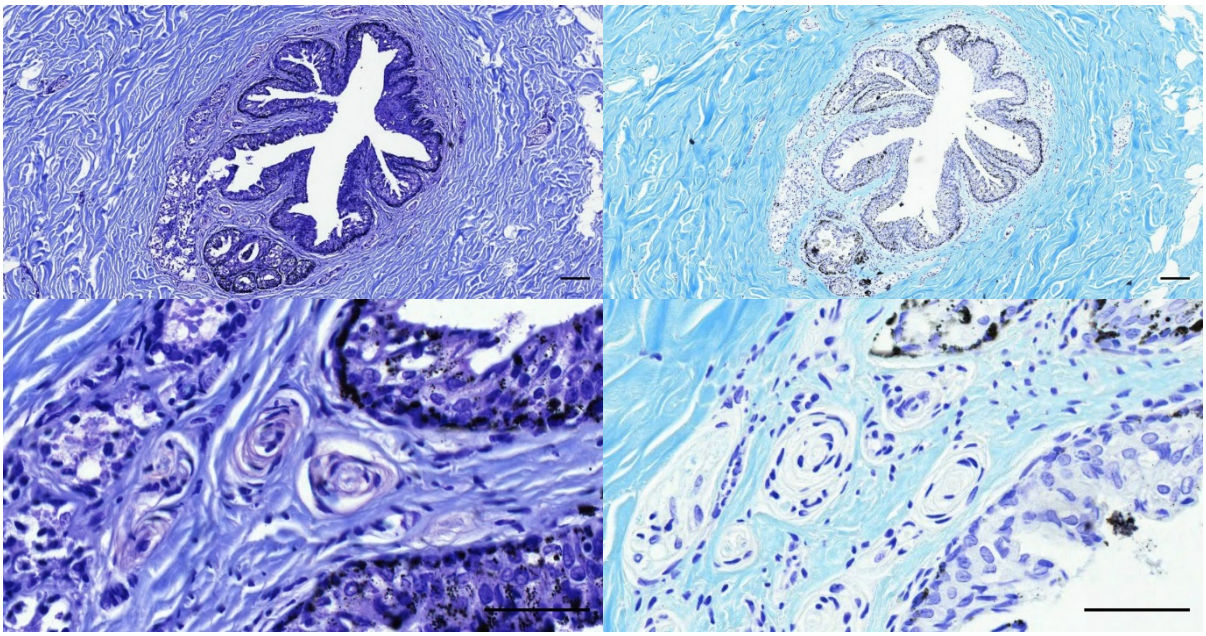

Figure 444. Two histological images of a transverse section through the ear canal of a striped dolphin (Sc1) stained with Luxol fast blue with two different staining times (left vs right). There is no clear distinction between nervous structures. Scale bar 100 µm top, 50 µm bottom.

2.1.4.3.4 Spaethe´s silver stain

Spaethe´s silver stain did not allow for the unambiguous identification of the lamellar corpuscles. Although nervous structures did stain dark brown to black as mentioned in the protocol (Figure 445, Figure 446, Figure 447, Figure 448, Figure 449, Figure 450), there were other structures of unknown nature staining equally intensely dark (might have been artefacts), which complicated the analysis and left the image unsuitable for image processing, and automatic tissue segmentation. Consecutively, a bleaching protocol was applied, leaving the epithelium of the ear canal, and most of the unknown dark structures unstained (Figure 444), but at the same time also nerves, lamellar corpuscles, and vasculature were bleached and remained visible as fully pale structures, equally unsuitable for image segmentation (Figure 451).

The nervous tissue showed the following reaction in the non-bleached sections:

Nerve fibres: Perineurium: darker than connective tissue; Schwann cell nuclei: intense dark brown; Axons: brown like perineurium; Schwann cell cytoplasm: golden brown;

Corpuscles: Axon: dark brown; Schwann cell nuclei: brown; Schwann cell cytoplasm: golden brown; peripheral: brown

Figure 445. Histological image (Spaethe's stain) of the ear canal and glands in a striped dolphin (Sc1_EAM02). Scale bar 100 µm

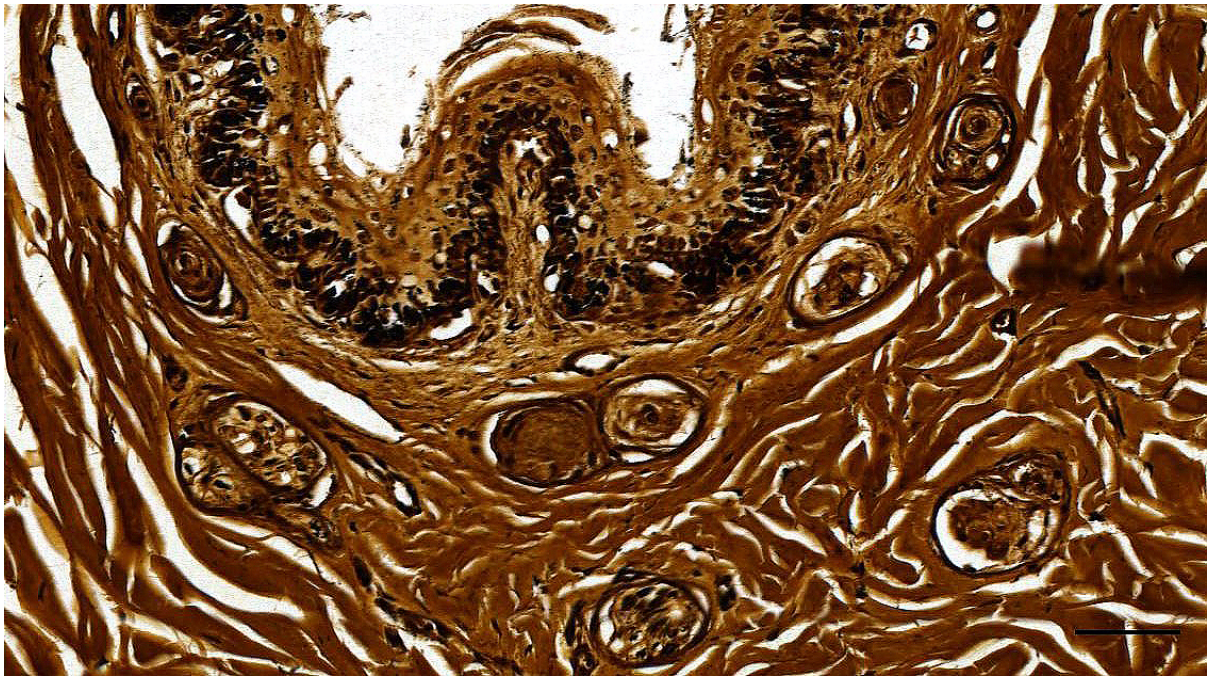

Figure 446. Histological detail image (Speathe's stain) of the nervous sructures around the ear canal in a striped dolphin (Sc1_EAM02). Scale bar 50 µm

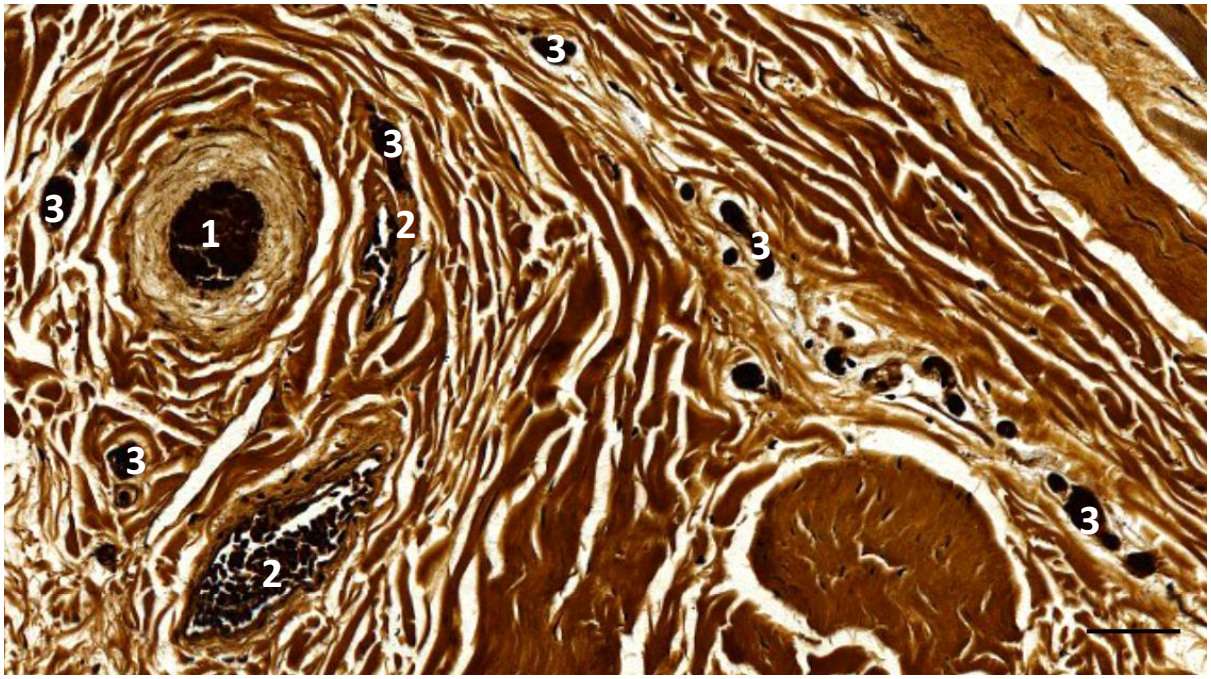

Figure 447. Histological detail image (Speathe's stain) of vascular structures and a small nerve in the vicinity of the ear canal in a striped dolphin (Sc1_EAM02). 1: artery; 2: veins; 3. Small nerves embedded in connective tissue. Scale bar 50 µm

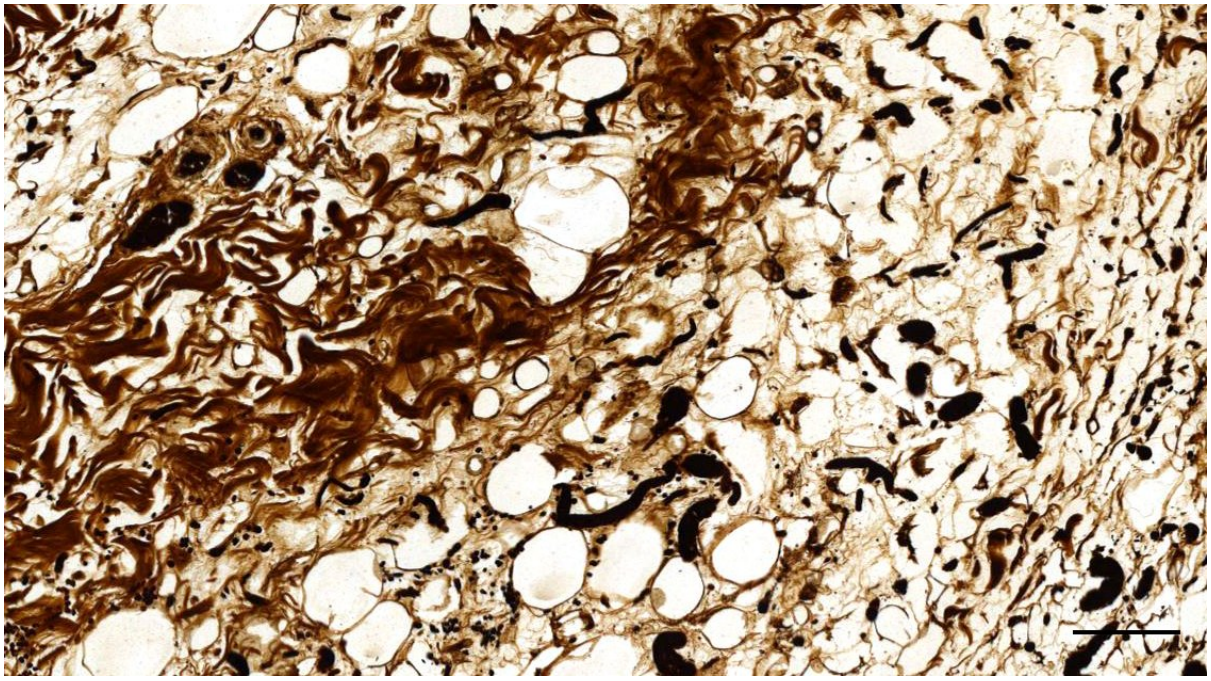

Figure 448. Histological detail image (Speathe's stain) of immunoreactive structures of unknown origin embedded in the adipoconnective tissue in the vicinity of the ear canal in a striped dolphin (Sc1_EAM02). Scale bar 100 µm

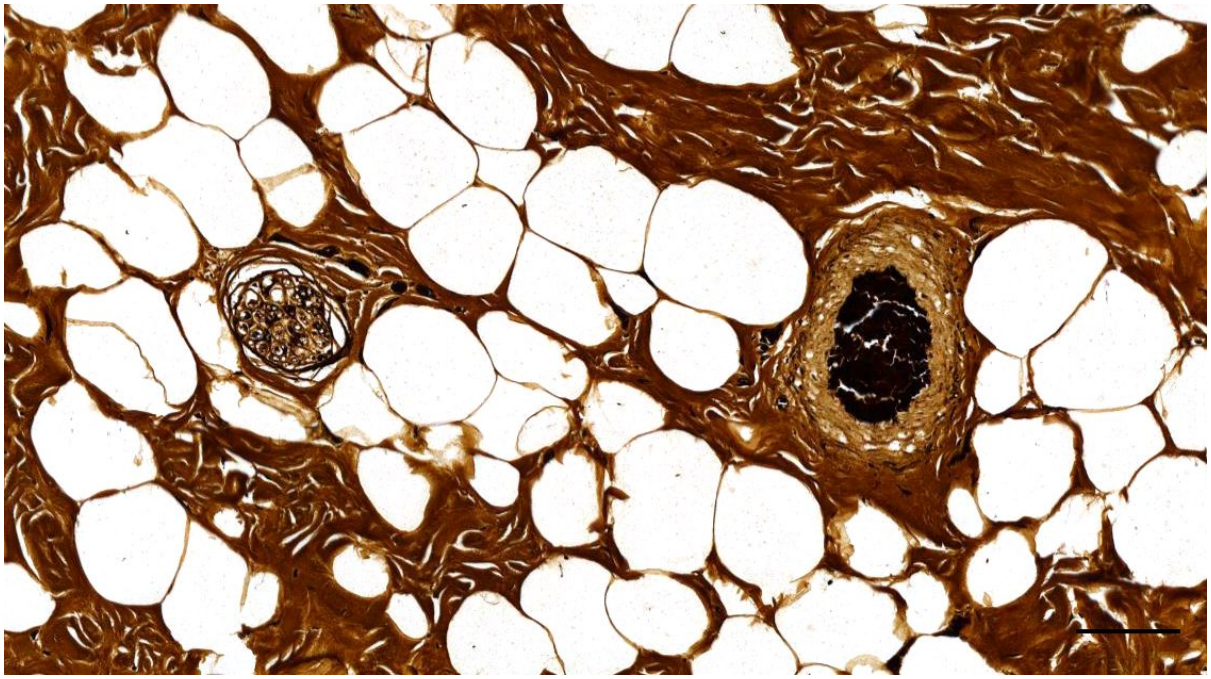

Figure 449. Histological detail image (Speathe's stain) of a small nerve fascicle and artery in the adipoconnective tissue associated with the external ear canal in a striped dolphin (Sc1_EAM02, Spaethe). Scale bar 100 µm

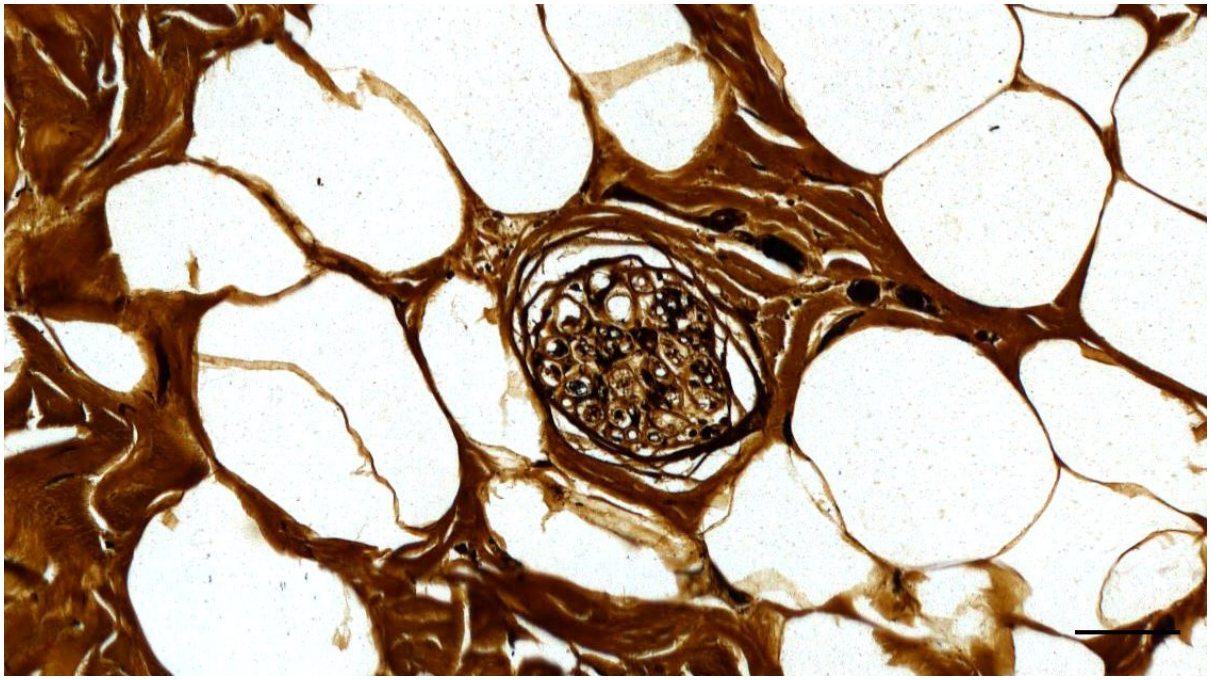

Figure 450. Histological detail image (Speathe's stain) of a small nerve fascicle in the adipoconnective tissue associated with the external ear canal in a striped dolphin (Sc1_EAM02, Spaethe). Scale bar 50 µm

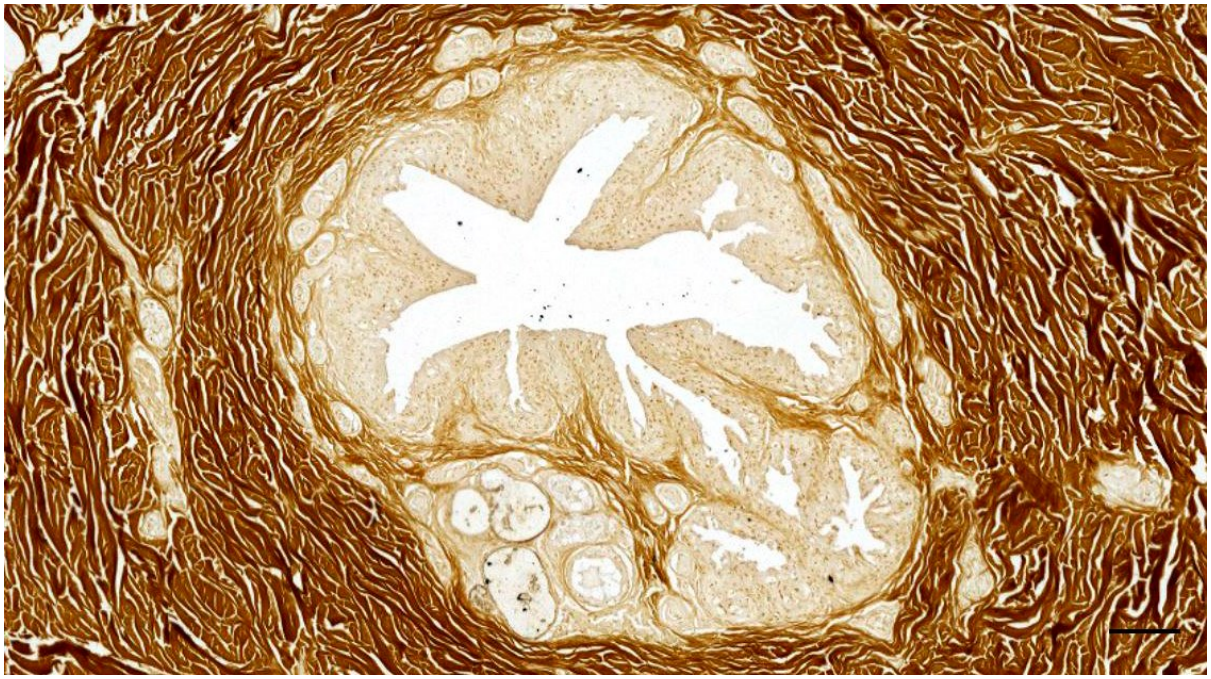

Figure 451. Histological image (Speathe's stain, after melanin bleaching) of the external ear canal in a striped dolphin (Sc1_EAM02). Note the ear canal and glands. Also note that all nervous and vascular structures are pale in a similar fashion as the epithelium. Scale bar 100 µm

2.1.4.4 PAS, and Pancytokeratin

The combination of these two stainings proved successful for the detection/exclusion of parasites in the ear canal lumen (See 1.1.2 - Striped dolphin (ID2926)). Interestingly, the lamellar corpuscle's peripheral layer stained PAS-positive, similar to the nerve fibre perineurium (Figure 452).

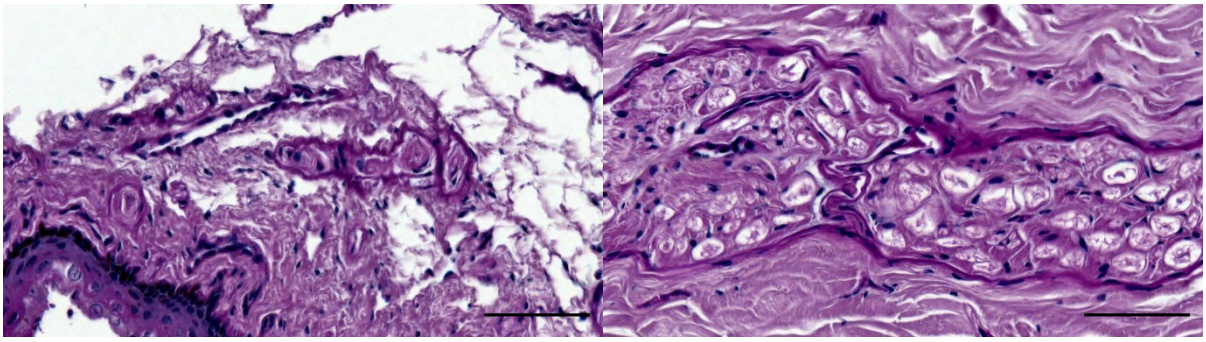

Figure 452. PAS staining of lamellar corpuscles (left) and a nerve fibre (right) in the vicinity of the ear canal in a striped dolphin. Note the peripheral layer of the corpuscles and the perineurium of the nerve fibre stain in a similar fashion darker than the internal structures and the surrounding connective tissue. Scale bars 50 µm

2.1.4.5 GRAM1 and 2

The results of the GRAM stains for bacteria were indicative but non-conclusive.

2.1.4.6 Stains for elastic fibres: Weigert´s elastic stain – Acid Orcein Giemsa

Both stains proved successful for the identification of elastic fibres, although the Acid Orcein Giemsa stain provided slightly more contrast, facilitating the interpretation of the histological slides.

2.1.5 Immunohistochemical techniques

Immunohistochemistry was the only technique that came close to allowing for the unambiguous identification of the lamellar corpuscles, and small nerve fibres, using a combination of anti-PGP9.5,

anti-NF, anti-S100 antibodies. However, in some cases, there was still confusion, and only with consecutive slides and a magnification of 400x, the distinction was clear in all cases. Anti-NSE was quite aspecific in staining nervous structures.

2.1.6 Transmission electron microscopy

This technique proved useful for assessing the ultrastructural characteristics of the lamellar corpuscles and nerve fibres, and epithelium.

2.1.7 Quantitative assessment of nervous structures

The results of the quantitative data on several cross-sections of lamellar corpuscles along the ear canal have been published and described above. Although the initial idea was to apply stereological methods, we did not attempt to calculate the numerical density of the lamellar corpuscles in 3D space, and we did not attempt to apply stereological methods for such number estimation. Rather, we applied simple morphometrical methods that took into account the physical characteristics and restriction of the dolphin ear canal, and the current limited knowledge on the 3-dimensional structure of the lamellar corpuscles (Work in Progress – See Confocal Microscopy). As such, we were able to extract information from 2D planes without attempting to obtain 3-dimensional information about the corpuscles, nor of the density distribution of the structures of interest.

Once we have more profound knowledge on the structural characteristics of the lamellar corpuscles, we could apply stereological methods, including systematic uniform random sampling to get to number estimation of the corpuscles, and a volume estimation of the ear canal, vertical sections to calculate and the surface area of the ear canal and corpuscles, although some of this data could also be obtained with calculations done on accurate 3D renders. For this, the techniques for preparing the sample have been prepared and tested (antithetic slicer), but the unambiguous identification and 2D delineation of the lamellar corpuscles have not been fully ascertained using the various histochemical staining protocols or machine learning techniques mentioned in this dissertation.

2.1.8 Tissue segmentation for modelling

2.1.8.1 Masson´s trichrome stain + Trainable Weka segmentation (ImageJ)

Proved successful on a small scale (Figure 454). Although it lacked the flexibility that ILastik offered in this process, see below.

Figure 453. Sc1_ Masson's trichromic staining of a section of the ear canal of a striped dolphin, at the level of the glands

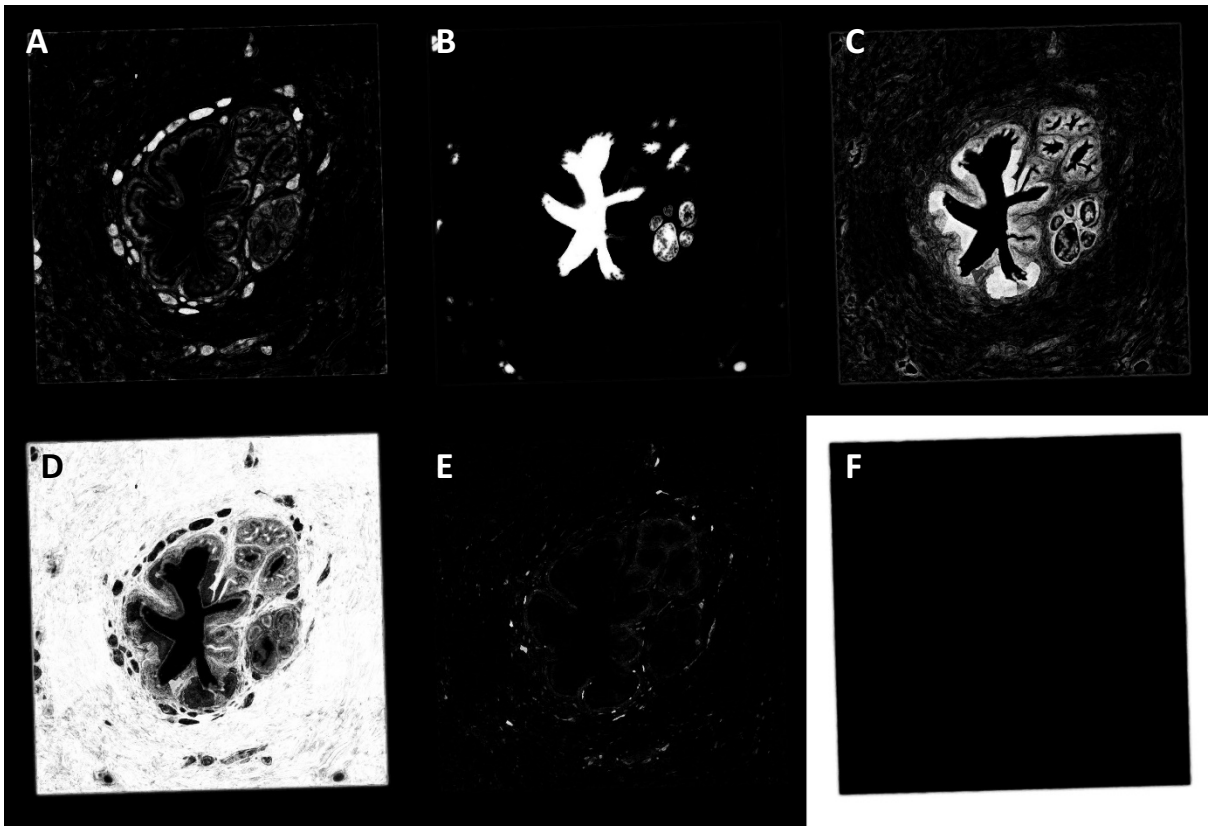

Figure 454. Montage of Probability maps as output of the trainable WEKA segmentation in FIJI applied to Figure 453. White = high probability; Black = low probability; 1. Nervous tissue; 2. Lumen; 3. Epithelium; 4. Connective tissue; 5. Vascular tissue; 6. Background

2.1.8.2 Masson´s trichromic stain + Split channels

The digital images were split into 8 or more colour channels that would encompass and separate the soft tissues of interest (e.g. muscle = red, blood yellow), but did not prove successful for the segmentation of nervous structures, vascular structures and others, so this technique was not elaborated further.

2.1.8.3 Masson´s trichromic stain + Ilastik

This technique proved the most efficient in segmentation of the tissues of interest: lumen, epithelium, vascular structures, nervous structures, fat, muscle, connective tissue, cartilage, and bone, and was therefore used for the 3D reconstruction of the ear canal and associated tissues.

2.2 Discussion

2.2.1 Techniques to study the morphology and function of sensory nerve formations

The techniques that have been used for studying the morphology of SNFs include

- Histological techniques (histochemical and immunohistochemical techniques), possibly in combination with confocal microscopy and immunofluorescence (Guinard et al., 2000; Vega et al., 1996a; Zachar and Jonz, 2012), or with 3D reconstruction from serial sections (e.g. Kim et al., 2018)
- Ultrastructural techniques: TEM and SEM (e.g. Nafstad and Andersen, 1970; Poláček and Halata, 1970; Spencer and Schaumburg, 1973; Bryden and Molyneux, 1986)
- Molecular techniques for the identification of proteins and the biochemical processes that take place inside the receptor (e.g. Cherepnov and Chadaeva, 1981)
- Receptor response techniques to mechanical stimuli in live animals (in vivo)(e.g. (Mountcastle et al., 1972) or in live tissue (ex vivo electrophysiological studies)(e.g. Williams et al., 2010)
- Biomechanical modelling for evaluation of the properties of the different structures that make up the SNFs (Biswas, 2015; Quindlen et al., 2015)

The current study has successfully applied various histochemical and immunohistochemical techniques for the identification of the cellular nature of the various components of the lamellar corpuscles and other SNFs.

The use of TEM has proven useful for the analysis of the ultrastructural components of the corpuscles. The use of SEM was considered an essential step in the first evaluation of the corpuscle morphology and could be considered in future steps.

The combination of immunohistochemical labelling with immunofluorescence and confocal microscopy is currently ongoing and has provided some preliminary results. This will be carried out further to characterize the 3D morphology of the corpuscles, their innervation patterns (single providing axon or multiple; axonal ending or continuation), and the nervous network with branching and merging of nervous structures. The results of this project will provide the base for the biomechanical modelling of the lamellar corpuscles in cetaceans, and could narrow down the focus of likely molecular techniques.

2.2.2 Transmission electron microscopy

In this study focused on the typical morphology of the external ear canal epithelium and subepithelial tissue with particular attention to the fine nervous innervation and sensory nerve formations. Besides

the ‘normal’ morphological results, there were several interesting findings, such as the epithelium showing indications of exocytotic processes with the lumen, the myelin in- and outfolding of the small nerve in the subepithelial tissue, and the morphology of the axon terminal of the lamellar corpuscles, of which it is not clear to what extent degenerative and/or pathological processes have played a role in the appearance of the tissues. For instance, there were various indications of degenerative processes, such as in the epithelium and the nerves, although the latter might have been subjected to an axonopathy. However, because both processes might have been concurrent and would be non-exclusive for each other, we cannot draw any conclusions. To our knowledge, the TEM findings contribute to a first description of a possible peripheral axonopathy in cetaceans. It also provides the first ultrastructural description of lamellar corpuscles in cetaceans and compares it to encapsulated receptors found in mammals.

2.2.3 Macroscopic techniques: dissection

Macroscopic dissection techniques were very useful for a general understanding of all the tissues involved, the interspecific differences, and the various tissue conservation codes. It did, however, not prove successful on a first run for the full and comprehensive identification and tracking of macroscopic nerves fibres and the various striated muscles. Additional samples, in good condition code, would be needed to compare results and draw conclusions, and, in the best-case scenario, these would be accompanied by medical imaging techniques (see below).

Of the two heads dedicated to macroscopic dissection of the tissues surrounding the ear canal, the ear canal was not present in one specimen as the soft tissues in that area had been cut, and in the other specimen, it was barely present, with many of the soft tissues dorso-caudal to the EAM not being present.

2.2.4 Macroscopic techniques: Sihler’s stain

This technique did not prove successful, most likely due to the fatty nature of the tissues associated with the external ear canal in toothed whales. The protocol should be revised and tested with other samples (cfr. Mu and Sanders, 2009).

Figure 455. Example of the typical state of the Sihler’s stain samples when the process was halted.

2.2.5 Histology – sample processing

The standard protocols for histological sample processing were also valid for processing tissue from the toothed whale ear canal and other tissues. In some cases, some additional steps were involved, such as melanin bleaching or decalcification, similar to the standard processing techniques in anatomical and pathological laboratories.

2.2.6 Histochemical stains

Regarding the various additional histochemical staining techniques, including specialized silver stains applied to formalin-fixed tissues, these did not contribute to a better understanding of the morphology of the lamellar corpuscles. However, all stains were applied to opportunistically obtained formalin-fixed tissue, which is what also impeded us from applying other techniques. Future prospective studies could look at appropriate fixation protocols to comply with various histochemical techniques, especially regarding specialized silver stains, for the visualization of the peripheral nervous structures (De Vreese et al., 2020). Some of these techniques did provide exciting results on the nature of other tissue, such as the subepithelial connective tissue.

2.2.6.1 Silver stains: Palmgren, Bielschowsky, Luxol Fast Blue/Cresyl Violet, Speathe

The silver impregnation techniques in this study did not provide any additional information on the morphology of the SNFs, nor did they provide consistent results on the unambiguous identification of nervous structures. In contrast, similar techniques have been used successfully. For example, El-Oteify et al. (2011) used a silver impregnation technique (Linder, 1978) that worked well for the identification of various SNFs, including lamellar corpuscles. These authors describe Pacinian corpuscles as stained by silver staining and immunohistochemical staining with S100 protein. The picture of the silver staining depicts lamellar corpuscles labelled as Pacinian corpuscles that show remarkable resemblance to the lamellar corpuscles in this study, with a central axon surrounded by concentric lamellae of nerve fibres and Schwann cells, and in terms of number of lamellae and the clustering of corpuscles, except that they noted a ‘well-developed connective tissue capsule’.

The significance in the staining intensity of the connective tissue around the ear canal and further away, between Bielschowsky´s and Palmgren´s stain is not well understood. The results have to be examined with care since the staining of reticulin and elastin fibres by these methods has been subject to confusion, and only under carefully controlled conditions would there be selective staining of nerve fibres. It would be interesting to apply these techniques to other tissues to see if there is a trend in the staining intensity between different types of stromal tissue.

2.2.7 Immunohistochemistry

The herein investigated antibodies cross-reacted against formalin-fixed, paraffin-embedded tissues of stiped and bottlenose dolphins, reflecting the immune reaction patterns already showed in other species of terrestrial mammals. To validate antibody specificity, other than the correct use of positive

and negative samples, the immunoreactivity against the proper cetacean antigen was proved by Wester Blotting analyses, as suggested by standard guidelines for veterinary laboratories (Ramos-Vara et al., 2008)(De Vreese et al., 2020).

The positivity beneath the basement membrane was variable but consistent for all antibodies used in this study. Although this could be false positive due to non-specific staining or an artefact that caused melanin from the epithelium to be present in the subepithelial tissue, we noted that routine histological staining did not show this reaction, nor did IHC with antibodies for the identification of other tissue types using the similar immunohistochemical procedures.

The IHC research with anti-PGP9.5 showed results as expected, as it is commonly used as a panneuronnal marker (according to manufacturer and Wilson et al., 1988), and as a neuroepithelial markers of the peripheral nerve system (e.g. Veres et al., 2007). It has also been used to identify (neuro-)endocirine cells (Suarez-Mier and Buckwalter, 2015; Thompson et al., 1983; Wilson et al., 1988), thecal gland cells and endothelial cells (Kimaro and Madekurozwa, 2006), single axons (Ji et al., 2018; Kelly et al., 2005; Saffari et al., 2018; Suarez-Mier and Buckwalter, 2015), entire nerve bundles (Kimaro and Madekurozwa, 2006; Suarez-Mier and Buckwalter, 2015; Thompson et al., 1983) and a large variety of sensory nerve formations including Meissner corpuscles (Wang et al., 1990), free nerve endings (Kelly et al., 2005; Soda and Yamamoto, 2012), and motor end plates (Day and Thompson, 2010).

There was an overlap in distribution of anti-PGP 9.5 and -NSE in the lamellar corpuscles in this study, which supports the suggestion of a functional or structural relation between the two (cfr. Wilson et al., 1988), although its significance has not been elucidad yet.

NSE stained axons of both corpuscles and nerves, but has also been mentioned to stain neuroendocrine cells (Kimaro and Madekurozwa, 2006; Schmechel et al., 1978). Interestingly, there was a difference in the staining of slides with or without casein blocking reagent. In the sections without blocking, the anti-NSE antibody stained the central axons in the corpuscles intensely positive, while there was also positivity of the lamellae, more specifically of the cytoplasm of the Schwann cells. The slides with the blocking agent also showed positivity of the central axons, but with a subtle positivity of the lamellae with the Schwann cell scantly labeled nuclei staining more intensely than the cytoplasm, and an inconsistent darker labeling of the peripheral layer of the corpuscle, similar in intensity to the perineurium of the small nerves. NSE staining of the capsule was inconsistent and less intense than for the axon.

The Western blot showed that the expression of the NF antigen lied around 150-160 kDa, corresponding to Neurofilament protein M, while the manufacturer's technical sheath mentioned a reaction with the 70 kDa subunit of neurofilament, Neurofilament protein L. Nerves fibres are known

to react to anti-bodies to all three subunits of neurofilament protein (Iwanaga et al., 1982), and our results correspond to studies showing IR to NFm in the central axon of Meissner's corpuscles (Iwanaga et al., 1982)

Anti-S100 is used particularly for the identification of (modified) Schwann cells, and although previously considered to be a nervous-system-specific protein, S100 is present in cells originated from the neural crest, but has been shown in a large variety of tissues. It has been used to identify (modified) Schwann cells (Bock, 1978; Del Valle et al., 1998; Iwanaga et al., 1982; Soda and Yamamoto, 2012; Stefansson et al., 1982; Suarez-Mier and Buckwalter, 2015), free nerve endings (Del Valle et al., 1998), Langerhans cells (Cocchia et al., 1981; Takahashi and Nakano, 1989), and other cells like e.g. bronchial epithelial cells (Suarez-Mier and Buckwalter, 2015) and satellite cells of adrenal medulla (Cocchia et al., 1981), and other. Anti-S100 has also highlights the presence of myoepthelial cells (Chung et al., 2017), which was not apparent in the current study.

According to the manufacturer, staining with anti-S100 is confined to the cytoplasm, while our findings indicate also a nuclear staining of the lamellar cells. However, the reaction is usually very intense, which could create colour masking of non-staining structures such as the nucleus.

Anti-S100 has also been used to localize Langerhans cells in the epidermis of the external ear canal in humans, with reactivity in the perikaryal and cytoplasmic processes of melanocytes and Langerhans cells in normal human skin, without positivity in any keratinocyte within the epidermis. There were few reative cells in the stratum spinosum of healthy samples, with higher number in samples with cholesteatoma (Cocchia et al., 1981; Takahashi and Nakano, 1989).

For PanCK, both corpuscles and nerve fibres were entirely negative in one section, while in another section there were indications of positivity in both the perineurium and the outer layer of the corpuscles. However, the latter section also contained non-specific background stain, therefore, this was not considered a positive reaction, while the epithelium of the ear canal and the glands did show IR. This is conform the literature, as there is no cytokeratin in Pacinian or Meissner corpuscles to form the intermediate filaments (Haro et al., 1991; Vega et al., 1996b). The only study that did report IR to cytokeratins in lamellar corpuscles, specifically of lamellar cells (and perineural cells of nerves), was in the snout of the pig, while it proved negative in other mammalian species (Ortonne et al., 1987).

In contrast, both cytoplasm and cell membrane of the epithelial cells were positive, while nuclei were negative. Basal cells showed less intense stain, likely because they were less differentiated. It would be interesting to perform a characterization of the cytokeratins in the ear canal epithelium, to understand the distribution of specific keratins, the nature of the canal's obstruction or full closure as

in baleen whales (together with a characterization of the earplug and getting a better understanding of its genesis and development, and to compare with terrestrial ear canals.

Table 20 presents the distribution of various cytokeratins, and proliferation markers like Ki-67 and Proliferating cell nuclear antigen (PCNA) as can be found in the epithelium of the ear canal (Broekaert and Boedts, 2009; Kakoi et al., 1997; Lepercquel et al., 1993, 1993; Sanjuan et al., 2007; Vennix et al., 1996). It also presents Ki-67, which is a nuclear and nucleolar antigen associated with cell proliferation, and PCNA, an antigen found in mitotic cells, both of which are (hyper)proliferative-characteristic antigens and seem to be located in the region the annulus tympanicus. Similar proliferation has been suggested in baleen whales, where the earplug originates from the glove finger and the epithelium of the deepest region of the ear canal (Ichihara, 1959, 1964).

Table 20. IHC labelling in healthy external auditory canal structures in humans 1: Broekaert and Boedts, 2009; 2: Lepercquel et al., 1993; 3: Vennix et al., 1996; 4: Kakoi et al., 1997; 5: Sanjuan et al., 2007, using cultured cells; 6: Broekaert and Boedts, 1993. Ki67 and PCNA presence everywhere but with significant variation in distribution and number of positive nuclei; Question marks are uncertainties; Brackets indicate weak reactivity

		CYTOKERATIN												KI-67	PCNA
		4	**5**	**6**	**7**	**8**	**10**	**13**	**14**	**16**	**17**	**18**	**19**		
CARTILAGENOUS PART	Basal cells		1,2?, 3,5,6				2?	6	1, 2?, 3	6				4	4
	Suprabasal cells		2?				1,2?,3, 5,6		2?					4	4
OSSEOUS PART	Basal cells		3,5,6	(3)			3	6	3	6	3			4	4
	Suprabasal cells		3	3			3,5,6		3	1,3,6	3			4	4
TYMPANIC MEMBRANE	Basal cells		1,2?, 3,6				2?		1,2?,3,6	(6)				4	4
	Suprabasal cells		2?,6				1, 2?, 3,6		2?	1,2,6				4	4
FIBROCARTILAGENOUS RING	Basal cells							6		6			1,2,3,6	4	4
	Suprabasal cells							6		3,6	3			4	4
	Tense part									3	3		3	4	4
	Flat part									3	3		3	4	4
	Umbo area									3	3		3	4	4

2.2.8 3D reconstruction from histological slides

3D reconstruction of tissue from histological slides proves very useful for anatomic goals as well as for histopathology and the study of normal and pathological processes (Braumann et al., 2005; Roberts et al., 2012). The reconstruction of the toothed whale's ear canal proved successful, although there is room for improvement as discussed below. Importantly, the entire process can be recreated using only open-source software and can therefore be implemented by anyone or any institution that cannot afford specialized software such as Amira (FEI software)(See Clendenon et al., 2006 for other programs).

Sampling and tissue blocks preparation

After sampling and fixation, the tissue was cut into tissue blocks for paraffin embedding. The tissue was either cut manually, or with a specially-developed antithetic slicer that maintained the tissues fixed in space and direction, and allowed for creating tissue blocks of equal thickness. Both were valid, although they would have to be taken into account in the registration steps.

Paraffin embedding and slide preparation

Both steps were carried out according to conventional methods. As it was a time-consuming process that had to be executed preferably within the same day to avoid tissue deformation and damage with temperature changes (room temperature – fridge temperature 6°C – freezer -16°C), it is best to plan this step well, and maybe even automate it if possible (Kokubo et al., 2002). It would be great to organize a system for the storage of non-used tissue sections. For every reconstruction, at least two histological slides were prepared, and the best quality one was chosen for reconstruction, and in the rare case that both slides were too damaged, these were discarded, and the previous slide was copied (cfr. Woodward and Maina, 2005).

Staining

The Masson´s trichrome staining with aniline blue, with a slightly adjusted protocol for manual staining in batches, gave the best results for the trainable, automatic tissue segmentation (ILastik) of the tissues of interest. If needed, the colour of the digital images could be matched to produce more homogenous results, although if the staining protocols are carried out in a standardized manner, we noted there was no need for such as step for the segmentation to be successful. It must be noted that the choice of staining protocol should be adapted to the structures of interested. For the lamellar corpuscles, after discarding Silver impregnation techniques and other histochemical stainings, immunohistochemical staining with several markers would be the best option (work in progress, confocal microscopy).

(Automated) slide digitization

For batch scanning of hundreds of slides, the collaboration with the Hospital of Rovigo was essential for the progress of the work. The manual scanning using D-sight was a time-consuming process that was only used for the reconstruction of a part of the nervous network. The automated scanning results often came with inconsistent results, artefacts of the acquisition such as vertical line noise, artefacts of the tissue such as creases or ruptures, or defects such as dust (Figure 456). In the best case, these should be rescanned or corrected digitally. Also, even though deconvolution techniques have been widely used in histological optical image processing to enhance the image quality in 2D or 3D (Clendenon et al., 2006; Sibarita, 2005), this step was not considered essential for the current research purposes.

Image processing

This required a manual export of the region of interest, in part because the scanning and image analysis software did not allow for batch processing of the SVS or jp2 image format (manual scanning: D-sight, Menarini Diagnostics + associated software; and automated scanning: Scanscope XT + Leica ImageScope Pathology software), and second because of the great variety in type and size of tissues. It would be great to look into automating these image processing methods if they are to be implemented in routine analyses (cfr. Roberts et al., 2012).

Image registration (rigid alignment: rotation and translation only).

The automatic registration using various ImageJ plugins did not prove useful for the alignment of images between consecutive tissue blocks, but only within the same block. Therefore, there was opted for a fully manual registration, which did not provide perfect or unbiased results (cfr. Roberts et al., 2012, Fig. 3). Because of the tissue deformation, related to tissue manipulation, cutting into blocks, and paraffin embedding, it would be useful for future reconstructions to add physical fiducial markers to the tissue (e.g. surgical sutures), before cutting into blocks, even though they are not recommended (Wang et al., 2015). It could be interesting to apply non-rigid registration (similarity (= translation + rotation + isotropic scaling), affine, or others) as a second step after the initial rigid registration, in order to compensate for local errors and smooth out the models.

2D segmentation (ILastik)

The development of the tissue classifier was a slow process, which depended on computing power and the size of the training images and required manual correction until a satisfactory level was obtained (unsupervised classification). Once trained, the application of the classifier on the image data stacks was relatively fast and could be done automatically in one or two nights. At least three tissue classifiers were developed for the various resolutions, after which, the steps of segmenting and downsizing were reversed to optimize the processing time.

Image downsizing – cropping (ImageJ)

The downsizing of the image was done without averaging or interpolation in order to not to change the values of the original segmentation image (Figure 457). As such, the originals values of the pixels were not changed, and in the downsizing, the priority was given to lower values (lumen > epithelium > nervous tissue > … > background)

3D segmentation (3Dslicer)

3Dslicer was the biggest bottleneck in this process, as it would preferably not handle images with dimensions larger than 500 pixels. Therefore, this step was anticipated by various image processing techniques, which resulted in sequences of images of various resolutions, but always with the same absolute dimensions, to be imported into 3DSlicer and positioned in space according to the values of the cropping step. The cropping involved two parallel processes, the first of which was to cut the sigmoid ear canal into sections that correspond and match in horizontal space, i.e. where the ear canal lumen has similar X and Y coordinates, and to remove excess areas of the images without tissue. The second was to create images sequences of varying resolution to be cropped and inserted into 3Dslicer according to their cropping coordinates. This process should be revised as there are automated that do not require for compromising the original resolution (e.g. using the DICOM image format).

Stl file size reduction (Meshlab)

This was realized using consecutive steps of Quadric Edge Collaps Decimation at 50%, which provided the best results for the integrity of the model. The model was decimated until the file was manageable (<50MB) for next steps.

Model combination, Texturing and rendering (Blender)

The models of each tissue segmentation, obtained from the various resolutions, were Boolean subtracted using a rectangular cuboid obtained the coordinates of the high-resolution model and merged in order to obtain a single model with a single resolution but with great detail around the ear canal, and lower detail (in single or in various degrading steps) of the surrounding tissues.

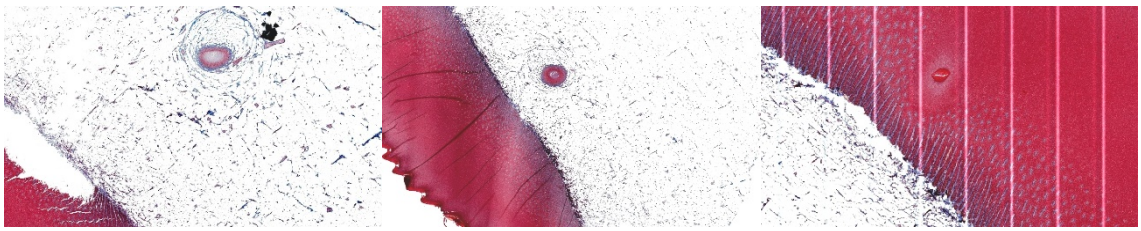

Figure 456. Examples of digital image artefacts. Left: dust and tissue missing; Middle: tissue creases and inhomogeneous scanning intensity; Right: vertical scanning lines.

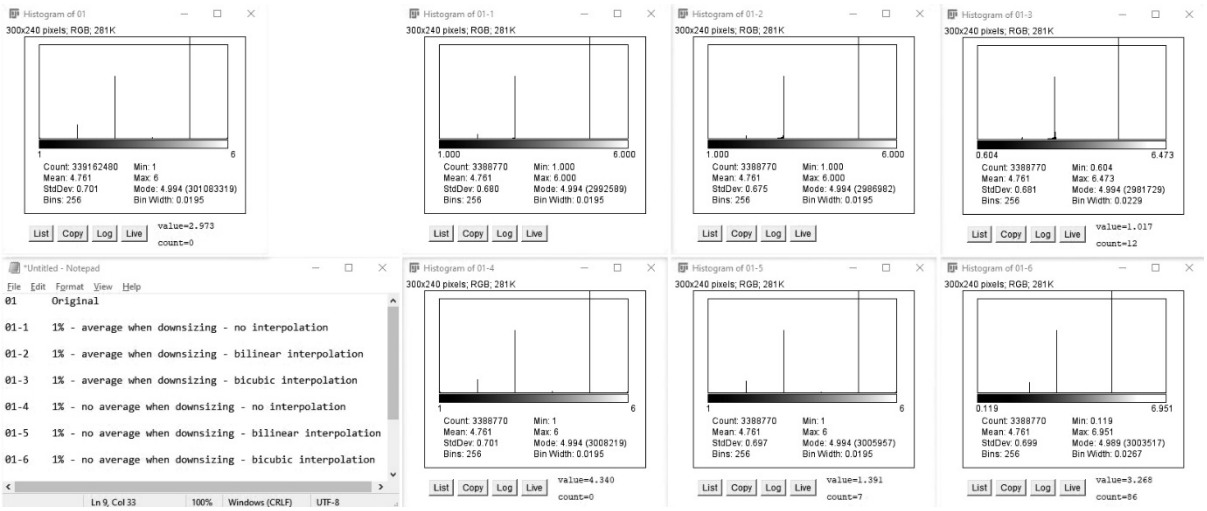

Figure 457. Comparison of the downsizing techniques using histograms of the results compared to the original. With or without averaging, and with or without interpolation. The best result was obtained without averaging or interpolation (01-4). Averaging caused additional values to appear (top row, notice the appearance of slopes in the graph), while the six values were the tissue segmentation results, while interpolation (bottom row) caused a change in the distribution of the values, which would make images no longer comparable among each other.

2.2.9 Lamellar corpuscle modelling

A functional model of the lamellar corpuscles, together with a network simulation or reconstruction of the lamellar corpuscles in a variety of tissues, would help to understand the sensitivity for biomechanical stimuli and to understand the physiology and pathology related to the corpuscles and the peripheral nervous system. The work on such a model was part of an optional work package that was based on the results of the confocal microscopy studies. For several reasons, this was not feasible within the timeframe but is currently (Oct 2020) being resumed. First of all, such models could provide the valuable information on the lamellar corpuscle morphology, and the nervous network they are part of, and could provide the base for biomechanical models, as has been developed for other SNF such as the Pacinian corpuscle (Biswas et al., 2013, 2014, 2015; Quindlen et al., 2015).

2.2.10 Computer tomography

The CT-scans of a bottlenose dolphin (University of Padova) and a harbour porpoise (University of Utrecht, the NL´s) did not provide additional information on the structure and components of the external ear canal in these species. Even though the external ear opening, and the medial end of the ear canal, where it transitions into the middle ear, could be noted, the lack in the contrast of the soft tissue attenuation was minute. There were few indications of the auricular cartilage, similar to the mention of a slightly hyperattenuated cartilage in striped dolphin foetuses (García de los Ríos y Loshuertos et al., 2019). Other medical imaging techniques could be more useful for segmentation of soft tissues (see below).